Chemical Engineering Journal 478 (2023) 147302

Contents lists available at ScienceDirect

Chemical Engineering Journal

journal homepage: www.elsevier.com/locate/cej

Review

Metal-organic framework-based composites for biogas and natural gas uptake: An overview of adsorption and storage mechanisms of gaseous fuels

Mohammed Yusuf [a,1], Ramesh Kumar [a,1], Moonis Ali Khan [b], M.J. Ahmed [c], Marta Otero [d], Subbaiah Muthu Prabhu [e], Moon Son [f,g], Jae-Hoon Hwang [h], Woo Hyoung Lee [h], Byong-Hun Jeon [a,*]

[a] Department of Earth Resources and Environmental Engineering, Hanyang University, 2226 Wangsimni-ro, Seongdong-gu, Seoul 04763, South Korea
[b] Chemistry Department, College of Science, King Saud University, Riyadh 11451, Saudi Arabia
[c] Department of Chemical Engineering, College of Engineering, University of Baghdad, 10071, Baghdad, Iraq
[d] Departmento de Química y Física Aplicadas, Universidad de Leon, Campus de Vegazana s/n, 24071 Leon, Spain
[e] Department of Chemistry, School of Advanced Sciences, VIT-AP University, Vijayawada 522237, Andhra Pradesh, India
[f] Center for Water Cycle Research, Korea Institute of Science and Technology (KIST), Seoul 02792, Republic of Korea
[g] Division of Energy and Environment Technology, KIST-School, University of Science and Technology, Seoul 02792, Republic of Korea
[h] Department of Civil, Environmental, And Construction Engineering, University of Central Florida, Orlando, FL, 32816, USA

ARTICLE INFO

Keywords:
MOF-based adsorbents
Synthetic methods
Biogas and natural gas upgrading
Adsorption and storage
Storage mechanism

ABSTRACT

Biogas and natural gas are potential renewable energy sources. They primarily contain CH_4, H_2, CO_2, CO, C_2H_6, C_3H_8, H_2S, N_2, and moisture. To be used as fuel, raw biogas and natural gas require upgrading to enrich the CH_4 content (≥97 %). The development of a practical technique to effectively trap gas molecules in a limited space for a variety of uses has been acknowledged as a major technical difficulty. Among the various practical enrichment processes, the adsorption-based method is particularly attractive for upgrading because of its ease of use and economy. A new family of versatile porous solid-state materials, metal–organic frameworks (MOFs), possess controllable structures, tunable thickness and pore size, chemically adjustable architectures, vast surface areas, and favorable mechanical flexibility. Therefore, MOF-based adsorbents can play an exceptional role in the adsorption of gas molecules like CO_2, CH_4, H_2, and C_2H_2 for gaseous fuel uptake and eliminating greenhouse gases from the atmosphere. The mechanism of gaseous molecule adsorption/separation using MOF materials was critically evaluated. Fluorinated MOFs, such as ZIF-8, ZIF-67, UiO-66, and nanosheets (2D MOFs), are considered potential adsorbents for moisture-stable, cost-effective, and efficient biogas and natural gas adsorption. Moreover, the prospects and further research ought to concentrate on comprehending the dynamics of gas adsorption and desorption in massive columns loaded with MOFs, effectively packing MOF particles, cost-effective manufacturing, and enhancing the reusable nature of MOFs. The comprehensive review provides an in-depth understanding of MOFs by focusing on the most recent advancements in gas storage and adsorption.

1. Introduction

Modern society has witnessed significant improvement in living standards owing to technological advancements, which have contributed to the enhancement of global energy demand. Currently, fossil fuels cover 80 % of the global energy requirements, which leads to the emission of hazardous gases, such as NO_x, SO_x, CO, H_2S, and NH_3, and deteriorates the states of the global ecosystem and human health

Abbreviations: ANG, adsorbed natural gas; AMX, amoxicillin; BET, Brunauer–Emmett–Teller; BTC, 1,3,5-benzene tricarboxylic acid; CB, carbon black; CNG, compressed natural gas; DMF, dimethylformamide; DOE, U.S. Department of Energy; FTO, fluorine-doped tin oxide; GCMC, grand canonical Monte Carlo; GHG, greenhouse gas; HKUST, Hong Kong University of Science and Technology; IRMOF, isoreticular metal-organic framework; LCD, largest cavity diameter; LNG, liquefied natural gas; MEM, maximum entropy method; MOF, metal-organic frameworks; MW, microwave; OMS, open metal site; rGO, reduced graphene oxide; STP, standard temperature and pressure; ZIF, zeolitic imidazole framework; EDA, electron-donator-acceptor; SSA, specific surface area; vdW, van der Walls.

* Corresponding author.
E-mail address: bhjeon@hanyang.ac.kr (B.-H. Jeon).
[1] These authors contributed equally to this work.

https://doi.org/10.1016/j.cej.2023.147302
Received 6 September 2023; Received in revised form 8 November 2023; Accepted 10 November 2023
Available online 20 November 2023

[1,2]. Consequently, efficient detection and replacement of these chemicals from bio-based sources is crucial for preserving the ecosystem and human health. The use of renewable energy sources as a sustainable alternative to conventional fossil fuels is being investigated by researchers throughout the world [3]. One of the crucial renewable energy sources is biogas and bio-H_2 produced from waste lignocellulosic biomass, food waste, organic waste, animal waste, and sewage sludge [4,5]. Biogas is similar to natural gases, which is composed of CO_2 (25–50 %), CH_4 (50–75 %), N_2 (0–10 %), H_2S (0–3 %), H_2 (0–1 %), and a trace amount of other gases that significantly affect the reduction of greenhouse gases (GHGs) [6,7].

Biogas is produced through the anaerobic fermentation of organic waste materials and has numerous advantages, such as cost-effectiveness, ease of handling, and high flexibility during commercial scale-up [8,9]. The United Kingdom and Germany produce 60 % of biogas from landfills and install several industrial plants to upgrade biogas for smooth injection into their natural gas supply [10]. The amount of biogas supplied by the global energy sector is currently 10–14 % and is expected to increase to 25 % within the next few years [7,11]. CH_4 is the predominant component of natural gas, along with C2 + hydrocarbons, H_2S, CO_2, N_2, H_2O, and other gases [12]. The CH_4 content in biogas and natural gas must be enriched to a minimum of 97 % to optimize its burning capacity and flammability limit for use as a valuable energy source [13]. Various methods for gas enrichment, such as absorption, pressure swing adsorption, porous material adsorption, chemical adsorption, water scrubbing, membrane-based separation, and cryogenic recovery, have been reported [7,14,15].

Absorption, chemical adsorption, cryogenic, and membrane processes encounter challenges such as chemical prerequisites, high pressures, elevated temperatures, and multistage procedures. Using solid-state porous materials has been demonstrated to be a successful strategy for separating and enriching desired gases through adsorption. Adsorption can separate the desired gas through adhesion or bonding to specific components in a mixture over a microporous solid matrix with a high surface area/mass. Subsequently, the adsorbent and gas are recovered through desorption at low pressure [16]. However, the synthesis of ultrahigh porosity adsorbing materials with a balanced volumetric and gravimetric surface area is a significant challenge for successful onboard storage of H_2 and CH_4 [15]. MOFs are coordination polymers with highly ordered crystalline porous materials obtained from metal clusters or ions combined with organic groups as linkers (ligands) [17]. In the history of MOF development, Hofmann and Küspert [18] were the first to describe a network of coordination connected by cyanide groups of 2D layers linked by cyanide ions, using the formula $Ni(CN)_2(NH_3)\cdot C_6H_6$, known as Hofmann clathrate. Rayner and Powell later verified the crystal structure of the coordinate network [19]. In 2002, a group of Zn dicarboxylates gained popularity because of the concept of isoreticular chemistry [20] to manipulate the porous structure design and functionality of MOF-5. In 2002, imidazolate-based compounds were introduced to the category of MOFs and are now referred to as zeolitic imidazole frameworks (ZIFs) [21].

Because MOFs have outstanding structural properties, research on their industrial and technological applications has increased dramatically over the past two decades. One representative field is in traditional gas capture and separation techniques, such as CO_2 absorption [22], H_2 gas attraction [23], NH_3 capture [24], and effective CO_2 and CH_4 separation [25]. A physisorption mechanism controlled by thermodynamic equilibrium typically governs gas removal through the adsorption process on porous materials. In this method, gases are reversibly adsorbed over nanopores at higher densities compared to the bulk densities [26]. The controlling mechanisms, such as equilibrium, kinetic, and steric, are essential components of creating functional MOFs for gas separation and selectivity, which are the most important factors in addition to the surface area, stability, and heat of adsorption. The thermodynamic component is one of the most significant variables influencing the dynamic structural alterations of some flexible MOFs to improve materials for guest sorption and other uses [27,28]. Rosen et al., showed the structural deformation of ZIF-8 by evaluating changes in thermodynamic data during CO_2 molecule adsorption [29]. A successful structure-deformation-thermodynamic-energy-modulation method was demonstrated to allow flexible MOF for selective adsorption of guest molecules [30].

Using lanthanide MOFs, aqueous-phase differentiation, and speciation between Fe(III) and ferrous Fe(II), researchers have demonstrated excellent detection sensitivities, rapid reaction times, and appropriate detection limits [31]. In addition, studies on the specific sensing and detection of Fe(III) [32], ciprofloxacin [33], and Cr(VI) [34] in water and acetone [35] and p-nitrophenol [36] have been reported. These studies demonstrate the extraordinary abilities of MOF-based sensing devices. A pressure-assisted sintering technique can produce macroporous MOF monoliths for industrial-scale applications, offering a platform for exploring gas–solid interactions [37]. Because of their steric and electronic tunability at the molecular level, MOFs may provide special prospects in selective gas adsorption and storage [38]. Chen et al., reported a simulation-inspired fabrication of an ultra-porous MOF (NU-1501-Al/Fe), a trinuclear cluster of metals that exhibit 7310 m^2/g of gravimetric surface area and 2060 m^2/cm^3 of volumetric area [15]. However, conventional MOFs suffer from structural instability, aggregation, restacking phenomenon, and poor electrical conductivity [39]. Moreover, because of different topologies and compositions, manipulating and comprehending both compositional [40] and structural complexity is a synthetic problem in the field [41]. Additionally, poor selectivity and inefficient adsorption capability are shown by MOFs for gas molecules with low and comparable polarizabilities, such as CH_4/Kr or N_2/O_2 [42].

This review mainly focuses on critically analyzing recent developments in MOF-based materials, including the ongoing development of various synthesis techniques and exceptional effectiveness in gaseous fuel storage and adsorption. A comprehensive summary of recent representative progress in MOFs' utilization in gas storage and their storage mechanisms, influencing parameters, and upgradation strategies have been analyzed. The challenges and potential directions for future work in the vital field of MOF-derived adsorbents are discussed. This review provides direction and motivation for future research on high-performance biogas and natural gas storage and energy applications using MOF-based adsorbents.

2. Synthesis strategies of MOFs

Depending on the type of energy or source and the synthesis process, the fabricated MOFs have different characteristics and properties [17]. The main characteristics of the synthesized MOFs, such as particle size, distribution size, and morphology, determine their application or usefulness [43]. The porosity of the synthesized MOFs depends on the kind of heat energy produced during manufacturing and the heat source used [44,45]. The time, temperature, and pressure during the synthesis process, as well as the compositional factors, affect the types of MOFs produced (linker substituent, pH, metal ion concentration, and solvent) [46]. In addition, metal salts, ligands, and solvents can be used to synthesize MOFs. The various MOF synthesis methods are illustrated in Fig. 1.

2.1. Electrochemical synthesis

The electrochemical procedure is a promising and ecologically friendly technique for synthesizing MOFs with numerous advantages over other methodologies (such as shorter and milder synthesis conditions) [48]. Both indirect and direct methods can be used to produce and place MOFs on a substrate. Ideal MOFs are produced by direct electrochemical synthesis using an electrochemical process occurring on the surface of an electrode, such as reductive electrochemical synthesis or anodic dissolution [49]. This direct technique controls the synthesis of

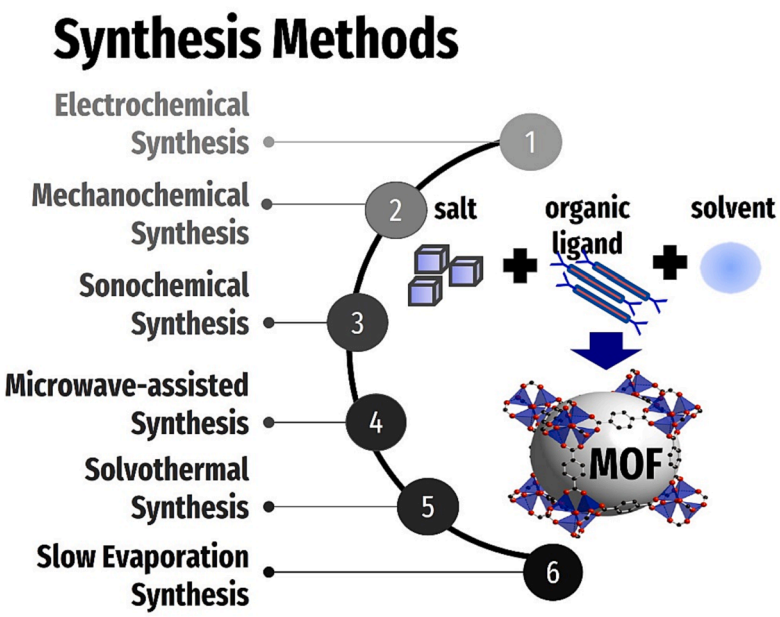

Synthesis conditions		
Energy	Time	Temperature (K)
Electrical energy	10 - 30 min	273 - 303
Mechanical energy	30 min – 2 h	298
Ultrasonic radiation	30 min – 3 h	273 -313
Microwave radiation	4 min – 4 h	303 – 373
Thermal energy	48 – 96 h	353 - 453
No external energy	7 days – 7 months	298

Fig. 1. Various MOFs synthesis techniques. The time and temperature of MOFs synthesized using different methods are shown (Reprinted (adapted) from [47]).

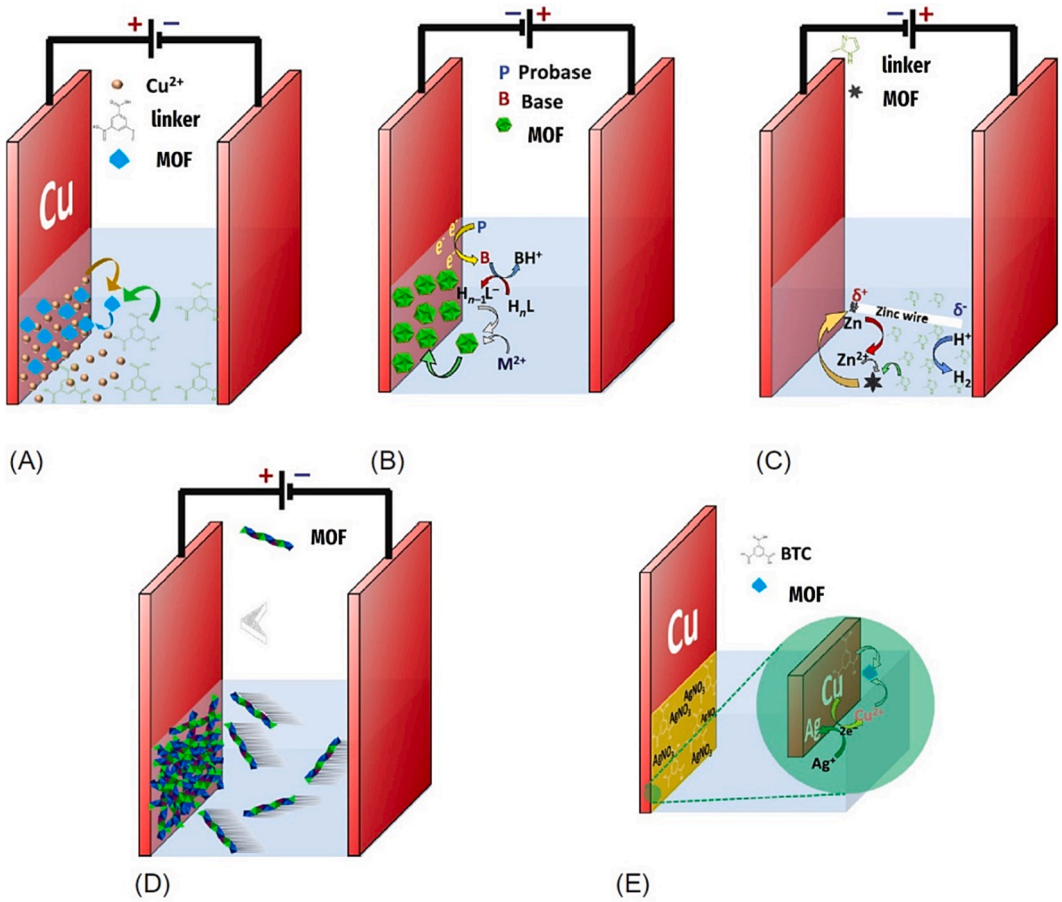

Fig. 2. Schematic of electrochemical synthesis methods of MOFs following (A) anodic dissolution, (B) reductive electrosynthesis, (C) bipolar electrosynthesis, (D) electrophoretic deposition, and (E) galvanic displacement (Reprinted (adapted) from [62] with copyright permission from Elsevier with License Number 5507940921270).

the MOFs, enabling real-time electrochemical tuning. The electrochemical response is one of the steps involved in synthesizing MOFs using indirect methods, such as self-templating, electrophoretic deposition, and galvanic displacement.

Mueller et al., developed the electrochemical synthesis technique for MOFs, known as anodic or anodic disintegration [50]. This technique involves the addition of metal ions through electrochemical reactions rather than through a solution of metal salts. The metal ion, via anodic dissolution, is oxidized and released into a mixture of an organic linker and sustaining electrolytes as a metal ion source when an electric current is applied. The dissolved metal ions immediately respond to the organic linker, and a MOF formation takes place close to the electrode's surface [51]. Fig. 2 **(A)** shows a schematic of the anodic dissolution technique. The interaction of metal ions with organic binders in the solution near the electrode surface produces a thin MOF coating. In contrast to other synthesis methods, MOF formation associated with the metal precursor can be avoided because no salt is used in anodic dissolution [52]. Additionally, altering the electrochemical conditions allows the metal to exist in various oxidation states, allowing control over the MOF characteristics. Jiao et al., reported the properties of Hong Kong University of Science and Technology (HKUST)-1 prepared through anoxic dissolution [53]. They applied the oxidation potential method to dissolution.

Reductive deprotonation is a relatively recent electrosynthesis method for down-producing MOFs on conductive substrates. This method uses an electrical technique to increase pH and deprotonate the linker. In contrast to the anodic dissolution approach, this method relies on the electrolytic production of an agent known as the "probase," such as a nitrate (NO_3^-) or perchlorate (ClO_4^-) ion, at the cathode surface (Fig. 2 **(B)**). An MOF-5 thin sheet was developed on a fluorine-doped tin oxide electrode using this technique [54]. The bipolar electrosynthesis technique for electrodeposition involves simultaneous anodic and cathodic reactions, placing the conducting substrate under a small amount of electrolyte at a specific angle. A conductive item is polarized between its two sides (anodic and cathodic sides), allowing various redox reactions to occur [55]. In one study, site-selective bipolar electrosynthesis was used for electrodeposition of the ZIF and HKUST structures onto Zn wire [56]. The potential gradient that produced the ionic metals was the deposition site of the MOF layer on the hemisphere of the conductive object. Zinc ions were produced on the Zn surface wires. Then, the organic linker 2-methylimidazole chemically interacted with the metal ions (Fig. 2 **(C)**). A novel family of MOFs was made using single organic crystals that transmit through bipolar electrodes [57].

Electrophoretic deposition uses a strong electric field to apply charged granular particles to a surface (e.g., conductive glass electrodes, metallic substrates, and glassy carbon) to synthesize MOF film [58,59] (Fig. 2 **D**). Among the numerous well-known MOF thin sheets synthesized, Hod et al., were the first to use electrophoretic coatings (ZIF-8, UiO-66, HKUST-1, and NU-1000) [60]. Ameloot et al., developed the technique of growing HKUST-1 cells on glass [61]. To prepare HKUST-1, spin-coating was used to apply a BTC ligand and $AgNO_3$ solution to a Cu-based glass electrode at 808 °C. Accordingly, Cu(II) ions were freed, and Ag(I) ions were reduced (Fig. 2(E)).

2.2. Mechanochemical synthesis

Mechanochemistry considers the effects of mechanical forces on chemical reactions and structural alterations [63]. In mechanochemical production, the initial mechanical dissociation of intramolecular interactions occurs before chemical transformation [28]. Several industries, such as the pharmaceutical, mining, manufacturing, and building sectors, use mechanochemical technologies [64]. This synthesis technique accelerates chemical responses by grinding solids or milling starting materials with little to no solvent (or even without any solvent). The liquid coordination phase procedure involves dissolving organic ligands and metal salts in appropriate liquids and is typically the basis for synthesizing MOFs. Mechanical forces form connections between molecules when the substrates are ground in a mortar or ball mill. In addition, MOFs can be produced using a minimal quantity of solvent because of their mechanochemical properties (Fig. 3). For example, the ball-milling process does not require any solvent or, at the very least, only a small amount. Thus, problems with solvents (such as lack of solubility in organic linkers or metal salts) and creating a significant amount of trash can be avoided during mechanochemical synthesis [65].

Pichon et al., were the first to synthesize MOFs using a mechanochemical process [66]. A Cu(II) isonicotinate MOF, $Cu(INA)_2$ (INA = isonicotinate) was prepared by grinding a dry mixture of Cu acetate ($Cu(CH_3COO)_2$), and isonicotinic acid ($C_6H_5NO_2$). The reaction yields byproducts of acetic acid and water, partly clogging the pores. An increased temperature (150 °C) and a lengthy response period (48 h) are necessary for $Cu(INA)_2$ synthesis using conventional solvothermal methods. However, a mechanochemical process using a similar composite may produce a large output in only 10 min without the use of chemicals at room temperature. This study showed that quick, easy, and cost-effective synthesis of MOFs can be achieved through mechanochemistry.

2.3. Sonochemical synthesis

Sonochemical synthesis (a combination of the terms "sono" and "chemical") is a process in which heat is generated from ultrasound, which, in turn, triggers the response mechanisms of the chemicals. The production of organic metal crystals through sonochemical MOF synthesis is an effective and environmentally benign process. The preparation of small samples in the laboratory to complete the commercial manufacturing of MOFs can be linearly scaled up using ultrasound (Fig. 4 **(A)**). In this novel approach, a Pyrex reactor in a moldable horn with a sonicator bar and variable power output is equipped with a substrate–solution mixture to obtain a specific MOF structure without external cooling. Acoustic cavitation occurs during the process, leading to the formation of droplets (gas bubbles). These bubbles enlarge (by a few thousand micrometers) under varying pressures owing to the diffusion of solute vapor into the surrounding area, resulting in the build-up of acoustic energy. Subsequently, acoustic cavitation leads to the formation and decay of bubbles after sonication, resulting in 5000 K and 1000 bar of temperature and pressure, respectively [67]. Acoustic cavitation causes changes in the temperature at heating rates > 1010 K/s to form delicate crystallites [68]. This technique has the advantages of a shorter crystallization period and smaller particle size owing to uniform and faster nucleation [67].

2.4. Microwave-assisted synthesis

Despite microwave (MW) heating being a fast and uniform method, providing precise control over the irradiation power or temperature gradient within the reaction vessel is challenging, potentially affecting MOF quality or reproducibility during mass synthesis [51,70]. Prolonged reaction times at high temperatures are the main issues in MOF synthesis using conventional processes. During the synthesis of MOF-808, seven days of heat treatment (100 °C) is required [71]. Reducing the heating time is crucial for retaining the MOF yield, topology, and properties while bridging the gaps between academia and industry. One solution that addresses this issue is MW-assisted synthesis. In MW-assisted synthesis, the energy derived from MW radiation in a mixture of solid or liquid states activates electromagnetic radiation and mobile electric charge coupling. The orientation of polar molecules in a solution change over time in an oscillating electromagnetic field. Thus, by using a suitable frequency, collisions occur between the molecules, increasing the kinetic energy and, consequently, the system's temperature. This synthesis process is an excellent example of an energy-efficient heating approach because of its high reaction speed, short reaction time, and direct reactant-radiation interaction [72]. MW-assisted heating is an

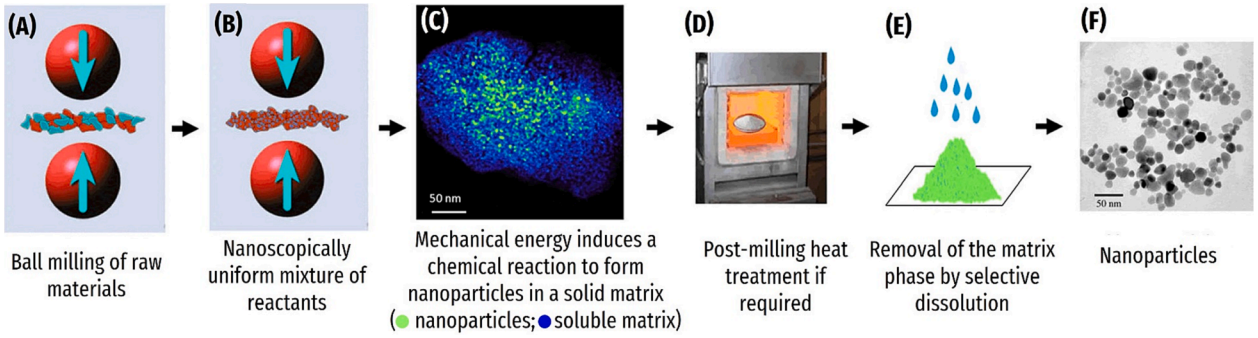

Fig. 3. Standard mechanochemical processing stages for a solid-state displacement reaction that yields nanoparticles: (A) a milling receptacle is filled with milling balls and dry raw reactant ingredients; (B) a nanocomposite of the reactants is created during ball milling owing to the repeated fracture and welding of raw materials; (C) a reactive nanocomposite is mechanically energized, triggering a chemical process that develops nanoparticles in a solid matrix (Reprinted (adapted) from [259] with permission from Springer, License Number 5671680749013); (D) if required, a post-milling heat treatment is performed to complete the chemical reaction or to regulate the size, shape, or crystallinity of the nanoparticles; and (E) the matrix layer of soluble byproducts is eliminated. (F) The resultant produced nanoparticles (Figs. A, B, D, E, and F are Reprinted (adapted) from [69]).

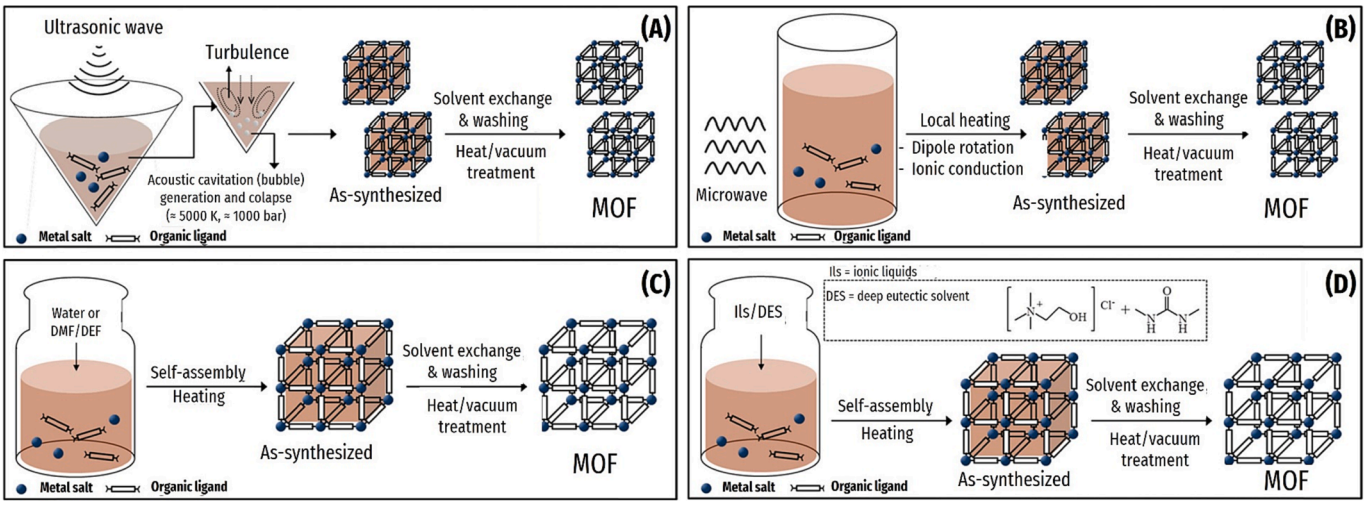

Fig 4. Different synthesis procedures of MOFs: (A) sonochemical synthesis, (B) MW-assisted synthesis, (C) solvothermal method, and (D) ionothermal synthesis (Reprinted (adapted) from [90] with copyright permission from Springer Nature with License Number 5,510,050,580,622 (Fig. 4 A, B, C) and License Number 5,510,050,759,057 (Fig. 4 D).

energy-efficient approach for heating a solution or performing a reaction because radiation comes into direct contact with the substance. Thus, high heating speeds and uniform heating across samples are feasible. Other advantages of this technique include rapid crystallization, phase selectivity [73], narrow particle size distribution [74], and ease of morphology control [75]. Fe-MIL-53 [76], Fe-MIL-101-NH_2 [77], isoreticular MOF (IRMOF)-3 (H_2BDC-NH_2) [78], and ZIF-8 (HMeIm) [79] were synthesized via MW-assisted synthesis. Fig. 4 **(B)** shows different approaches to the MW-based fabrication of the MOFs.

Numerous investigations have been conducted up to this point to determine how the structure of MOFs is affected by the MW-assisted synthesis technique. The impact of concentration on the textural qualities of HKUST-1 was examined through experiments involving temperature, reaction time, MW power, and starting materials [80]. As per their assertion, the reaction mixture containing copper nitrate trihydrate dissolved in trimesic acid, dimethylformamide, ethanol, and H_2O at 360 W for 10 min was accompanied by a specific surface area (SSA) of 1863 m^2/g of resulting HKUST-1. The production of (Na, Cd)-MOF was achieved by MW heating, containing open metal sites (Na(I) ions) in the framework structure [81]. The total synthesis time was decreased to 1 h from 5 days compared to the conventional synthesis process with improved volumetric CO_2 adsorption capability (5.2 mmol/cm^3 at 25 °C and 1 bar), better selectivity (over N_2) and stability (even at 95 % humidity). Furthermore, it retained the CO_2 adsorption capability after 15 cycles, which is an essential characteristic, particularly in the case of industrial utilization.

2.5. Solvothermal synthesis

Solvothermal synthesis is a commonly and extensively used approach for producing MOF-based nanomaterials. In general, this method requires no complicated techniques or expensive tools. Most often, during solvothermal synthesis, solvents other than water are used, leading to a subsequent increase in pressure and high temperatures (depending on the desired MOF structure, usually 100–120 °C) [82]. The dissolved chemicals are continuously combined in a Teflon-lined reactor or a sealed bottle. After the reaction is over, the mixture is cooled to room temperature and washed with water several times, followed by vacuum drying and cleaning the product with anhydrous ethanol at a predetermined temperature to obtain pure MOFs (Fig. 4 **(C)**).[83]. The solvent selection is an essential consideration. The typical high-boiling organic solvents used during the synthesis include dimethylformamide (DMF), acetonitrile, methanol, and ethanol. Using a template, such as organic amines or alkylammonium cations, can facilitate the required shape for a structure. However, these templates often block pores.

The solvothermal synthesis process is fast and requires simple

equipment, which can be suitable for reactants that are insoluble at or below room temperature. MOFs with kinetically inert ions require higher reaction temperatures to form crystals and achieve suitable reaction rates. By altering the conditions, crystal growth with the nucleation rate can be regulated during MOF synthesis [84]. To obtain a transparent crystal, the concentration of critical nucleation must be greater than the concentration of the reactant, which can be done by altering the reaction conditions or by letting the solvent evaporate. The responding temperature gradient and the effects of solution layering, reactant solution evaporation, and sluggish reactant diffusion on the temperature gradient aid the development of MOFs. Dense-structure MOFs are produced by changing the reaction temperature. Xu et al., synthesized many Cu-TCPP nanosheets with a thickness of 15 nm using solvothermal synthesis [85]. MOFs prepared through solvothermal synthesis include MOF-177, ZIP-8, MOF-5, and MOF-74 [86]. Long reaction duration during solvothermal synthesis was associated with unfavorable effects, such as the loss of crystallization and the weakening of pores [87].

2.6. Ionothermal synthesis

Ionic liquids or eutectic mixtures are used concurrently in the ionothermal synthesis of MOFs as solvents and potential templates or structure-directing agents in the formation of solids (Fig. 4 **(D)**). They are fluids at room temperature (<100 °C) and essentially contain only ions [88]. The most appealing characteristic of ionic liquids is their extremely low vapor pressures. This makes them safer than solvothermal methods that generate high vapor pressures [88]. Ionic liquids also possess qualities that are useful for chemical synthesis, including cyclability, good modifiability, and excellent thermal stability. For example, HUSK-1 has been prepared using choline chloride/DMF solvents [86]. Another intriguing aspect is that, in addition to serving as solvents, these ionic liquids can function as structural-directing agents [89]. The benefits and drawbacks of these synthetic techniques are listed in Table 1.

3. Applications of MOFs for biogas and natural gas storage and its mechanisms

Gas molecules are adsorbed on MOFs and MOF-based materials because of their porosity and increased surface area. Consequently, they can store gaseous fuels, such as H_2, CH_4, and C_2H_2, and capture GHGs and other toxic gases, such as CO_2 and CO, from biogas and the atmosphere.

3.1. Bio-H_2/H_2 storage

With the depletion of conventional fossil resources and the environmental impact of CO_2 emissions, significant attempts have been made in the development of alternative fuels. Alternative fuels have several advantages; for example, H_2 has long been considered a perfect clean energy carrier (142 kJ/g) to replace current carbon-based energy sources. Hydrogen contains no carbon and, when oxidized in a motor, only produces water residue, making it a "zero emissions" fuel. In addition, H_2 has a significant energy density that can reach almost three times that of fuel per unit mass. Bio-H_2 can be produced from CH_4 through steam reforming and photo-/dark-fermentation by converting organic and carbohydrate-enriched biomass waste [4]. Furthermore, bio-H_2 can be produced using microbial electrolysis cells (by fermenting waste organic materials), algae (*Chlamydomonas reinhardtii*) under anaerobic conditions, and biological/solar water-splitting processes [93]. The bio-H_2 productivity and yield could reach 324 mL/L·h and 2.59 mol/mol in sequential batch fermentation operated in three batches for 13.5 h using algal biomass (*Spirogyra*) hydrolyzates [94].

However, the lack of sufficient onboard storage space continues to be a significant barrier to its widespread adoption, making H_2

Table 1
Benefits and drawbacks of MOF manufacturing techniques.

Synthesis method	Advantages	Disadvantages	Reference
Electrochemical synthesis	(1) Higher solid content can be yielded through continuous synthesis. (2) It has the potential for commercial production of MOFs.	(1) A constant electrical connection between the entire metallic pattern is required for MOF solid particle formation via anodic oxidation.	[68]
Ionothermal synthesis	(1) Regarded as an ecological synthesis technique. (2) The physicochemical characteristics of MOFs can be controlled by adjusting the chemical composition of the ionic liquid. (3) Stable performance at high temperature. (4) Without a reflux condenser, moderate-to-higher temperature synthesis can be performed.	(1) Even the tiniest minute impurity or residue can decrease the thermal stability of the ionic liquid.	[91]
Microwave-assisted synthesis	(1) Quick response time and high reaction rate. (2) The ability to regulate particle size. (3) Greater output with astounding phase purity and selectivity. (4) Utilization of small synthesis devices. (5) The synthesis machinery consumes less energy and produces fewer chemical pollutants.	(1) Adjusting irradiation strength for modification of reaction conditions is difficult. (2) The reaction duration and temperature are also restricted because different instruments cannot provide the same conditions consistently, ultimately hindering reproducibility. (3) Maintaining temperature gradient within the reaction vessel is challenging, potentially affecting MOF quality or reproducibility regarding mass synthesis.	[72]
Sonochemical synthesis	(1) Quick, sustainable, and cost-effective synthesis of nanocrystalline particles at room temperature.	(1) Although the process is performed at room temperature, there are instances where	[68]

(*continued on next page*)

Table 1 (*continued*)

Synthesis method	Advantages	Disadvantages	Reference
		controlling the synthesis temperature in the vicinity of the reactive mixture becomes difficult.	
Solvothermal synthesis	(1) Acquiring single crystals is simple. (2) Structural analysis can be accomplished using single-crystal X-ray diffraction.	(1) Precursors must be in solution form. (2) Regency dissolution requires either heat or strong reagents (acids, bases, organic solvents). (3) The solvent residue is produced in abundance. (4) Metal salts (nitrates/ chlorides) could be explosive or corrosive when present with organic materials. Reactions produce unwanted mineral compounds or acids.	[92]
Mechanochemical synthesis	The ball-milling synthesis is a solvent-free process or requires minimal co-solvent, which should avoid problems associated with solvents, such as poor solubility of metal salts and/or organic linkers.	(1) The formation of undesired by-products owing to competing reactions and the generation of structurally amorphous products.	[65]

uncompetitive with gasoline [95]. In addition, the storage of adequate amounts of fuel in automobiles presents another significant challenge in realizing an H_2 economy. Owing to the porous, crystalline, and large surface areas of MOFs, their potential use in H_2 storage has attracted considerable attention from the scientific community [96]. The H_2 adsorbed onto the pores of a MOF can be rapidly desorbed by increasing the pressure or temperature owing to the weakened van der Waals attraction. MOFs can offer high storage capacity on a mass basis, but volumetric H_2 storage densities are always lower compared to liquid H_2 or compressed gas storage. The volumetric H_2 storage densities of MOFs largely depend upon its interaction with H_2, packing of the materials, and its structure [97,98]. Physisorption enables fast kinetics with total reversibility, making it a secure and effective H_2 storage process.

Recently, adsorption using porous matrices has been investigated as a possible replacement for H_2 storage. The aforementioned storage objectives can be accomplished using MOFs. In 2003, a study provided the principle account of the H_2 storage potential of MOF-5 [97]. MOF-210 exhibits a total H_2 gravimetric uptake of 17.6 wt% at 80 bar and 77 K, making it stand out with the largest SSA and the highest H_2 storage capacity among other MOFs [99]. Although it has been estimated that the capacity for total gravimetric H_2 storage (at elevated pressure and a low temperature of 77 K) is proportional to the MOF-SSA, it is impossible to indefinitely increase these areas due to the complexity of creating MOFs with large SSAs. Alternatively, the addition of Li(I) and Mg(II) ions, metal nanoparticles, open metal sites (OMSs), and tiny holes can improve the ability of MOFs to store H_2 [100]. A maximum H_2 storage capacity by MOFs can be achieved through engineered morphology and proper crystal size distributions that can improve packing efficiency and volumetric H_2 gas packing density. A system model predicted 25 g/L H_2 in volumetric capacity in the compressed storage system (700 bar), exceeding the Department of Energy (DOE, US) objective for H_2 storage of 30 g/L (in 2020) using engineering crystal shape/size or bimodal distribution of cubic crystal size in tandem [101].

MOFs and H_2 molecules only interact through physisorption based on weak forces of physical interactions and isosteric heat. The most accurate measure of a MOF's ability to store H_2 is its interaction enthalpy, particularly its isosteric heat (Qst), which is released after binding H_2 to the adsorbent surface. Based on the Langmuir–Freundlich adsorption isotherm equation, it is possible to calculate Qst using the H_2 adsorption isotherms observed at two dissimilar temperatures, most commonly 77 K and 87 K. The Qst of most MOFs is in the range of 3–10 kJ/mol; however, it must be increased to 15–20 kJ/mol for use in real-world scenarios at room temperature. Coordinatively unsaturated metal centers and aromatic benzene rings are two techniques that have been shown to increase Qst; however, to date, exceptional H_2 storage capacities have only been attained from MOFs at low temperatures. Therefore, the DOE established a specific goal for onboard H_2 storage systems. With a highest delivery pressure of 100 atm and a working temperature of − 40 °C to 60 °C, the storage goals in terms of volumetric and gravimetric capacities are 40 g H_2/L and 5.5 wt% H_2, respectively [102]. These objectives require a system that includes valves, tanks, regulators, materials, pipes, a powerful cooling system, mounting brackets, insulation, and other balance-of-plant components [103,104].

Hydrogen storage hybrid materials, incorporating metals, complex materials, chemicals, biomass, and organic, inorganic, and AC, have been explored for H_2 gas storage [105–112]. MIL-100, MIL-101, MOF-5, MOF-74, MOF-177, and HKUST-1 are MOF-based materials used for H_2 storage. These materials exhibit exceptional H_2 storage and gas adsorption efficacy and distinctive crystal formation (Fig. 5 **(A)**).

Wong-Foy et al., [113] reported that MOF-5 exhibits 5 wt% of H_2 adsorption at 77 K and 90 bar. They also examined the effect of pressure on the adsorption of saturated H_2 at 77 K on different MOFs, covering a wide pressure range from 25 bar (MOF-74) to 80 bar (MOF-20). They found that with an increase in the SSA of MOF, the saturated H_2 storage also increased (Fig. 5 **(B)**). MOF-177 exhibited exceptional and consistent H_2 storage capacity, with volumetric and gravimetric capacities of approximately 32 g/L and 7.5 wt%, respectively [114]. In another example, UiO-66 exhibits a 4.2 wt% H_2 absorption at 77 K and 60 bar [115]. The potential for boosting the ability of MOFs to store H_2 has been investigated by creating coordinated unsaturated metal centers in MOF or doping alkali metal ions (Na(I), Mg(II), and Li(I)) in the MOFs framework. Lin et al., [116] used binuclear paddlewheel devices similar to those found in MOF-505 to investigate H_2 accumulation in various MOFs $[Cu_2(L)(H_2O)_2]$ at 78 K (L = quaterphenyl tetracarboxylate, terphenyl, and biphenyl). At 1 and 20 bar, the average H_2 storage quantities were 2.45 wt% and 4.62–6.07 wt%, respectively. Chen et al., developed a high surface area (7310 m^2/g) of ultra-porous MOFs (NU-1501-Al) with an H_2 storage capacity of 14 wt% (46.2 g/L) at 77 K and 100 bar [15].

Rosnes et al., conducted a similar investigation on H_2 adsorption on Mn_2(dobdc) and Cu_2(dobdc) [117]. They reported significant variations in the adsorption behavior of the two compounds, which were ascribed to variations in the interactions between the metal cations present in each framework and H_2. According to their experimental findings, Cu_2(dobdc) has the lowest Qst for H_2 adsorption of any M_2(dobdc) (M = Co, Ni, Mg, Mn, Fe, or Zn) material observed thus far, whereas Mn_2(dobdc) exhibits the second lowest Qst. Xiao et al., [118] investigated H_2 storage on HKUST-1 $[Cu_3(BTC)_2]$ Cu spots in HKUST-1 $[Cu_3(BTC)_2]$-unsaturated MOFs. Villajos et al., [119] reported the production of mixed metal M_2(dobdc) based on Co/Ni and its H_2 adsorption

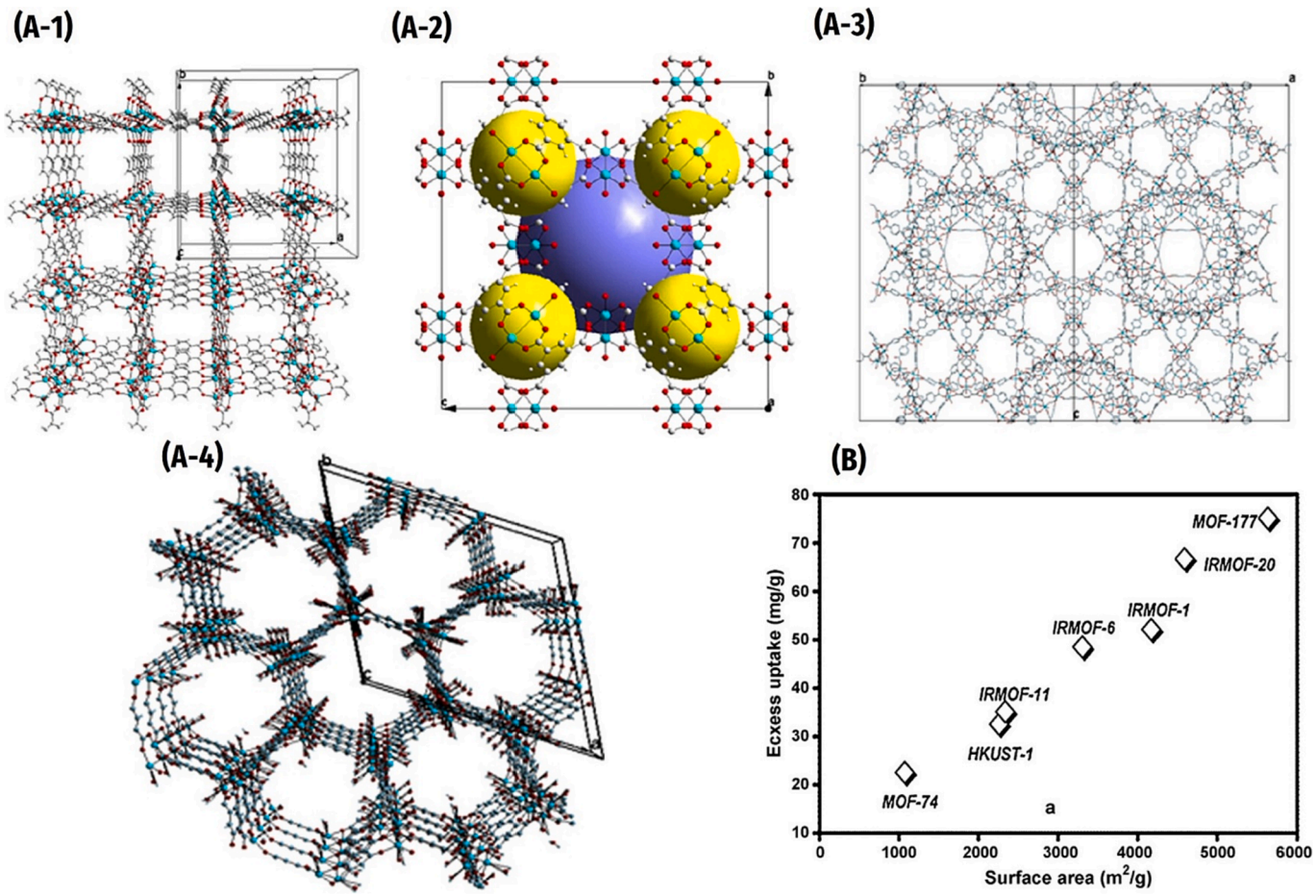

Fig. 5. (A) Crystal structures of different MOFs: (A-1) MOF-5; (A-2) HKUST-1 (cavities: yellow and blue spheres); (A-3) MIL-101; and (A-4) CPO-27-Co(Ni) (metals: cyan; oxygen: red; carbon: grey) or MOF-74 (adapted from [124] with permission from Elsevier License Number 5510051265267). (B) Plot of Langmuir surface area versus H_2 adsorption saturation at 77 K (Reprinted (adapted) with permission from [113]. Copyright (2006) American Chemical Society). (For interpretation of the references to colour in this figure legend, the reader is referred to the web version of this article.)

characteristics. Co_2(dobdc) enhanced the strength of the H_2 interaction and its potential for adsorption when a certain quantity of Ni was present. The maximum H_2 adsorption capacity was observed at 298 K and 77 K, along with Qst, when 40 % Co was isomorphically replaced. Researchers hypothesized that the retention of H_2 molecules with this type of porous material may be due to synergistic interconnections between the transition metal cations and smaller pores.

In another study, various Pd-doped MIL-101 materials with varied Pd concentrations were examined to determine their ability to store H_2 [120]. The H_2 absorption by Pd/MIL-101 was 3 wt% at 7.3 MPa and 298 K. The Pd-loaded MOF is 2.3-fold greater compared to pristine MOF. Additionally, Kim et al., [121] reported the creation of an amalgam of carbon black (CB)/Pt/MOF-5 by adding Pt nanoparticles to the perimeter of MOF-5 with (Pt) nanoparticles and covering it with hydrophobic microporous CB. At 298 K and 1 bar, H_2 uptake by CB/Pt/MOF-5 was 0.62 wt%, i.e., 41 % higher than pristine MOF-5 (0.44 wt%). Barman et al., developed MOF-649 and MOF-650 (two new MOFs) comprising inwardly polarized 2,6-azulenedicarboxylate (2,6-azd) [122]. At 77 K and 1 bar, the H_2 uptake by MOF-650 was 14.8 mg/g, and its preliminary Qst was 6.8 kJ/mol. According to a density functional theory study, the interactions for H_2 adsorption in MOF-650 were predominantly observed near the $Zn_4O(CO_2)_6$ units. MIL-100 and MIL-101 chromium carboxylates were produced using the same method as that used for the synthesis of MIL-53, but they had OMSs and larger specific surface areas (2800 m^2/g to 5900 m^2/g). Accordingly, they were expected to store more H_2 than MIL-53. MIL-53, MIL-100, and MIL-101 exhibit H_2 storage capacities of 3.28 wt% (26.5 bar) and 4.5 wt% (40 bar), respectively [123]. Table 2 briefly lists the H_2 storage capacities of various MOFs.

3.2. Methane storage

Methane is an abundant gas obtained from biogas (during the anaerobic digestion of organic waste) or natural sources [149]. It is a significant source of clean and renewable energy that can partially replace petroleum, coal, and other conventional energy sources [150]. Hydrocarbons with high hydrogen-to-carbon ratios, such as CH_4, are the main components of natural gas, which has a high octane rating (research octane number = 107) and emits the fewest CO_2 ions. The development of secure, practical, and affordable high-capacity CH_4 storage technologies for biogas/gas-powered vehicles is essential. For increasing CH_4 storage density, currently, supercritical fluid storage at room temperature and 200–300 bar pressure as compressed natural gas (CNG) or liquefied natural gas (LNG) is used to store in thick and heavy metal or expensive light carbon fiber tanks.

The selective adsorption found in gas–solid interactions can be utilized to hold CH_4 from biogas using porous adsorbents [151]. Researchers have studied zeolites, activated carbon, and activated carbon fibers as conventional porous materials for storage containers. The constrained surface areas and pore sizes of these materials result in an inadequate CH_4 storage capacity. MOFs can be used as promising strategies for adsorbed natural gas (ANG) for storage of CH_4 in a tank filled with porous material at modest pressure because of their substantial SSA and active sites [152,153]. However, the CH_4 storage density of MOFs (i.

Table 2
Overview of H_2 storage on various MOFs.

MOF Catalyst	Co-catalyst	Specific surface area (m^2/g)	Temp. (K)	Pressure (bar)	H_2 uptake/adsorption (wt.%)	Reference
Fe-BTT	N/A	2195	77	98	4.1	[125]
			298		1	
UIO-66	N/A	1413	77	100	4.6	[126]
			298		0.8	
UiO-66(Zr)	ZTC/PIM-1	1767–2433	77	1	1.22–1.87	[127]
NOTT-400,	N/A	1350	77	20	3.84	[128]
NOTT-401		1515			4.44	
ZIF-8,	Mg	118.45	623	40	–	[129]
ZIF-67,		33.572			5.3	
MOF-74		19.057			–	
Zr-MOF	rGO	1480	77	1	1.8	[130]
Zn (1,4-BDP)	N/A	1710	77	1	1.6	[131]
				40	4.7	
Zn (1,3-BDP)		820		1	1.6	
				40	2.1	
MOF-650	Mg/Ca-$B(OH)_2$	N/A	77	20	10	[132]
MOF-5	N/A	2136	77	20	5	[133]
CS-900,	N/A	1410	77	1	2	[134]
CS1000,		1629			2.2	
CB-900,		1526			–	
CB-1000		1825			–	
Cr-MIL-10,	LiCrw	2159	298	170	0.7	[135]
Fe-MIL- 100,		742			0.5	
Ni-MOF-74		595			–	
MOF-519a,	N/A	2400	77	1	2.13	[136]
			298		0.97	
MOF-520b		3290	77		1.94	
			298		1.27	
COMFA-ZTCethy	N/A	3341	77	1	2.75	[137]
COMFA-ZTCpy		3254			2.55	
COM-ZTCethy		2765			2.5	
COM-ZTCpy		2189			1.9	
PIM-1	PAF-1	681	77	100	2.6	[138]
PIM-1/PAF-1(0.225)		1197			4.08	
PIM-1/PAF-1(0.375)		1639			4.79	
PAF-1		3787			9.2	
MOF-5	N/A	3512	77	40	6.8	[139]
DUT-32	N/A	6411	77	53	7.8	[140]
				82	14.21	
MFM-132	N/A	2466	77	60	5.2	[141]
$SrCe_2(MoO_4)_4$	Ho^{3+}/Yb^{3+}	3.952	–	–	3.2	[142]
IRMOF-20	N/A	4590	77	70	6.7	[98]
MIL-101	5500			40	6.1	
CXFAETS	N/A	2841	77	20	6.3	[143]
MOF-177	Pt (0.43)	867	298	144	2.5	[144]
Mg-MOF-74	Ti	1206	298	1	1.29	[145]
she-MOF-1	N/A	4300	77	100	12.6	[146]
Mg-MOF-74	Ammonia borane	1206	393	–	11	[147]
Mg@SNU-90′c	N/A	1371	473	30	0.71	[148]
NU-1501-Al	N/A	7310	77	100	14	[15]

N/A, not available.

e., ANG) on a volumetric basis is relatively low compared to CNG or LNG. This may require larger storage tanks or systems to store the same amount of CH_4. Certain MOFs can store more than 170 cm^3/cm^3 of CH_4 (273.15 K; P = 101.325 kPa) [154].

Furthermore, the storage of CH_4 in MOF is cost-effective and secure, making it a new research focus because of high SSA, enhanced porosity, and structural diversity [155]. In 2012, the United States DOE set a volume storage capacity of 263 v/v or gravimetric storage capacity of 0.5 g/g (under STP conditions) for CH_4 in order to promote the development of ANG solutions. These targets are challenging to attain with most of the porous materials, but MOFs have been pointed as promissory materials to approach them under certain conditions. As an illustration, Fig. 6 (**A** and **B**) depicts the ideal crystallographic structures of MOFs for meeting the DOE 2012 volumetric and gravimetric CH_4 storage goals.

Kondo et al., [156] created a three-dimensional (3D) structure by controlling the voids of $[M_2(4,4'\text{-bpy})_3(NO_3)_4H_2O]_n$(M = Co, Ni, or Zn). At 298 K and pressures between 1 and 36 bar, they conducted an initial CH_4 adsorption test. In the IRMOF series, Eddaoudi et al., [20] created a stable MOF-5 ($Zn_4O(BDC)_3$) and utilized for CH_4 uptake studies. At a pressure of 36 bar and ambient temperature, this series exhibited a good propensity to absorb CH_4. The CH_4 uptakes of six MOFs, PCN-14, UTSA-20, HKUST-1, Ni_2(dobdc), NU-111, and NU-125, were investigated [157]. According to these findings, the volumetric absorption of CH_4 by HKUST-1 was greater than that of other MOFs at room temperature. The total CH_4 uptake on HKUST-1 was in line with the latest DOE volumetric goal, measuring approximately 230 cm^3/cm^3 and 270 cm^3/cm^3 at 35 and 65 bar, respectively. Hulvey et al., [158] thoroughly analyzed the underlying mechanisms of CH_4 uptake by combining computational and experimental data. The data for CH_4 adsorption onto HKUST-1 and the volumetric adsorption capacity were not significantly altered when the metal center was changed, as demonstrated by its isostructural analog $Cr_3(BTC)_2$. Their data on in situ neutron diffraction of granules revealed that the adsorption sites were mainly located at the small octahedral cage of the structure and its surroundings. In a separate study, Liu et al., [142] reported the strong CH_4 adsorption capability of MAF-38, which is an OMS-free MOF. According to their research, the CH_4 adsorption

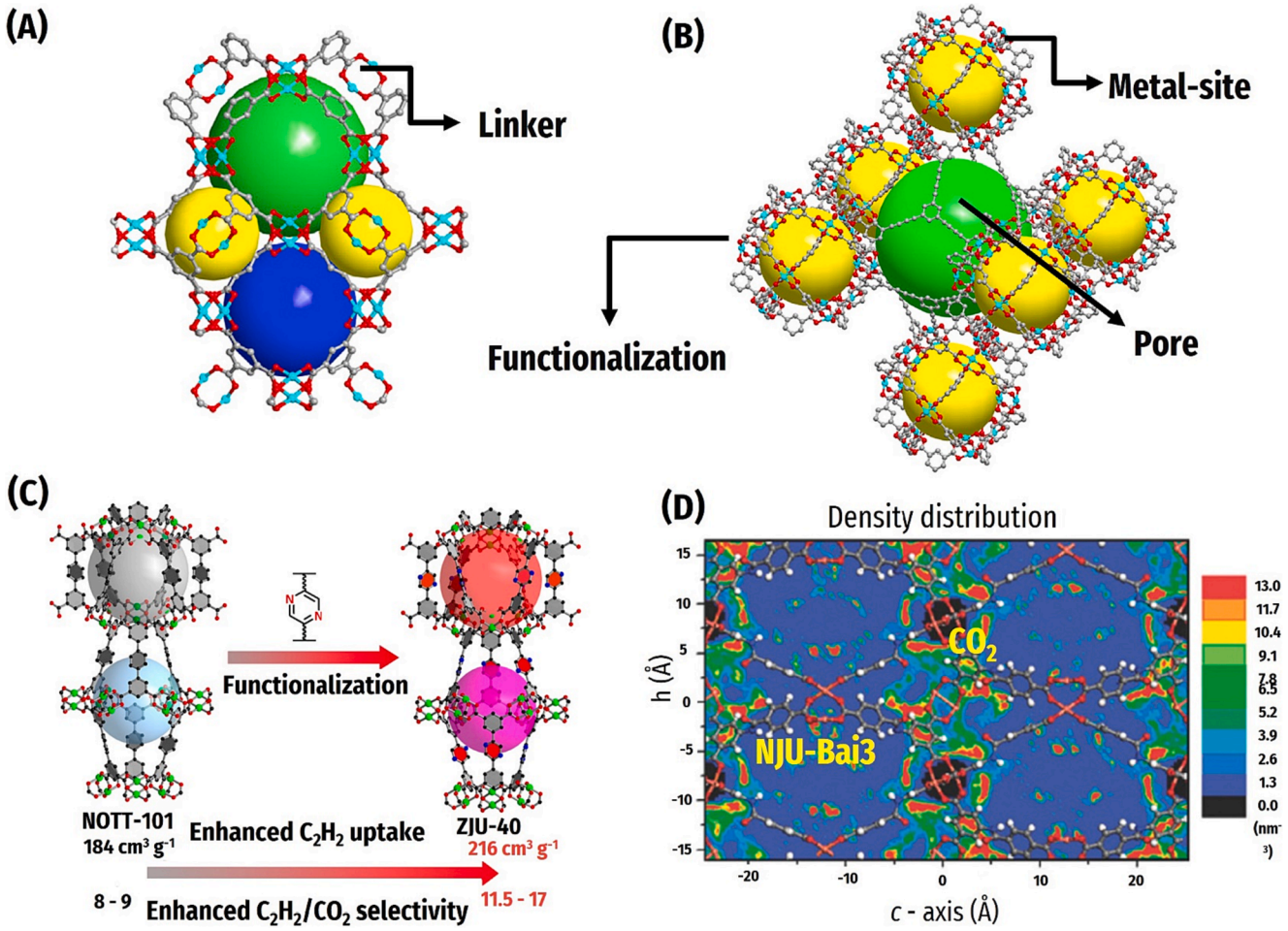

Fig. 6. (A) and (B) are hypothetical X-ray crystal structures of ideal MOFs to meet gravimetric and volumetric CH_4 storage goals for 2012 set by the DOE (Reprinted (adapted) from [153] with permission Elsevier Nature License Number 5671690247426): The 3D representation of HKUST-1 (A) reveals that it possesses some characteristics that can be helpful in achieving the volumetric goal, with relatively small cavity diameter (LCD) and high density while NU-111 (B) has relatively large LCD and reduced density, which could be helpful in achieving the gravimetric goal of 0.5 g CH_4/g of MOFs. (C) Single-crystal structures of NOTT-101 and ZJU-40 showing the functionalization of the nanocages within ZJU-40 by pyrazine groups, which allowed for an enhanced C_2H_2 uptake of selectivity in comparison with NOTT-101 (Reprinted (adapted) with permission from [191] Copyright (2016) American Chemical Society). (D). The density distribution of CO_2 molecules perpendicular to the NJU-Bai3 b-axis at 1 atm and 273 K (Reprinted (adapted)from [210] with permission from Copyright 2012 Royal Society of Chemistry).

values of MAF-38 were 76, 226, 263, and 273 cm^3/cm^3 at 5, 35, 65, and 80 bar, respectively. Among the upper limit pressures of 35, 65, and 80 bar and a lower limit pressure of 5 bar, working capabilities of 150, 187, and 197 cm^3/cm^3 were achieved, respectively. In the smaller cage, the apex of the carboxylate group of the BTC3 ligand was used as the secondary adsorption site while the quadrangular window crossed the large cage as the ternary adsorption site. The large cages had a weaker pore-confinement effect and contained ternary adsorption sites.

Barin et al., [159] synthesized NU-138, NU-139, and NU-140, which are equivalent to (3,24)- linked MOFs. NU-140 showed a gravimetric CH_4 absorption of 0.34 g/g at 65 bar and 298 K and had an operating capacity (65 bar to 5 bar) of 170 cm^3/cm^3. Moreover, the early Qst of the CH_4 uptake was approximately 14 kJ/mol. To increase the working capacity of CH_4, Mason et al., [160] reported a novel technique that used flexible MOFs as adsorbents. These materials undergo phase changes in response to the exoteric stimuli. A novel MOF material (NU-1501-Al) fabricated and designed by simulation with a high SSA of 7310 m^2/g could be able to store 0.66 g/g of CH_4, surpassing the US DOE target of 0.5 g/g [15].

Based on the gate-opening behavior, $[Co(bdp)]_n$(bdp^{2-}=1,4-benzenedipyrazolate) can store CH_4 at a high operating capacity of 197 cm^3/cm^3 at standard temperature and pressure (STP). Although MOF's gravimetric and volumetric storage or working capacities are better than those of other porous materials for CH_4 storage, providing the required adsorbents for currently widely used adsorbed natural gas technologies remains challenging. Seki and Mori [161] investigated using MOFs in CH_4 storage. With 1891 m^2/g SSA, 0.70 cm^3/g pore volume, and 0.87 g/cm^3 solid density, $Cu_2(bdc)_2(dabco)$ is isostructural with a Cu porous MOF [162]. By extending the ligand from styrene dicarboxylate ligand to benzene dicarboxylate, the pore capacity increases to 1.26 cm^3/g, and the SSA significantly increases to 3265 m^2/g [161]. Table 3 lists the main MOFs used for storing CH_4.

3.3. Acetylene storage

In addition to its use as a fuel for welding technologies, C_2H_2 has long been a crucial chemical feedstock in modern industries. It is frequently used in the production of chemicals and electrical materials [185]. Owing to its explosive nature when compacted at pressures higher than 2 bar at ambient temperature, C_2H_2 is challenging to move and store safely. Currently, acetone and porous materials are used to store C_2H_2 in specialized cylinders. However, this method is expensive and produces acetone pollutants. Thus, developing new methods to secure C_2H_2 is difficult. Owing to their high potential for gas storage, porous MOFs have emerged as promising solutions to the issues mentioned above. MOFs are useful for C_2H_2 storage at moderate pressures, resulting in

Table 3
CH_4 uptake capability of MOFs under specific conditions.

Materials	BET specific surface area (m^2/g)	Vp (cm^3/g)	CH_4 total uptake				CH_4 excess uptake				References
			mg/g	cm^3/cm^3	T(K)	P(bar)	mg/g	cm^3/cm^3	T(K)	P(bar)	
HKUST-1	1850	0.78	216	267	298	65	178	220	298	65	[163]
Al-soc-MOF-1	5590	2.30	410	197	298	65	–	–	–	–	[164]
monoHKUST-1	1193	0.52	177	267	298	69	151	227	298	69	[165]
LIFM-82	1624	0.71	210	271	298	80	–	–	–	–	[166]
MAF-38	2022	–	247	263	298	65	–	–	–	–	[167]
MFM-115a	3394	1.38	278	238	298	65	–	–	–	–	[168]
MIL-53(Al)	1100	0.59	≥96	155	304	35	–	–	–	–	[169]
MIL-53(Cr)	1100	0.56	≥96	165	304	35	–	–	–	–	[169]
MIL-10[p0(Cr)	1900	1.10	152	150	303	60	–	–	–	–	[170]
MIL-101(Cr)	4230	2.15	217.6	135	303	60	–	–	–	–	[171]
MOF-5	3800	1.55	–	132	298	35	–	300	60	–	[97]
MOF-177	4700	1.83	–	208	298	80	–	–	–	–	[172]
MOF-200	4530	3.59	–	–	–	–	234	–	298	80	[99]
MOF-210	6240	3.6	–	–	–	–	264	–	298	80	[99]
MOF-519	2400	0.928	190	259	298	65	–	–	–	–	[173]
MOF-905	3490	1.34	270	206	298	65	–	–	–	–	[172]
MOF-905-Naph	3640	1.39	–	211	298	80	–	–	–	–	[172]
MOF-905-Me2	3310	1.25	–	217	298	80	–	–	–	–	[172]
MOF-905-NO2	3380	1.29	–	203	298	80	–	–	–	–	[172]
MOF-950	3440	1.30	–	209	298	80	–	–	–	–	[172]
Ni-MOF-74	1350	0.51	148	251	298	65	125	210	298	65	[174]
NJU-Bai43	3090	1.22	283	254	298	65	–	–	–	–	[175]
NOTT-101a	2805	1.08	247	237	298	65	–	–	–	–	[176]
NU-111	4930	2.09	360	205	298	65	262	150	298	65	[177]
NU-125	3120	1.29	287	232	298	65	223	181	298	65	[157]
NU-135	2600	1.02	219	230	298	65	–	–	–	–	[178]
NU-1500-Al	3560	1.46	290	200	296	65	–	–	–	–	[179]
NU-1501-Al	7310	2.91	410	163	296	65	–	–	–	–	[179]
NU-1501-Fe	7140	2.90	400	168	296	65	–	–	–	–	[179]
PCN-14	2000	0.85	197	230	298	65	157	183	298	65	[180]
PCN-66	4000	1.63	–	187	398	65	177.6	110	298	35	[181]
PCN-68	5109	2.13	–	187	298	65	185.6	99	298	35	[182]
UTSA-20	1620	0.66	181	230	298	65	150	191	298	65	[157]
UTSA-76	2820	1.09	263	257	298	65	–	–	–	–	[183]
UTSA-110a	3241	1.263	288	241	298	65	–	–	–	–	[176]
ZIF-8	–	–	~85	–	300	36	70		300	36	[184]
ZJU-70	1791	0.676	–	211	298	65	–	–	–	–	[181]
NU-1501-Al	7310	–	660	262	270	100	–	–	–	–	[15]

effective storage with minimal energy. MOFs, as a novel class of solid permeable substances, facilitate energy-efficient C_2H_2 storage at reduced pressures. Multiple research organizations have been involved in MOF projects and have made remarkable progress [186].

Matsuda et al., [187] studied C_2H_2 storage on $Cu_2(pzdc)_2(pyz)$ (pzdc = pyrazine-2,3-dicarboxylate, pyz = pyrazine). Using the maximum entropy method (MEM) or Rietveld analysis, the crystal structure of $Cu_2(pzdc)_2(pyz)$ was identified after being loaded with C_2H_2. This analysis showed that C_2H_2 was spread on the unsaturated carboxyl oxygen atoms via H_2 bonding. The substance demonstrated excellent attraction for C_2H_2, with maximal entropy and adsorption capacity of 42.5 kJ/mol and 42 cm^3/g, respectively. The following approaches have been efficient in improving the C_2H_2 framework interactions and attaining large C_2H_2 storage capacities in MOFs: (1) optimizing the pore area and size, (2) including open metal locations, and (3) functionalizing organic linkers to create specific C_2H_2 molecule binding sites.

Xiang et al., [188] evaluated the C_2H_2 storage capabilities of six MOFs with different shapes and porosities (MIL-53, MOF-5, ZIF-8, HKUST-1, MOF-505, MOF-508, MIL-53, and MOF-8). MOFs with exposed metal sites, such as HKUST-1, exhibit the highest C_2H_2 capability of 201 cm^3/g at 295 K and 1 atm. According to the first-principles calculations and high-resolution neutron diffraction, HKUST-1 has strong binding locations at the preferred adsorption spots and OMSs. Hence, powerful interactions of the C_2H_2 molecules cause a high gas storage capacity by HKUST-1. In a related study, Xiang et al., [189] examined the uptake of C_2H_2 by M−MOF−74 with more accessible metal sites (M = Mn(II), Co(II), Zn(II), and Mg(II)). The most effective volumetric C_2H_2 adsorption of 230 cm^3/cm^3 was achieved using Co-MOF-74 at 295 K and 1.01 bar. This is due to the strong interfaces of Co-open MOF-74 Co sites and C_2H_2 molecules.

Rao et al., [190] substituted the benzene ring in the middle of a 1,4-benzenediisophthalate ligand with a functional N-site-containing pyridine ring in NOTT-101 to synthesize ZJU-5. According to their studies, ZJU-5 exhibited a significantly high C_2H_2 uptake density of 193 cm^3/g at 1 bar and 298 K, with a volume that was 9 cm^3/g larger than NOTT-101 (184 cm^3/g). This high C_2H_2 uptake density of ZJU-5 was due to the Lewis base sites of the pyridine ring, which improved contact with the acidic H_2 atoms of C_2H_2 by H_2 bonding. In a similar approach, as represented in Fig. 6C, ZJUT-40 MOF was created by Wen et al., [191], whereas pyrazine was used instead of benzene to increase the nitrogen density. Under the same conditions of 1 bar and 298 K, ZJUT-40 exhibited a higher C_2H_2 uptake density of 216 cm^3/g and higher C_2H_2/CO_2 selectivity than NOTT-101 (Fig. 6C). Such improved performance was related to stronger H_2 bonding between the nitrogen sites and the C_2H_2 molecules on ZJUT-40 in comparison with NOTT-101.

Moreau et al., [192] synthesized a Cu-based MOF, MFM-188, which contains CO and NH-bifunctional sites in a 5,5′,5″,5‴-([1,1-biphenyl]-3,3′,5,5″-tetracarbonyl) Tetrakis (azanediyl) tetra isophthalic acid. Despite its decent porosity (1.12 cm^3/g) and high surface area (2568 m^2/g), MFM-188 exhibited a very high C_2H_2 adsorption of 232 cm^3/g at 1.0 bar and 295 K. C_2H_2 molecules associated with the bi-functional C = O and NH sites of the amide groups were convincingly demonstrated using inelastic neutron scattering experiments and neutron diffraction. Their research demonstrated that vacant metal locations, amide groups, and proper pore geometry were responsible for high C_2H_2 uptake. Zhang et al., [193] studied the development of MOF-505, a NJU-Bai 17 amide-

modified material. Using first-principles calculations and the Monte Carlo method, it was determined that the amide groups were the primary C_2H_2 adsorption sites (in addition to the exposed metal sites for NJU-Bai 17) at 1 bar and 296 K, indicating that the amide groups and C_2H_2 formed H-bonds. This resulted in a C_2H_2 uptake of up to 222.4 cm^3/g.

FJI-H8 is a novel MOF with appropriate pore size and OMSs. In contrast to Co-MOF-74 and HKUST-1 at 1 atm and 295 K, FJI-H8 exhibited record-breaking gravimetric C_2H_2 adsorption of 224 cm^3/g and an equivalent adsorption intake of 196 cm^3/cm^3 by Pang et al., [194]. Traditional Monte Carlo calculations showed that C_2H_2 adsorption on FJI-H8 depended more on the pore space than on the OMSs. Additionally, FJI-H8 exhibited a lower temperature-dependent change in C_2H_2 adsorption capacity (2.2 cm^3/g) relative to other previously described MOFs. The C_2H_2 absorption of FJI-H8 decreased by only 3.8 % after five adsorption–desorption tests, showing good repeatability. Owing to its superior gravimetric and volumetric adsorption capacities, negligible C_2H_2 adsorption reduction rate, and high reusability, FJI-H8 is considered a superior adsorbent for practical applicability. Table 4 summarizes the C_2H_2 uptake capabilities using the developed MOFs.

3.4. Carbon dioxide storage

Global warming and anthropogenic climate change are caused by drastically elevated concentrations of CO_2, a primary GHG in the atmosphere. Consequently, significant efforts have been made in recent years to reduce CO_2 pollution. To tackle such issues, various CO_2 capture and sequestration processes have been practiced. MOFs have been regarded as a promising method for capturing and separating CO_2 [201,202]. CO_2 removal from biogas resources (e.g., landfills or anaerobic digesters) is required to enrich CH_4 for its utilization as a fuel. Furthermore, the recovered CO_2 from biogas or industrial sources can be valorized into various useful chemicals [7]. For instance, CO_2 from different sources can be turned into CH_4 in the presence of H_2 using power-to-gas technology using biological or chemical catalysts. Biological H_2 methanation utilizes methanogenic microbes in mild temperature (37 to 65 °C) and pressure (1 to 15 bars) ranges, but low H_2 solubility and mass transfer limitation in the fermentation medium result in a long operating time and large bioreactor volumes [203]. The CO_2 present in synthetic gas (obtained from coal or biomass combustion from power plants) can be converted to CH_4 using a catalytic methanation reactor [204]. Additionally, separated CO_2 can be utilized in industry (e.g., carbonation of bauxite residue), agriculture (e.g., nutrients for plant growth), energy generation (e.g., during oil and gas recovery), and the production of useful chemicals through carbon sequestration and reduction [205]. High-purity (≥95.5 %) CO_2 is required to be injected into a pipeline for carbon capture and storage applications [206,207].

The selective adsorption of CO_2 by porous solid-state compounds is reversible and consumes less energy. MOFs have attracted the most interest among solid-state porous materials because of their extraordinary porosity, strong adsorption capacity, enhanced selectivity through strong functional tenability, and high crystallinity for simple structural characterization. For efficient carbon storage, CO_2 is generally collected first because it typically produces more powerful intermolecular connections with OMSs and provides additional MOF features relative to H_2 storage [208]. Several techniques have been used to enhance the CO_2 capture potential of MOFs, such as the production of high-density OMSs, attachment of functional polar groups to unsaturated metal centers or organic backbones, infusion of metal ions, and constriction of internal pores.

Currently, MOF-200 and MOF-210 have superior adsorption densities for all porous materials, retaining 71 wt% of CO_2 at 50 bar and 25 °C, respectively [99]. The capture of flue gas CO_2 is more pertinent to the CO_2 storage capability of MOFs at atmospheric pressure, as affected by the significant adsorbent CO_2 interconnections and surface area. The Mg-MOF-74 structure at 1 bar and 298 K is currently the MOF with the most remarkable performance at atmospheric pressure. It has open Mg^{2+} sites and large (35.2 wt%) CO_2 storage capability [209]. Another study used a (3,4,6)-linked agw-MOF with an L4 linker built into an amide and two distinct types of secondary building units to produce an extremely porous material (NJU-Bai3) with a 2690 m^2/g specific surface area [210]. The amide-inserted MOF (NJU-Bai3) is indicated as one of the excellent MOFs for CO_2 capture due to its better storage and selectivity for CO_2. Three different types of cages are well packed in the overall structure, and each of the cavities is directly exposed to amide units. The amide groups in NJU-Bai3 and Cu(II) metal sites for CO_2 molecule adsorption in the framework [211]. As predicted by the ideal adsorbed solution theory (used to evaluate the selectivity of the MOF material for gas adsorption), NJU-Bai3 exhibited a high CO_2 adsorption of 6.21 mmol/g at 1 bar and 273 K. Moreover, it exhibited good selectivity for CO_2 over N_2 (25–61) at elevated pressures (20 bar) and over CH_4 (14–47) in the pressure range of 0–20 bar [210]. First-principles computations revealed amide groups with dense decoration, specifically the AC@OA groups in NJU-Bai3, which significantly increased the attraction between the NJU-Bai3 structure and CO_2, leading to strong selectivity and CO_2 uptake. Accordingly, it appears to outperform other MOFs, such as MOF-210, MOF-177, and NU-100, which have high CO_2 uptake but poor selectivity [99]. Fig. 6 **(D)** illustrates the density distribution of the center-of-mass of CO_2 molecules perpendicular to the b-axis of NJU-Bai3 [210,212].

In another study, an elegant txt-type MOF stage was purposefully

Table 4
C_2H_2 uptake potential of a few samples of MOFs at room temperature and 1 bar ().

MOFs	BET specific surface area (m^2/g)	Temperature (K)	Gravimetric uptake (cm^3/g)	Volumetric uptake (cm^3/cm^3)	Reference
HKUST-1	1780	295	201	177	[195]
MOF-505	1694	295	148	137	[195]
Co-MOF-74	1056	295	197	230	[189]
Mn-MOF-74	1102	295	168	182	[189]
Mg-MOF-74	1332	295	184	167	[189]
NOTT-101	2316	296	184	N.A.	[196]
SIFSIX-1-Cu	1178	298	190	164	[197]
ZJU-5	2823	298	193	N.A.	[190]
ZJU-8	2501	298	195	134	[198]
ZJU-40	2858	298	216	N.A.	[191]
NJU-Bai 17	2423	296	222.4	176	[193]
FJI-H8	2025	295	224	196	[194]
MFM-188	2568	295	232	N.A.	[192]
MAF-2	N.A.	298	70	82	[199]
$[Cd_3(vtz)_6]$	N.A.	298	50	77	[200]

N.A., not available.
adapted from [163]

built with many pores or an SSA of 5142 m^2/g for the mesoporous substance NJU-Bai23 [213]. The study showed that linkers for the amide groups in pyridine-based diisophthalates are easily incorporated. Owing to the presence of amide groups with a large density, the NJUBai21, 22, and 23 txt-MOFs exhibited comparable selectivity for CO_2/CH_4 and CO_2/N_2, as well as relatively strong CO_2 uptake at high pressures compared to NJU-Bai20 (without amide groups). Fig. 7 shows the adsorption of CO_2 onto NJU-Bai20 to 23, the corresponding heat of adsorption, and the selectivity of these txt-MOFs for CO_2/CH_4 and CO_2/N_2 [213]. The amide bond spacer, present in NJU-Bai21, shows high adsorption capacity for CO_2 (206 cm^3/g to 115 cm^3/g at 0 °C to 25 °C and 1 bar) compared to triple bond spacer NJU-Bai20 (136 cm^3/g and 68 cm^3/g at 0 °C to 25 °C, respectively and 1 bar of pressure) (Fig. 7 a and b). Similarly, a sharp increase in CO_2 adsorption enthalpy is reflected in NJU-Bai21 (25.9 kJ/mol) compared to -Bai20 (22.2 kJ/mol) (Fig. 7 c). Despite ligand expansion, the high selectivity trend of NJU-Bai21 > -Bai22 > -Bai23 is observed as 93, 81, and 72 for the binary gas mixture (15:85 of CO_2 and N_2) and 7.8, 6.7, and 5.8 for 1:1 gas mixture of CO_2 and CH_4 (Fig. 7 d). Furthermore, a higher CO_2 storage amount was observed in NJU-Bai21, specifically in the pressure range of 0 to 10 bar, compared to -Bai20 due to the presence of amide groups, which would promote CO_2 uptake (Fig. 7 e). Therefore, considering the simplicity of incorporating amide groups, it is an appropriate strategy to obtain MOFs superior to NJU-Bai20 for CO_2 storage applications. Qasem et al., examined CO_2 storage using MOF-177 and MOF-5 via adsorption [214]. They noted that MOF-177 and MOF-5 exhibit high storage pressures and sizable CO_2 adsorption capacities. The charging process was completed within the first 500 s for each of the examined adsorptive storage pressures (5, 10, 20, 30, 40, and 50 bar), followed by a cooling process lasting approximately 2500 s.

3.5. Gas storage mechanisms of MOFs

3.5.1. Hydrogen gas storage mechanisms

The most well-known approach for storing H_2 is the spillover mechanism, which is represented in Fig. 8(A). In the mechanism, the atomic H migrates from the dissociated H_2 molecules to the supportive materials. This mechanism operates at ambient temperatures and performs better when metal-based catalysts are used. To enhance the H_2 storage capacity, H_2 molecules move from the catalyst to the substrate [215]. Fig. 8 **(A)** shows the movement of H_2 through the MOF by spillover. As it may be seen in Fig. 8 **(A)**, H_2 migration in storage by spillover occurs through three primary reaction stages: (1) H_2 molecules chemisorption and dissociation on a catalyst made of a transitional metal; (2) spillover of H atoms from the catalyst to the substrate; and (3) H atom diffusion on the substrate surface. Then, the subsequent release may occur by (4) desorption of H_2 resulting from the recombination of two chemisorbed H atoms; (5) desorption of a chemisorbed H atom by a gas-phase H atom through Eley-Rideal recombination; (6) reverse spillover of H from the substrate to the catalyst; and (7) recombination of two H atoms resulting into a H_2 molecule. The energy required for H_2 chemisorption is 0.8–1.8 eV; thus, the catalyst in stage (1) must possess a remarkable ability to adsorb H_2. The H_2 particle in (2) must cross a sizable energy barrier of 2.45–3.2 eV to move toward support. The C–H bond is significantly strong, and the energy barrier on the MOF surface ranges from 1.05 eV to 2.16 eV; therefore, it is challenging for the H_2

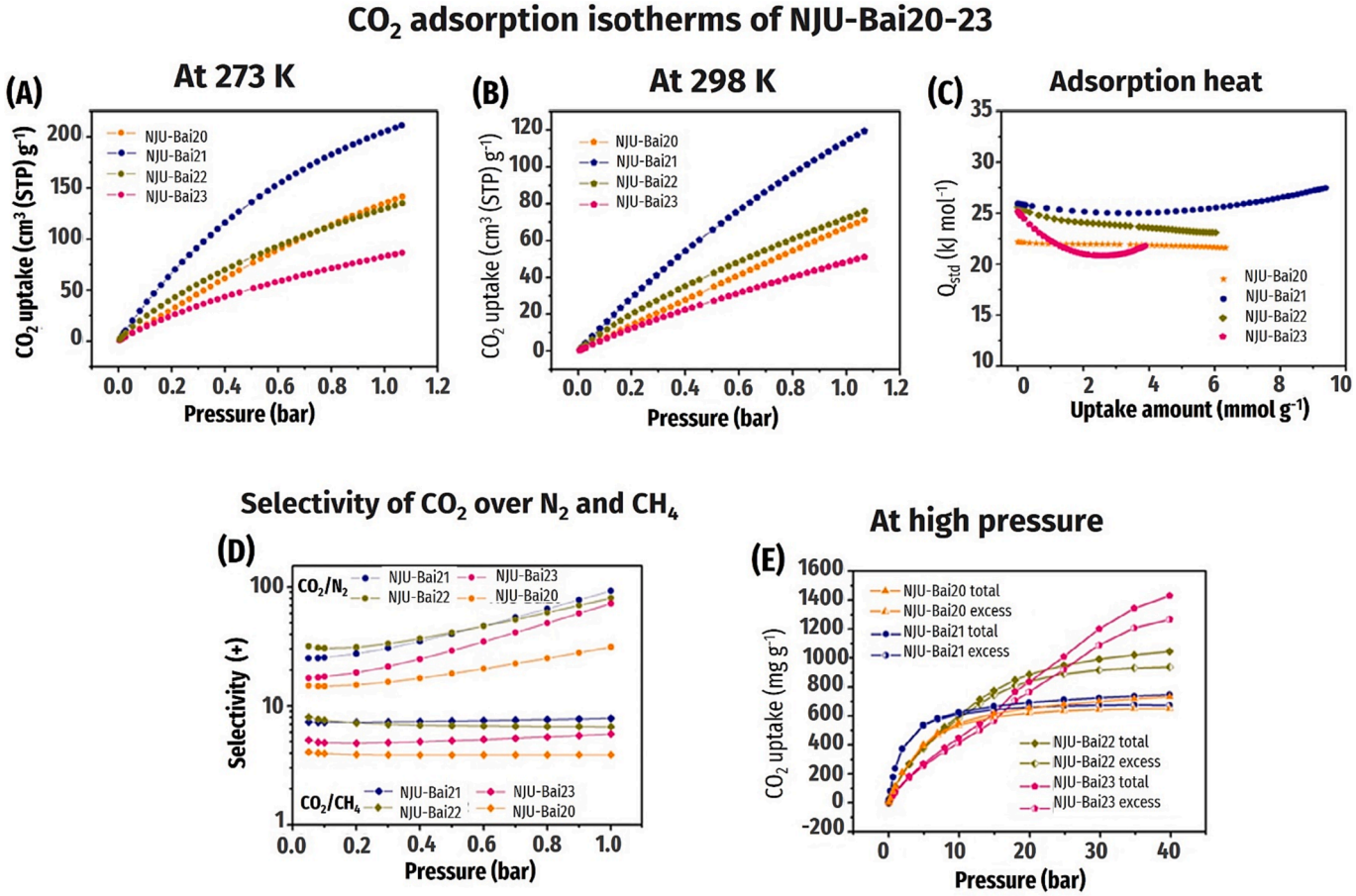

Fig. 7. CO_2 adsorption isotherms for NJU-Bai20-23 at (A) 273 K and (B) 298 K. (C) Heat of CO_2 adsorption for NJU-Bai20-23. (D) NJU-Bai20-23 selectivity for CO_2 over N_2 and CH_4. (E) CO_2 adsorption isotherms for NJU-Bai20-23 under high pressure (Reprinted (adapted) from [213] with permission from John Wiley and Sons License Number 5662890045515).

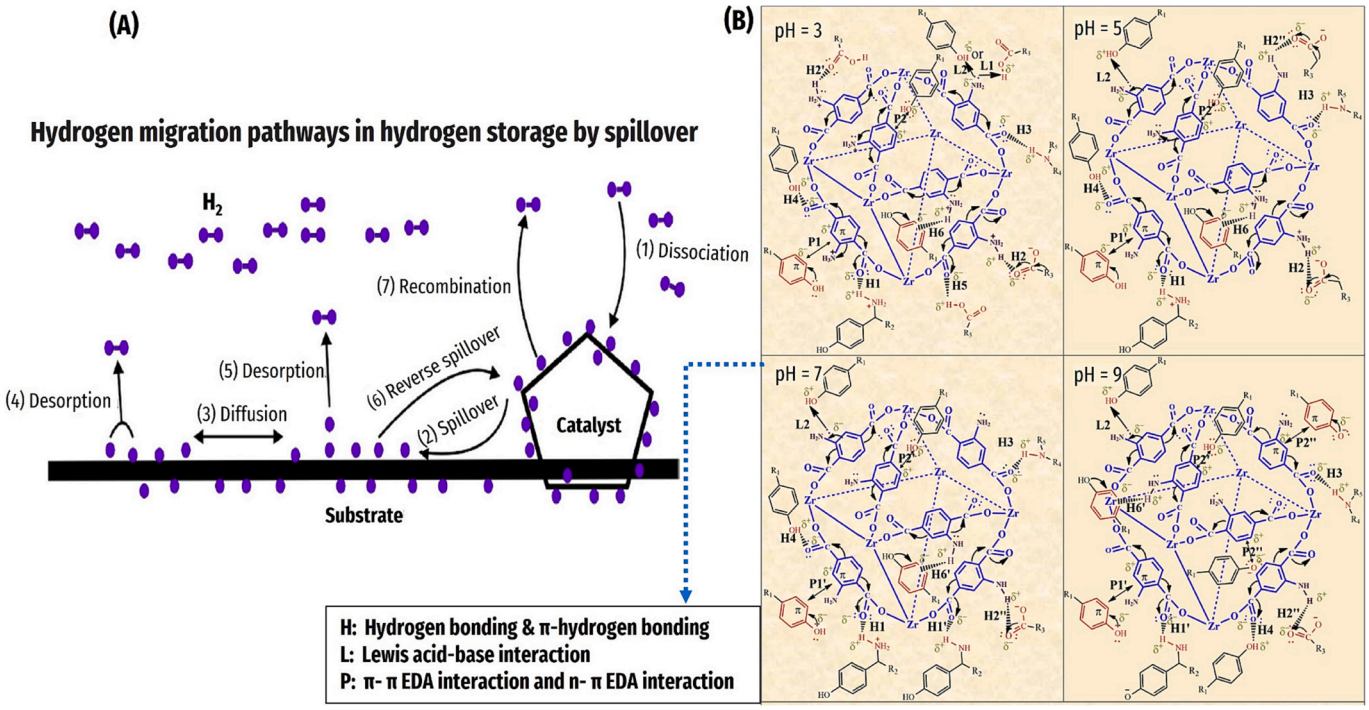

Fig. 8. (A) Spillover diagram of the H-migration routes in the storage of H_2 (Reprinted (adapted) from [222] with permission from Elsevier License Number 5510080993030). (B) Mechanisms for the adsorption of AMX on UiO-66-NH_2 at different pH values (Reprinted (adapted) from [219] with permission from Elsevier License Number 5510081295204).

atoms to diffuse through the substrate in stage (3).

Ensafi et al., [216] reported the use of stacked double hydroxides, reduced graphene oxide (rGO), and Al-M constructed using H_2 sorbents. The spillover impact was evaluated using Pd#Al-M/LDH-rGO-ophenylenediamine. Al was used as the chemical hydride, M (Ni, Cu, and Zn) was used as the metal hydride, o-phenylenediamine was used to improve the kinetics of H_2 desorption/adsorption, and rGO was used because of its sp^2 hybrid carbon acceptors with large surface areas [217]. At the site of the spillover material catalyst, H_2 molecules dissociate. These molecules are then transferred to the receptors with large surface areas. There are two steps in the H_2 spillover process: first, the highly active hydrogen was generated by dissociating H_2 at a metal surface. Secondly, through some tunnels or metal-support contacts, the dissociated hydrogen enters the substrate molecule. In addition to acting as reactants in the related catalytic reaction, the dissociated hydrogen can also cause phase transitions or defects in the support, which can modify the energy band and enhance catalytic activity [218].

UiO-66-NH_2 performed better in terms of H_2 absorption because of the interaction between amoxicillin (AMX) and different Zr-MOFs. The adsorption interactions of AMX and UiO-66 were pH-dependent and varied at high pH due to the deprotonation of their functional groups. Lewis acid-base interaction was the primary adsorption impulse, as demonstrated by the clear FT-IR/XPS spectrum shift [219]. In addition, H-bond interaction and π-π/n-π EDA (electron-donator-acceptor) interaction were also considered for H_2 adsorption. The percentage of the amine group in UiO-66 mostly interacted with the phenolic hydroxyl group of AMX, determining the strength of the Lewis acid-base interaction. There were six different types of π-π/n-π EDA contacts and thirteen different types of hydrogen/π-hydrogen bonding interactions because of the variations in the charge distribution of functional groups. Furthermore, the adsorption of AMX was further facilitated by molecule attraction and electrostatic interaction. In summary, a deeper understanding of adsorption mechanisms and more effective utilization of functional adsorbents may be achieved by the examination of interactions between functional groups [219].

The mechanisms by which AMX may adsorbed onto UiO-66-NH2 at different pH values, namely pH 3, pH 5, pH 7, and pH 9, are shown in Fig. 8 (B) [219]. These mechanisms involve (i) H_2 and p-H_2 bonding, (ii) contact with the Lewis acid–base system, (iii) electrostatic interactions, and (iv) interactions between p-p and n-p electron donor–acceptors. In UiO-66-NH_2, the (i) benzene ring is the p-electron donor and the electron-removal substituent. The H_2 donors and acceptors are AMX and UiO- 66-NH_2 in (ii). With increasing pH, the interactions in (iii) between the MOF and the target pollutants increased [220]. The Lewis acid and base are oxygen-containing groups (e.g., carboxyl and phenol hydroxyl) on AMX and —NH_2 group onto molecule UiO- 66-NH_2, respectively. The main adsorption mechanism is purely pH-dependent via Lewis acid-base interactions [219,221].

3.5.2. *Methane gas storage mechanisms*

Although physical adsorption comprises most storage mechanisms of MOFs, the surface area significantly affects how well a gas adheres to the MOF. After CH_4 adsorption, Zhou [223] noticed comparatively homogeneous pore coverage as the van der Waals forces engaged the MOF surface when CH_4 molecules were present. However, one feature distinguishing MOF from other porous adsorbent materials is their OMSs, which makes it possible for the MOF to tightly bond to CH_4 molecules via Coulombic interactions [164].

Lin et al., [167] clarified the CH_4 adsorption process of MAF-38 using DFT and grand canonical Monte Carlo (GC-MC) simulations. A solvothermal process was applied to produce an OMS-free MOF, MAF-38, using Hpypz, Zn(II), and H3btc containing polyhedral cages of different sizes. The large cage comprised six $Zn_2py_2pz_2(RCOO)_2$ units, six isophthalate moieties from six btc, two complete btc, and 12 pypz ligands. The small cage was encircled by six $Zn_2py_2pz_2(RCOO)_2$ units, six pypz ligands, and two btc ligands, as shown in Fig. 9 **(A and B)**. The six open trigonal sides of the small and large cages result in a 3D hierarchical pore structure. MAF-38 had a total CH_4 adsorption density of 226 cm^3 at 35 bar, 65 bar, and 80 bar. Assuming a delivery pressure of 5 bar, the operating capacities of CH_4 at 35, 65, and 80 bar were 150, 187, and 197 cm^3/(STP) cm^3 (Fig. 9 **(C)**), respectively. The primary CH_4 adsorption site (as identified by computer simulations) is situated in the

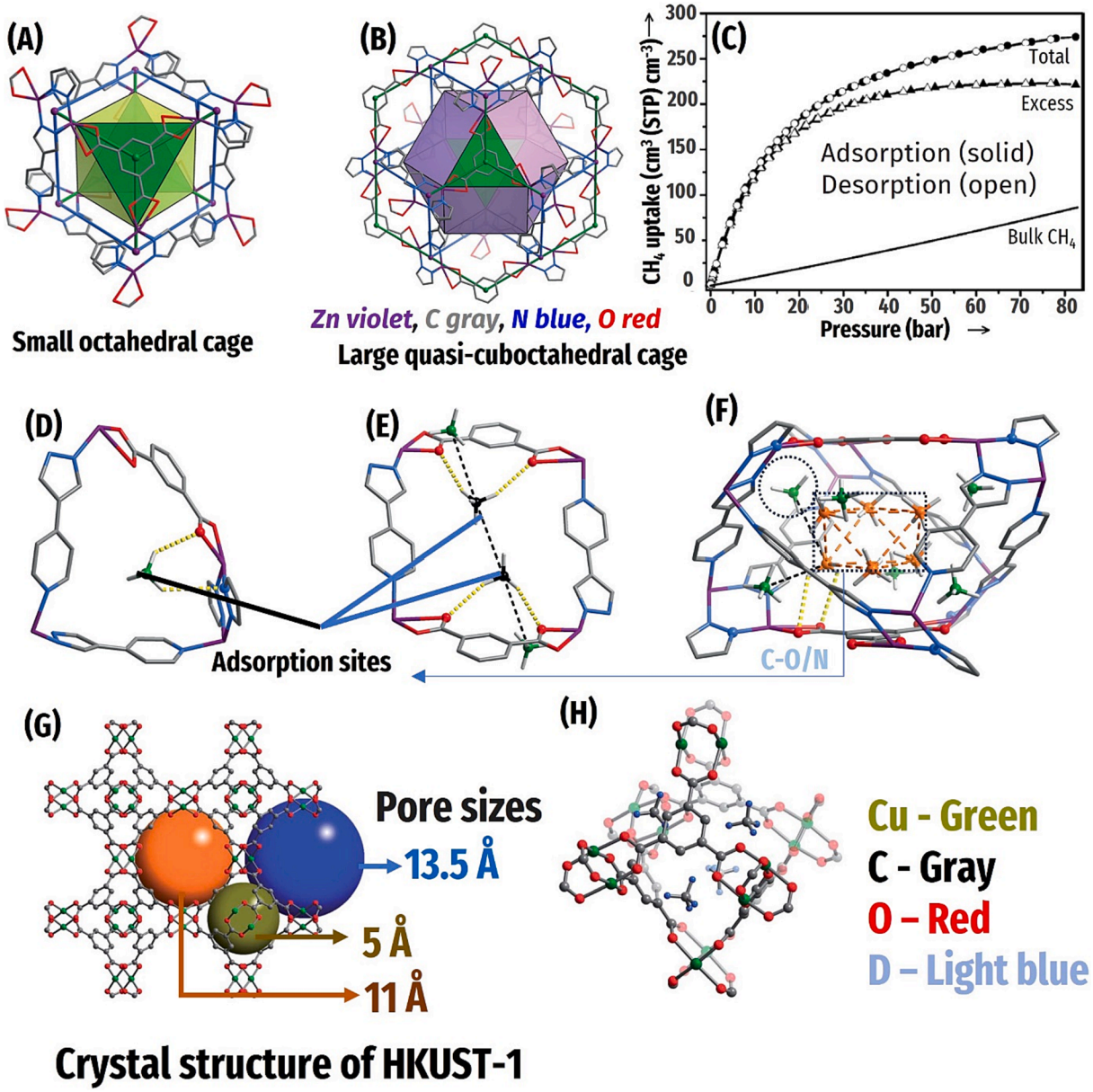

Fig. 9. Views from different angles of (A) the tiny octahedral cage as well as (B) a sizable quasi-cuboctahedral enclosed in MAF-38. (C) High-pressure excess and total CH_4 adsorption isotherms (298 K) on MAF-38. (D) Primary (green) CH_4 adsorption sites in MAF-38. (E) Secondary (black) CH_4 adsorption sites in MAF-38. (F) Ternary (orange) CH_4 adsorption sites in MAF-38 (Reprinted (adapted) from [167] with permission from John Wiley and Sons with License number 5510090505423). (G) Three different types of cages in HKUST-1. The diameters of the cages represented as dark green, orange, and blue spheres are 0.5 nm, 1.1 nm, and 1.35 nm, respectively, the exposed Cu(II) being only directed into the latter. (H) Four apertures of the octahedral cage of HKUST-1 where CH_4 molecules are adsorbed.(Reprinted (adapted) from [174] with permission from the Royal Society of Chemistry. (For interpretation of the references to colour in this figure legend, the reader is referred to the web version of this article.)

trigonometric window associated with the cages (small and large), where many connections exist in the host structure. Additionally, C-H···O and C-H···N H_2 bonds and C-H··· π interactions are produced (Fig. 9 **(D)**). The COOH group of the btc ligand present in the smaller cage and the quadrangular window linking the large and small cages are used as adsorption sites for secondary and tertiary CH_4 (Fig. 9 **(E** and **F)**).

Wu et al., [224] reported the CH_4 adsorption mechanism using three MOFs: PCN-14, HKUST-1, and PCN-11. According to their study, the CH_4 molecule rests immediately above the exposed Cu(II) ion OMS, which is one of the key CH_4 binding sites for all three MOFs. Along with the OMSs that have long been known to exist, pockets at the junction of the hole and cage were discovered as additional efficient guest molecule adsorption sites. Fig. 9 **(G)** represents the crystal structure of HKUST-1 with three different types of cages. The H atoms present in CH_4 were distributed toward the octahedral cage adjacent to the Cu(II) tetracarboxylate-paddlewheel units, and the small cage window site served as HKUST-1′s second main binding site. Fig. 9 **(H)** represents the localization of adsorbed CH_4 molecules at the four windows sites of an octahedral cage. A CH_4 capacity of approximately 160 cm^3(STP)/cm^3 was achieved once the Cu(II) open sites and small cage window sites were completely saturated. Two more secondary adsorption sites, one at the corner of the large cage and the other close to the small cage center, were discovered in addition to the previously mentioned main locations. Three others significant CH_4 binding sites and a sizable corner cage site were discovered in the PCN-11 two-site cage window (I and II). One hydrogen atom of each CH_4 molecule occupying the two cage window positions points toward the center of an extended cuboctahedral cage perfectly aligned along its threefold axis. Although those at window cage

site II pointed in the general direction of the organic linkers, the three remaining atoms of hydrogen in the CH_4 absorbed at the window cage site I pointed out the general direction of the Cu(II) tetracarboxylate-paddlewheel units. At the maximum saturation of these four primary binding sites, which corresponded to almost 75 % of the total CH_4 adsorption, the storage capacity was 160 cm^3(STP)/cm^3. The pore spaces and secondary adsorption sites of the three MOFs provide available storage space.

Hulvey et al., conducted a thorough study on the CH_4 uptake by HKUST-1 [158], and the results indicated that the adsorption sites are preferred over the exposed Cu(II) sites and are situated close to and inside the small octahedral framework of the structure. Wu et al., [225] calculated the CH_4 binding energies at the unsaturated metal sites of Mg-MOF-74 using first-principles calculations. The calculated binding energy was higher than that of conventional MOFs (30–35 kJ/mol). Based on previous findings for various gas molecules, it was demonstrated that OMS was the main adsorption site when the position of the CH_4 molecule was above the MgO_5 pyramidal square plane. The distance between the Mg and C atoms of the bound CH_4 in MAF-38 was 3.04 Å less than the carbon–carbon distance of CH_4 deposited over graphite (3.45 Å), indicating that the CH_4 molecules and Mg ions have strong interactions. The adsorbed CH_4 molecules reacted with the OMSs' CH_4 molecules and the framework at the second CH_4 site, which is another adsorption site. This interaction helped stabilize the adsorbed CH_4 molecules.

Kim et al., [162] used synchrotron X-rays to describe the CH_4 adsorption locations in $Zn_2(bdc)_2(dabco)$. X-ray structural analyses of CH_4 adsorbed on Zn2(bdc)2(dabco) using single-crystal X-ray analysis revealed that site B was located near the center of the minor windows along the a- and b-axes, and site C was situated at the center of the cavity, being associated with the $Zn_2(COO)_4$ paddlewheel units ($H_4C\cdots O1$, 3.74(2) Å). Additionally, the CH_4 molecules at site A formed incomplete π–HC interactions with the phenyl chain of the bdc ligands at a distance of 3.33(2) Å. At site B, the CH_4 molecules interacted ($H_4C\cdots C_3$, 3.99(1) Å) with phenyl ring. The CH_4 molecules at site C remained steady through contact with sites B and A. In addition, 4.02(2) Å and 3.91(4) CH_4-to-CH_4 separations existed between locations C and A and B, respectively. As they were significantly closer to each other, sites A and B could not be completely occupied simultaneously.

Lucena et al., [226] investigated the temperature dependence of PCN-14′s CH_4 adsorption. Interestingly, CH_4 was present at the unsaturated Cu(II) sites at 150 K rather than at 290 K. They also showed that no energy boundary existed between PCN-14′s weak and powerful binding sites at room temperature. Ma et al., [227] synthesized PCN-14 for CH_4 adsorption. Their findings showed a considerably higher CH_4 intake of 230 v/v at 290 K and 35 bar, relative to the earlier DOE goal of 180 v/v at 35 bar and 298 K. The small surface area of PCN-14 does not explain its highly potent CH_4 adsorption capacity of 1453 m^3/cm^3. Getzschmann et al., [228] computationally examined CH_4 adsorption in the pores of HKUST-1. They discovered through GC-MC simulations that CH_4 molecules first adsorb in the 5 tiny pores before moving on to larger holes (11 Å and 13.5 Å). Wu et al., used neutron powder diffraction to identify the locations and orientations of two archetypal MOF molecules with CH_4 (ZIF-8 and MOF-5) [229]. The apex of the organic linker (MeIM), serving as the first CH_4 adsorption site (IM site) in ZIF-8, was created by the early loading of CD_4/Zn. Another CH_4 adsorption location (channel site) situated in the middle of the channel comprised six ZnN4 tetrahedra and was determined using a loading of 2.33 CD_4/Zn. The vertex D atom in the CD4 and associated C = C bond were most tightly spaced at 2.98 and 3.21 in the IM and channel sites, respectively. In contrast, excess CH_4 molecules were contained within a nanocage with a diameter of approximately 5 Å formed by the CH_4 molecules present on these two sites. Orientationally disordered confined CH_4 randomly occupies four potential spots in the center of the cavity. Notably, a phase shift was observed after cooling. In this case, the location of the CH_4 molecules shifted, but the two primary sites remained unchanged.

In this type of nanocage, three confined CH_4 sites are observed, each encircled by four main CH_4 sites. According to the loading of 0.75 CD_4/Zn, the initial CH_4 adsorption site (cup site) in MOF-5 is situated in the middle of the triangular faces of the zinc oxide molecules. The CH_4 molecules in the cup site are properly aligned, with one C-D bond in the three-fold axis and three other points on the three ZnO_3 triangular sides. The cup sites were fully occupied by the increasing CH_4 loadings of 3CD_4/Zn, and two extra sites were visible: one overhead the hexagonal plane of the organic linkers and another ZnO_4 tetrahedron (ZnO_2 site) (hex sites) located above the O–O border. At the zinc oxide and hex sites, the CH_4 molecules lacked well-defined orientations compared to those at the cup site, suggesting significantly weaker CH_4–MOFs interactions. The central pore structure also contained a small number of totally disorganized CD_4 molecules in addition to the cup, hex, and ZnO_2 sites. With higher CH_4 loadings (2, 3, 4, and 6 CD_4/Zn), a phase transition occurred when the temperature was reduced below 60 K. The CH_4 molecules assemble in the core cavity of the structure and rearrange in response to this phase change. As a result of the phase shift, the three first adsorption sites remain basically unchanged. In addition to the three adsorption sites mentioned above, the other CH_4 molecules occupy large cages. They exhibit host–guest and guest–guest interactions similar to those at the secondary and tertiary sites.

Once the MOFs (MOF-5) are loaded with CH_4, the gas adsorbents are first drawn to the strongest binding site, which is the metal clusters in MOF-5 and the organic linkers in ZIF-8. The CH_4 orientation is defined by framework molecule interaction. The molecule orientations and adsorption sites remain consistent with temperature because of the comparatively high binding energy. Higher loading causes CH_4 molecules to begin settling into the secondary binding sites. ZIF-8′s second site features local 3-fold symmetry, making it suitable for a tetrahedral CH_4 molecule. The MOF-5′s second and third binding sites lack such an appropriate local shape. Adsorbed CH_4 exhibits orientational disorder at these sites and is stabilized through the framework-CH_4 interaction and a drop in temperature. The overall symmetry of the MOF-5 system is lowered as a result of the modest offset of the CH_4 location from the sites that fulfill the cubic symmetry caused by the mismatch between the molecule shape and the local framework geometry. Under both circumstances, the host pore shape serves as a template for the intriguing interconnected nanocage structures formed by the adsorbed CH_4 molecules [229]. On the other hand, as temperatures rise for PCN-14, the CH_4 saturation absorption of both absolute and excess adsorption decreases. At 125 K, the saturation of excess CH_4 adsorption in PCN-14 an adsorbed density of CH_4. The fully activated PCN-14 sample's nitrogen sorption isotherms demonstrate typical Type-I sorption behavior, demonstrating the activated PCN-14′s persistent porosity [104].

Higher gas loading causes the CH_4 molecules to concentrate in the center of these nanocages created by the adsorbed CH_4 molecules, where they primarily interact with the surrounding CH_4. At low temperatures (about 60 K), both MOFs loaded with a high concentration of CH_4 exhibit unique phase changes that are caused by the partial ordering of the confined CH_4 in the framework pores.

3.5.3. Acetylene gas storage mechanisms

Acetylene is usually produced by the thermal cracking of hydrocarbons or the combustion of natural gases that are accomplished with a significant amount of CO_2. It results in the necessity for the purification of C_2H_2 using an efficient technology to meet the quality to fulfill the demand in different domains, such as feedstocks for synthesizing several valuable commercial compounds and welding fuels [230]. Cryogenic distillation and solvent-based absorption are major processes currently practiced for separating C_2H_2 from the gaseous mixture. However, these methods are energy-intensive and require potentially hazardous chemicals. It leads to exploring novel, eco-friendly, and economical approaches, such as adsorption-based technology using highly porous MOFs with reduced energy footprint [231].

To rationally design and synthesize novel MOFs with enhanced C_2H_2 storage performance, it is crucial to understand the C_2H_2 adsorption

mechanism(s) at the active sites present in porous MOFs. Spectroscopic methods, such as high-resolution powder neutron diffraction, can be used to describe the C_2H_2 adsorption sites in MOFs. In MEM/Retiveld analysis, MOFs, in contrast to conventional activated carbons, have a highly crystalline nature and well-ordered structures, making them suitable for single-crystal X-ray diffraction. By using MEM/Rietveld analysis, it was determined that when a $Cu_2(pzdc)_2(pyz)$crystal structure was filled with C_2H_2 [187], the molecules of C_2H_2 comprised intermolecular bonds and was organized along a 1D channel of deuterated C_2H_2 gas (C_2H_2) at a distance of 4.8 Å. The crystal structure of $Cu_2(pzdc)_2$(pyz) filled with C_2H_2 at 170 K, as obtained by MEM/Rietveld analysis, is shown in Fig. 10 **(A).** C_2H_2 contains one H atom and one O atom of the uncontrolled carboxylate separated by 2.2 Å. Owing to C_2H_2 adsorption, a slight alteration in the structure of the framework also occurs, and the heat generated by the adsorption of C_2H_2 can offset the energy required for this structural transformation.

The large enthalpy associated with the adsorption of C_2H_2 in HKUST-1 was demonstrated by Xiang et al., where the strong interaction of C_2H_2 molecules was found with the open Cu(II) sites [188]. Fig. 10 **(B)** represents the Fourier map of HKUST-1 obtained by these authors after loading 0.62 C_2H_2 per Cu calculated by the difference of the current diffraction pattern with the one of the bare materials. The primary binding location was the Cu site open for the C_2H_2 molecule, which attached to it via Columbic reactions between the Cu atom and the C_2D_2 molecule at a Cu-C distance of 2.62 Å [188]. The C_2D_2 molecule binds to the open Cu(II) sites with C-D and C≡C bond lengths of 1.06 Å and 1.13 Å, respectively. This indicates bond stimulation by the open Cu^{2+} sites, which are slightly longer than those of the unbound C_2H_2 molecule. The tiny octahedral cage window entrance serves as the next adsorption site after the OMSs. The adsorbed C_2H_2 molecules are very disorganized, and the C_2H_2-structure interface is of the usual van der Walls (vdW) category. The extra-positive intensity, ascribed to the adsorbed C_2D_2 molecules, is indicated by pink spots above the open Cu(II) (green balls). This categorically refutes our earlier theory that the high adsorption enthalpy observed in HKUST-1 is caused by the open Cu(II) sites, owing to their strong C_2H_2-binding affinity. The same technique was used by Xiang et al., [189] to demonstrate that the open sites of Co(II) in Co-MOF-74 served as the leading sites for C_2H_2 adsorption. The accessible Co(II) site and the C_2D_2 molecule are separated by approximately 2.65 Å, as is the adjacent Co atom. The crystalline c-axis is the organizing principle for the C_2D_2 molecules in C_2D_2-loaded Co-MOF-74, forming pseudo-1D arrangements with approximately 4.0-Å intermolecular C_2D_2 distances (Fig. 10 **(C)**). This is similar to the 4.8-Å distance observed in $Cu^2(pzdc)_2(pyz)$. In another study, neutron powder diffraction clearly showed six distinct C_2H_2 atoms occupying various binding locations in MFM-188 [192].

As shown in Fig. 10 **(D-1)**, the C_2H_2 molecules that attach to site 1 (labeled C_2D_2 (1), similar to the one below) virtually encircle the

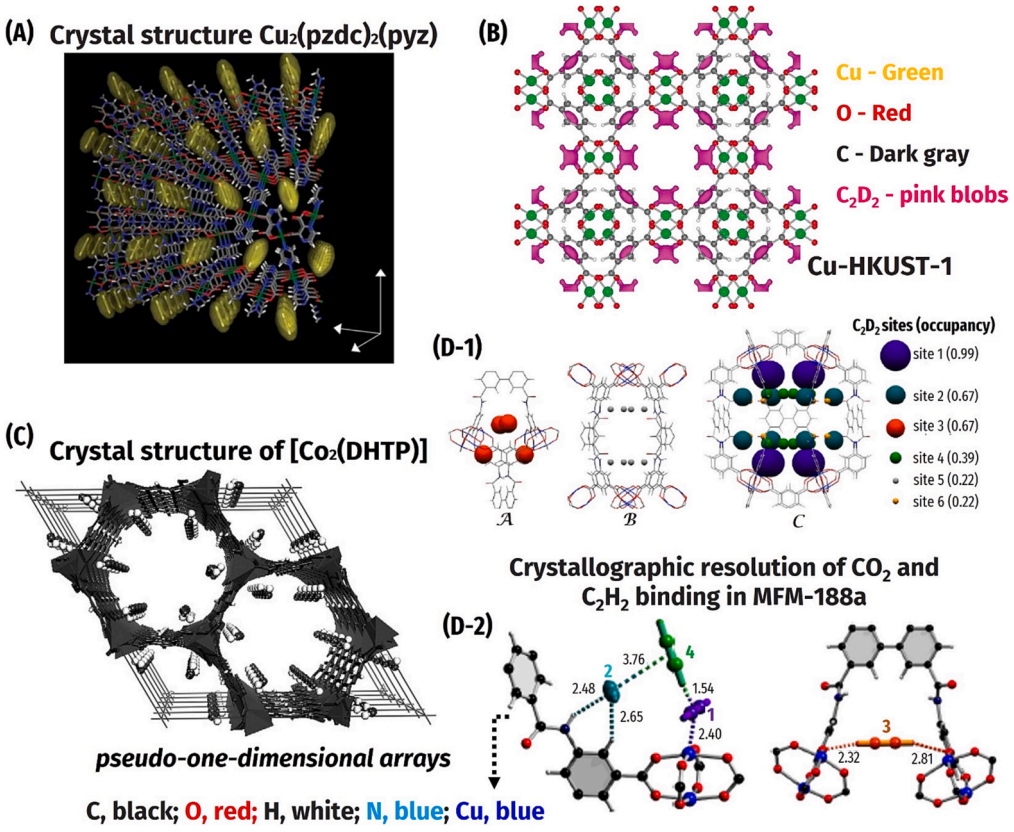

Fig. 10. (A) Perspective image of the $Cu_2(pzdc)_2(pyz)$ crystal structure determined by MEM/Rietveld studies. (Reprinted (adapted) from [187] with permission from Springer Nature with License Number 5510100189806). (B) The preferential binding sites of acetylene illustrated by the Positive Difference Data from powder neutron diffraction were used to compute the Fourier map of the loaded HKUST-1 with 0.62 C_2D_2 per Cu. The pink areas represent the first, strongest adsorption sites of open Cu(II), which have an extra-positive abundance of adsorbed C_2D_2 molecules attached to them. Atoms do not gravitate toward the gauge. The pink masses on top of the BTC rings are caused by C_2D_2 molecules that are connected to other open Cu sites (Reprinted (adapted) with permission from [188], Copyright (2009) American Chemical Society). (C) crystal structure of $[Co_2(DHTP)]1.08C_2D_2$, where high-density C_2H_2 molecules are organized in pseudo-1D arrays (Reprinted (adapted) [189] with permission from John Wiley and Sons with License Number 5510100594509). (D-1) Neutron powder diffraction was used to identify the deuterated C_2H_2 adsorption (sites 1 to 6, in order of decreasing occupancy) in cages A, B, and C of MFM-188a (sites are represented by spheres whose radii are proportional to the corresponding crystallographic occupancies); (D-2) crystallographic view (with measurements shown in Å) of the binding arrangements of the acetylene molecules adsorbed at sites 1 to 4 (Reprinted (adapted) from [192] with permission from Springer Nature). (For interpretation of the references to colour in this figure legend, the reader is referred to the web version of this article.)

available Cu locations in an aside-on manner. According to Xiang et al., [188], the distances at Site 1 between the nearest Cu atoms and carbon in the bound C_2H_2 molecules are 2.60(3) Å and 2.37(3) Å (Fig. 10 **(D-2)**), respectively, which are similar to those observed for HKUST-1 when filled with C_2D_2. With a 0.67 site occupancy, C_2D_2 (2) Cage C contained the compounds. In addition to the Lewis acid-base interactions between the C_2D_2 molecules and C-H groups from the nearby isophthalate group at this binding location [C···C acetylene = 3.47(1), C-H···C = 149°], connections also exist between the C_2D_2 molecules and N-H portions of the amide groups through hydrogen bonds [N···C acetylene = 3.24(5), N-H···C = 147°]. C_2D_2 (3) occupies the same location as C_2D_2 at the triangular aperture of the smallest octahedral cage. Atoms of oxygen in the carboxylate [C acetylene···O = 3.72(4), 3.37(4), C-D···O = 143, 169°] are hydrogen-bound to the C_2D_2 molecules at this binding site (Fig. 10 **(D(b))**. The fourth C_2H_2 absorption site in cage C was obtained by combining C_2D_2 (1) and C_2D_2 (2) with an occupancy rate of 0.49. The C_2H_2 adsorption of molecules at sites 5 and 6 did not appear to engage specifically with the MOF host. C_2H_2 plays a dual function by acting as an amide and aromatic C-H group to strengthen the bond between the C_2H_2 and MOF.

3.5.4. *Carbon dioxide gas storage mechanisms*

The separations between the metal elements and O_{CO2} are in the adsorption modes of 2.228 and 2.262 for respective Mg-MOF-74···CO_2 and Zn-MOF-74···CO_2.. While they are separated by 2.715 and 2.598 Å, the C_{CO2} atoms are directed with the closest oxygen atom. In the M···O-C-O compound created by the CO_2, Mg-O-C and Zn-O-C have positions of 129.8° and 136.8°, respectively. The angles for the Mg-O-C and average distance between magnesium and oxygen concur with the numbers of B3LYP-D* (129° and 2.310 Å) [232]. The O-C-O angle is bent due to Lewis acid-base interactions and sp hybridization of the carbon isotope variations. Neutron particle diffraction experiments also support the bending of CO_2 [233]. The energy for contact with Mg-MOF-74···CO_2 is −51.5 kJ/mol, according to the revPBEvdW method [234]. Similar interaction energy values were predicted by the hybrid-MP2:B3LYP + D* for Zn-MOF-74···CO_2 and Mg-MOF-74···CO_2 [232]. However, it is evident that, insofar as the predicted interaction energy, relative to Mg-MOF-74, Zn-MOF-74 has a lower CO_2 value. Fig. 11(A) shows no evident differences between the Zn-MOF-74···CO_2 electronic and exchange energies, and those MOFs such as Mg-MOF-74···CO_2, a larger repulsive energy, exist for Zn-MOF-74···CO_2. Compared to Mg-MOF-74···CO_2, Zn-MOF-74···CO_2 exhibits substantially stronger electron repulsions owing to its 3d10 Zn structure [235]. Fig. 11(B) displays the CO_2 adsorption isotherms in Zn-MOF-74 and Mg-MOF-74 at 298 K. W During a barometric transition from low to high pressure, Mg-MOF-74 always absorbs more than Zn-MOF-74. Saturation was visible in all the isotherms at approximately 2000 kPa. At 101 kPa and 298 K, Mg-MOF-74 absorbed CO_2 at a 9.5 mmol/g. Based on the data from the simulated adsorption isotherms, this was consistent with the experimental results of 8.0 mmol/g under these conditions [236].

The CO_2 binds in an end-to-end coordination fashion to the penta-coordinate Mg(II) sites [237]. The binding mode facilitates the collection and stability of CO_2 inside the MOF structure. The CO_2 adsorption on Mg-MOF-74 exhibits an initial high Qst value of 47 kJ/mol, indicating a significant binding affinity between the Mg-based node and CO_2. The greater Lewis acidity of Zn(II) in comparison to other metals (Mg(II)) was suggested as the reason for the high epichlorohydrin conversion of Zn-MOF-74 [238]. The smaller ionic radius of Zn(II) is the cause of its increased Lewis acidity. Lewis acidity is primarily influenced by ionic radius size since all metal ions under evaluation have the same charge.

As ionic radius size and charge increase, Lewis acidity increases for metal ions [239]. Because the Mg site has a partial positive charge on the metal core and is Lewis acidic, the Mg-O bond has a higher ionic character. The electron-rich oxygen atoms of CO_2 are drawn to this partial positive charge, which causes a coordination bond to form. The ionic

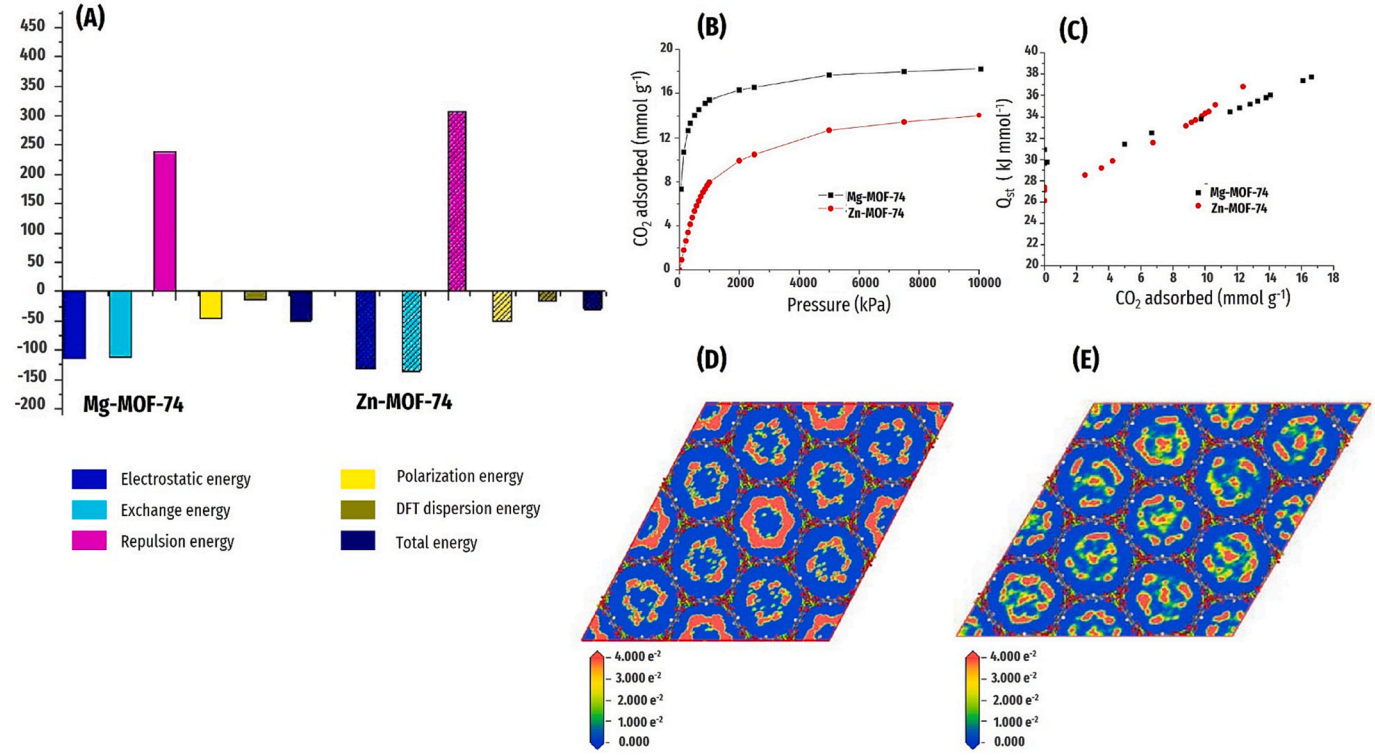

Fig. 11. (A) Contribution of different elements to the overall binding energy as determined by the LMO-EDA SVWN/3-21G level approach for the Mg-MOF-74···CO_2 and Zn-MOF-74 ···CO_2 combinations. (B) Simulated adsorption isotherms (298 K) of CO_2 onto Mg-MOF-74 and Zn-MOF-74. (C) Relationship between CO_2 adsorption isosteric heat (Qst) and the amount of CO_2 adsorbed; (D) Adsorption-related density distribution outlines 10 gas molecules on Mg-MOF-74. (E) Adsorption-related density distribution outlines of 200 gas molecules on Mg-MOF-74 (Reprinted (adapted) with permission from [235], Copyright (2013) American Chemical Society).

nature of this bond influences the degree to which Mg-MOF-74 and CO_2 interact. The mobility and reactivity of adsorbed CO_2 molecules (e.g., $MgCO_3$ formation) are restricted by the inflexible structure of Mg-MOF-74 [209,240]. In contrast, Zn-MOF-74 stimulates the opening of the epoxide ring more intensely due to the increased contact between Zn(II) ions and the epoxide's oxygen atom, which permits the bromide ion to effectively attack the less substituted carbon atom by nucleophilic attack [241].

Due to the partial positive charges on the metal centers, these MOFs have unsaturated metal sites that display Lewis acidity, which is beneficial for CO_2 capture. Interestingly, Zn-MOF-74 outperformed the other isostructural MOF-74 materials in the cycloaddition reaction between CO_2 and styrene oxide, demonstrating a 93 % epoxide conversion and complete selectivity to styrene carbonate. Divalent metal ions' effect on isostructural MOF-74 materials' CO_2 valorization at room temperature [242]. The polarization of CO_2 near Mg ions is considerable and adds significantly to the interaction energy, according to quantum mechanical estimates of CO_2 adsorption in Mg-MOF-74 [243,244]. Considering the very similar configurations of CO_2 inside Mg-MOF-74, no reaction is occurring, and no significant charge transfer is expected. An appropriate approximation for the polarization energy should be the orbital interaction energy [243].

Despite being less than the exact measurement of 296 K and 5.5 mmol/g at 1 atm, the predicted CO_2 absorption of Zn-MOF-74 is 1.6 mmol/g at 298 K and 101 kPa [240]. The investigational measurement showed 14.3 mmol/g [245] according to the anticipated adsorption isotherms in Mg and CO_2 up to approximately 16.6 mmol/g at 3300 kPa in MOF-74. The relationship between the uptake and predicted isosteric heat is shown in Fig. 11(C). The findings demonstrate that as the absorption increases when the Mg-MOF-74 and Zn-MOF-74′s isosteric heat curves intersect, they are at a concentration of approximately 9.7 mmol/g. Simmons et al., reported the rapid adsorption of CO_2 in Mg-MOF-74 compared to that in Zn-MOF-74 at low pressures, with starting Qst values of 30 and 26 kJ/mol, respectively [246].

This difference in the adsorption temperatures at low coverages was caused by the higher ionic character of the Mg–O bond. MgO produces $MgCO_3$ via the exothermic chemisorption of CO_2. Although Mg-MOF-74 cannot chemisorb CO_2, there is an incorrect description of the enhancement of the ionic nature of the Mg–O bond when using the GC-MC approach, which is a widely used physisorption modeling technique. When the pressure was increased (>0.1 kPa), the binding sites close to the M atoms were overwhelmed. When the pressure exceeds 0.1 kPa, the physisorption characteristic leads to an accurate GC-MC description of the adsorption temperatures and isotherms. Fig. 11(**D** and **E**) demonstrate how the CO_2 uptake in MOF-74 at various rates is compared in terms of the density distribution outlines, as shown by the tests [233]. CO_2 molecules are primarily adsorbed at the six corners of the hexagonal channels during minimal uptake. This variation in the adsorption temperature at limited coverage was caused by the higher ionic character of the Mg–O bond. MgO produces $MgCO_3$ via the exothermic chemical reaction with CO_2. Although, no chemisorption of CO_2 occurred in Mg-MOF-74, the Mg-O bond exhibited an enhanced ionic character. Nonetheless, this results in an erroneous description by the S-method, which is a widely used physisorption modeling methodology. As the pressure increased (greater than 0.1 kPa), the intake sites near the M atoms were overwhelmed. Owing to the evident physisorption characteristics, the adsorption heats and isotherms could be accurately described using the GC-MC technique.

4. Application of MOFs in biogas upgradation

The biogas composition during anaerobic digestion depends upon the chemical composition, feed organic matter, and other operating conditions, such as temperature, pH, retention time, and digestion technology [247]. Generally, biogas primarily contains CO_2 and CH_4, including trace amounts of ammonia, nitrogen, oxygen, hydrogen sulfide, siloxanes, and moisture [248]. During biogas purification, biomethane must be upgraded by $\geq$ 97 % by removing excess CO_2 for its potential use as commercial biofuels. MOFs, being porous, structurally diverse, versable, and tolerable, can be used for CO_2 removal through the specific passage of CH_4, MOF-based materials viz. ZIF-8, UiO-66, and ZIF-8 mixed with ZIF-67, 2D MOF, and functionalized MOF can be applied for economical and effective biogas upgradation [249]. Upgradation of biogas through selective CO_2 adsorption using MOFs, such as MOF-177, was found to have a 9-times higher amount of CO_2 separation compared to conventional adsorbent materials, such as activated carbon and zeolite [250].

Chidambaram et al., synthesized two MOFs made up of Al(III) and tetracarboxylate ligands based on pyrens (Al-PyMOF) and porphyrin (Al-PMOF) rings with a 7 Å distance of two parallel aromatic rings to make binding pockets for CO_2 [251]. The binding affinity and stability of porous MOF adsorbents were in the presence of water vapor at a relative humidity of 4 to 85 vol% in the feed gas. A strong affinity with CO_2 and hydrophobicity towards water vapor was observed in a column study at 30 °C and 1 bar with a 10 mL/min flow rate using synthetic biogas mixtures for dry (CO_2/CH_4, 50/50 v/v) and wet ($CO_2/CH_4/H_2O$, 50/46/4 v/v). Al-PMOF exhibited a high breakthrough time of 11 min/g for the separation of CO_2 and CH_4 with almost similar performance in wet and dry gas composition due to hydrophobic binding pocket nullifying the co-adsorption competition between CO_2 and water vapor.

The MOFs, such as ZIF-7, ZIF-90, UiO-66, MIL-101, MIL-53HKUST-1, and CuBDC, have attracted significant interest in fabricating mixed-matrix composite membranes to improve the selectivity and permeability due to large pore volume and tunable structure and properties [252,253]. The presence of organic moiety in MOFs can be easily mixed with membrane polymers owing to the high affinity of organic membrane polymers for fabricating defect-free composite membranes [254]. The morphological structure of MOFs in composite membranes can be exploited to enrich CH_4 from biogas by selective separation of CO_2. Gong et al., utilized $Zn(pyrz)_2(SiF_6)$ nanocrystals MOFs filler (20 wt%) material for the composite membrane to achieve high CO_2/CH_4 separation due to selective separation of CO_2 by $Zn(pyrz)_2(SiF_6)$ to surpass the upper limit of the polymeric membrane [253]. An ideal pore size of 3.8 Å and strong affinity of SiF_6^{2-} enabled nanocrystals for strong affinity with CO_2 in a mixed membrane matrix of 4,4′-(hexafluoroisopropylidene) diphthalic anhydride (6FDA), N,N,N,N-Tetramethyl-1,3-propanediamine (TMPDA). MOFs-based polymeric composite membrane with 2 wt% to 4 wt% loadings of copper 1,4-benzene-dicarboxylate nanosheet (CuBDC NS) in polymeric matrices (6FDA-DAM and PIM-1) enhanced 40 % of selectivity of CO_2/CH_4 [255]. The 2-D MOF material (CuBDC) with a high aspect ratio exhibits cavities with a pore pocket of ~ 5.2 Å to discriminate the gas molecule permeation based on kinetic diameter. It is a promising filler material in mixed matrix polymeric membranes in gas separation to concentrate CH_4 by removing CO_2.

The MOFs and MOFs composites have drawn a significant surge of research interest in developing novel materials for biogas upgradation. In the recent scenario, pollutants, such as H_2S and NH_3, are adsorbed before MOFs' application as an adsorbent or filler material for CO_2 removal from CH_4 [249]. However, future research should focus on the crucial challenges for practical applications, especially in acidic conditions, of MOFs and composite, such as fabrication cost and material stability or reproducibility. The production cost may be reduced by scaling up the fabrication process using cost-effective and abundantly available petroleum products. The non-reproducibility of MOFs can be handled by adopting hydrophobic materials for the synthesis of MOFs, such as 2D MOF, fluorinated MOF (ZIF-8), and a combination of ZIF-8 and ZIF-67 with appropriate polymers.

5. MOFs for gas adsorption and energy storage applications-major challenges

Although significant progress has been made in MOF-related fields of study, many difficulties and hurdles remain. MOF nanostructures, for example, produce framework adsorbents that are capable of separating well while also providing a variety of performance characteristics, including scalability, recyclability, easy regeneration, and mechanical stability; in particular, they may not meet the standards for some applications [256]. Because the interactions between ligands and metal centers play a major role in determining the durability of MOFs, it is imperative to synthesize MOFs with the best possible coordination between the organic linkers and metal clusters. All current preparation techniques can chemically or physically damage the MOF nanosheets, resulting in suboptimal structures and properties. Preparing a monolayer in a controlled manner with a high yield remains challenging because of the uneven thickness of the produced MOF nanosheets.

As a primary biofuel that will aid in overcoming the world's energy issues to attain environmental sustainability, biogas is recognized for its pivotal role in the renewable energy market. Absorption, adsorption, and cryogenic distillation processes are only a few of the numerous technologies used in industry to improve biogas [257]. High energy requirements, CH_4 loss, high capital, operating and maintenance expenses, and the need for a sizable footprint are the typical obstacles that stand in the way of the effective deployment of biogas upgrading systems. Furthermore, the non-reproducibility of these materials presents a difficulty to the commercialization of MOFs. The majority of MOFs are not long-term stable enough and can break down, especially when humid biogas and a trace amount of H_2S are present [249]. This is due to the fact that CO_2 must be removed from a biogas stream at considerably higher quantities than H_2S, which could alter how one MOF compares to another. Recently, MOFs have been used as a filler material for the mixed-matrix membrane for the improvement of CO_2/CH_4 by selective removal efficiency due to the selective diffusivity/solubility of gases through the composite membrane [258]. The MOF-based composite membrane is another way for gas upgradation with a lower footprint, ease of operation, energy efficiency, and cost-effectiveness; however, membrane swelling, wetting effect, and sensitivity to corrosive solvents are some of the key challenges [249].

There is uncertainty surrounding the exact mechanism of MOF growth. Owing to incomplete self-assembly knowledge in a confined response system, such as how synthetic conditions affect the MOFs' pore size and surface area, precisely controlling the target structures for pristine MOFs remains challenging. With regular or hierarchical pores, we can develop and produce MOFs with large surface areas and modifiable compositions with a thorough understanding of the self-assembly process. Different MOF nanosheets may have varying apertures based on their basal planes, potentially leading to noticeably different performances. Consequently, the creation of MOF nanosheets with various orientations remains extremely difficult. In addition, most MOF nanosheets exhibit poor stability and insufficient conductivity, restricting their gas adsorption and storage. Despite these significant obstacles, the successes to date have been inspiring, and the topics discussed in this review are merely the beginning of investigations into MOF-based materials. Owing to the remarkable gas adsorption performance and selectivity of MOFs, gas adsorption and storage represent suitable fields for the practical applications of MOF-based materials.

6. Conclusions and future research perspectives

MOFs are currently regarded as important new members of the permeable material family as they have a lot of accessible sites. MOFs, MOF composites, and MOF variants can replace traditional porous materials in many ways (e.g., metal oxides, porous carbons, metals, metal sulfides, and their composites), and their use has become more common. It was observed that the MOFs could be used as important porous materials for the selective adsorption and storage of strategically important biogas and natural gas to produce alternatives to fossil fuels and reduce GHGs. Owing to their unique characteristics, MOF is useful for upgrading biogas by separating CO_2 and H_2S from biogas in a custom-made manner or enriching natural gas, which would be an economical solution for sustainable energy demand. Despite the widespread use of conventional synthesis techniques, the synthesis of distinct MOFs is mainly practiced by mechanical, sonochemical, electrochemical, and MW-assisted syntheses. These techniques can typically be applied under mild reaction conditions to produce compounds with various characteristics and particle sizes. Future developments in MOF-derived materials with enhanced performance require the introduction of low-cost and effective synthetic routes with the ability to conduct precise manipulations.

Most studies on MOFs have used existing and popular MOF types such as MILs, PBAs, and ZIFs as precursors or sacrificial templates. Alternative MOFs, particularly those with specifically designed features, should be investigated to improve their performance. This can be explicitly attributed to the increased use of compounds and MOFs. By fully utilizing porosity for gas storage and applications, MOF composites can enhance adsorption capacities and stabilities and offer a positive outlook toward the widespread use of MOFs in energy storage. In recent years, remarkable developments have been made in the preparation and use of MOF-derived materials. Several foreseeable problems regarding gas adsorption and storage using MOF-based nanostructures must be resolved. This study offers several perspectives for future research in this field. The volumetric energy densities of MOF-derived hybrid materials are relatively low, although they have potential applications in energy storage and gas adsorption. Their porous, low-density construction is the primary reason for this restriction. These properties should be examined in the future.

Currently, the lack of long-term practicability and cost-effectiveness of MOF derivatives limits their potential for commercial applications, and significant efforts are required to improve these products for effective environmental cleanup and biogas storage. To develop an economical route for commercial biogas and natural gas upgrading and storage, the scaling of MOF synthesis using economical and abundantly available petroleum raw materials can be an alternative to replace expensive organic linkers. In addition, moisture-stable MOFs (e.g., fluorinated MOFs-ZIF-8, 67 and their mixtures) should be used for high-capacity CO_2 removal. However, their high production costs and poor yield delay the large-scale preparation of MOF precursors. In the near future, close collaboration between scientists and industry should be encouraged to bridge the gap between laboratory scale and industrial outputs.

Future research should focus on understanding the kinetics of gas adsorption and desorption in MOF-filled large columns, efficient packing of MOF particles, economical production, and increasing the reusability of MOFs. In addition, it is necessary to improve the pore sizes and volumes and expose the active sites more uniformly, particularly those caused by collapsing porous structures. This review outlines and critically evaluates the most recent developments using MOF-based adsorbents for gas uptake and storage. The authors expect this review to inspire researchers in the next stages of materials science and technology to better understand the pore environment in MOFs as gas adsorption/separation carriers.

Declaration of Competing Interest

The authors declare that they have no known competing financial interests or personal relationships that could have appeared to influence the work reported in this paper.

Data availability

No data was used for the research described in the article.

Acknowledgments

The authors acknowledge the Creative and Challenging Research Program (2021R1I1A1A01060846) and Mid-Career Researcher Program (2020R1A2C3004237) sponsored by the National Research Foundation (NRF) of the Republic of Korea

References

[1] A.A. Abd, M.R. Othman, S.Z. Naji, A.S. Hashim, Methane enrichment in biogas mixture using pressure swing adsorption: process fundamental and design parameters, Mater. Today Sustain. 11–12 (2021), 100063, https://doi.org/10.1016/j.mtsust.2021.100063.

[2] S. Chakrabortty, R. Kumar, J. Nayak, B.-H. Jeon, S.K. Dargar, S.K. Tripathy, P. Pal, G.-S. Ha, K.H. Kim, M. Jasiński, Green synthesis of MeOH derivatives through in situ catalytic transformations of captured CO2 in a membrane integrated photo-microreactor system: a state-of-art review for carbon capture and utilization, Renew. Sustain. Energy Rev. 182 (2023), 113417.

[3] B. Basak, R. Kumar, A. Bharadwaj, T.H. Kim, J.R. Kim, M. Jang, S.E. Oh, H.S. Roh, B.H. Jeon, Advances in physicochemical pretreatment strategies for lignocellulose biomass and their effectiveness in bioconversion for biofuel production, Bioresour Technol 369 (2023), 128413, https://doi.org/10.1016/j.biortech.2022.128413.

[4] R. Kumar, T.H. Kim, B. Basak, S.M. Patil, H.H. Kim, Y. Ahn, K.K. Yadav, M.M. S. Cabral-Pinto, B.-H. Jeon, Emerging approaches in lignocellulosic biomass pretreatment and anaerobic bioprocesses for sustainable biofuels production, J. Clean. Prod. 333 (2022), https://doi.org/10.1016/j.jclepro.2021.130180.

[5] B. Basak, B.-H. Jeon, T.H. Kim, J.-C. Lee, P.K. Chatterjee, H. Lim, Dark fermentative hydrogen production from pretreated lignocellulosic biomass: Effects of inhibitory byproducts and recent trends in mitigation strategies, Renew. Sustain. Energy Rev. 133 (2020), https://doi.org/10.1016/j.rser.2020.110338.

[6] B. Aghel, A. Gouran, S. Behaein, Intensified biogas upgrading via various wastewater using microchannel, Chem. Eng. Proc.-Process Intensif. 175 (2022), 108927.

[7] A. Roozitalab, F. Hamidavi, A. Kargari, A review of membrane material for biogas and natural gas upgrading, Gas Sci. Eng. 114 (2023), 204969, https://doi.org/10.1016/j.jgsce.2023.204969.

[8] B. Basak, S. Patil, R. Kumar, G.S. Ha, Y.K. Park, M. Ali Khan, K. Kumar Yadav, A. M. Fallatah, B.H. Jeon, Integrated hydrothermal and deep eutectic solvent-mediated fractionation of lignocellulosic biocomponents for enhanced accessibility and efficient conversion in anaerobic digestion, Bioresour Technol 351 (2022), 127034, https://doi.org/10.1016/j.biortech.2022.127034.

[9] R. Kumar, B. Basak, P. Pal, S. Chakrabortty, Y.K. Park, M. Ali Khan, W. Chung, S. Chang, Y. Ahn, B.H. Jeon, Feasibility assessment of bioethanol production from humic acid-assisted alkaline pretreated Kentucky bluegrass (Poa pratensis L.) followed by downstream enrichment using direct contact membrane distillation, Bioresour Technol 360 (2022), 127521, https://doi.org/10.1016/j.biortech.2022.127521.

[10] P. Cozma, W. Wukovits, I. Mămăligă, A. Friedl, M. Gavrilescu, Modeling and simulation of high pressure water scrubbing technology applied for biogas upgrading, Clean Technol. Environ. Policy 17 (2) (2015) 373–391, https://doi.org/10.1007/s10098-014-0787-7.

[11] J.B. Holm-Nielsen, T. Al Seadi, P. Oleskowicz-Popiel, The future of anaerobic digestion and biogas utilization, Bioresour. Technol. 100 (22) (2009) 5478–5484, https://doi.org/10.1016/j.biortech.2008.12.046.

[12] S. Faramawy, T. Zaki, A.A.E. Sakr, Natural gas origin, composition, and processing: a review, J. Nat. Gas Sci. Eng. 34 (2016) 34–54, https://doi.org/10.1016/j.jngse.2016.06.030.

[13] C.E. Wylock, W.M. Budzianowski, Performance evaluation of biogas upgrading by pressurized water scrubbing via modelling and simulation, Chem. Eng. Sci. 170 (2017) 639–652, https://doi.org/10.1016/j.ces.2017.01.012.

[14] J. Zhao, Y. Li, R. Dong, Recent progress towards in-situ biogas upgrading technologies, Sci. Total Environ. 800 (2021), 149667.

[15] Z. Chen, P. Li, R. Anderson, X. Wang, X. Zhang, L. Robison, L.R. Redfern, S. Moribe, T. Islamoglu, D.A. Gómez-Gualdrón, T. Yildirim, J.F. Stoddart, O. K. Farha, Balancing volumetric and gravimetric uptake in highly porous materials for clean energy, Science 368 (6488) (2020) 297–303, https://doi.org/10.1126/science.aaz8881.

[16] F. Karami, B. Aghel, P. Moradi, M. Karimi, Stripping of hydrogen sulfide from crude oil desalter effluent via different adsorbents, Int. J. Environ. Sci. Technol. 19 (6) (2022) 5119–5130, https://doi.org/10.1007/s13762-021-03718-z.

[17] M.-L. Hu, M.Y. Masoomi, A. Morsali, Template strategies with MOFs, Coord. Chem. Rev. 387 (2019) 415–435.

[18] K. Hofmann, F. Küspert, Verbindungen von kohlenwasserstoffen mit metallsalzen, Z. Anorg. Chem. 15 (1) (1897) 204–207.

[19] J. Rayner, H.M. Powell, 67. Structure of molecular compounds. Part X. Crystal structure of the compound of benzene with an ammonia–nickel cyanide complex, Journal of the Chemical Society (resumed) (1952) 319–328.

[20] M. Eddaoudi, J. Kim, N. Rosi, D. Vodak, J. Wachter, M. O'Keeffe, O.M. Yaghi, Systematic design of pore size and functionality in isoreticular MOFs and their application in methane storage, Science 295 (5554) (2002) 469–472.

[21] C. Jeong, Z. Ansari, A.H. Anwer, S.-H. Kim, A. Nasar, M. Shoeb, F. Mashkoor, A review on metal-organic frameworks for the removal of hazardous environmental contaminants, Sep. Purif. Technol. 122416 (2022).

[22] X. Xia, G. Hu, W. Li, S. Li, Understanding reduced CO2 uptake of ionic liquid/metal–organic framework (IL/MOF) composites, ACS Appl. Nano Mater. 2 (9) (2019) 6022–6029.

[23] K.S. Song, D. Kim, A. Coskun, Hierarchically porous reduced graphene oxide coated with metal–organic framework hkust-1 for enhanced hydrogen gas affinity, ACS Appl. Nano Mater. 3 (2) (2019) 985–991.

[24] Y. Chen, X. Zhang, K. Ma, Z. Chen, X. Wang, J. Knapp, S. Alayoglu, F. Wang, Q. Xia, Z. Li, Zirconium-based metal–organic framework with 9-connected nodes for ammonia capture, ACS Appl. Nano Mater. 2 (10) (2019) 6098–6102.

[25] T.J. Ferreira, R.P. Ribeiro, J.P. Mota, L.P. Rebelo, J.M. Esperança, I.A. Esteves, Ionic Liquid-Impregnated Metal-Organic Frameworks for CO2/CH4 Separation, ACS Appl. Nano Mater. 2 (12) (2019) 7933–7950.

[26] S. Keskin, T.M. van Heest, D.S. Sholl, Can metal-organic framework materials play a useful role in large-scale carbon dioxide separations? ChemSusChem 3 (8) (2010) 879–891, https://doi.org/10.1002/cssc.201000114.

[27] N. Novendra, J.M. Marrett, A.D. Katsenis, H.M. Titi, M. Arhangelskis, T. Friščić, A. Navrotsky, Linker substituents control the thermodynamic stability in metal-organic frameworks, J. Am. Chem. Soc. 142 (52) (2020) 21720–21729, https://doi.org/10.1021/jacs.0c09284.

[28] N. Calvo Galve, A. Abrishamkar, A. Sorrenti, L. Di Rienzo, M. Satta, M. D'Abramo, E. Coronado, A.J. de Mello, G. Mínguez Espallargas, J. Puigmartí-Luis, Exploiting reaction-diffusion conditions to trigger pathway complexity in the growth of a MOF, Angew. Chem. Int. Ed. 60 (29) (2021) 15920–15927, https://doi.org/10.1002/anie.202101611.

[29] P.F. Rosen, M.S. Dickson, J.J. Calvin, N.L. Ross, T. Friščić, A. Navrotsky, B. F. Woodfield, Thermodynamic evidence of structural transformations in CO2-loaded metal-organic framework Zn(MeIm)2 from heat capacity measurements, J. Am. Chem. Soc. 142 (10) (2020) 4833–4841, https://doi.org/10.1021/jacs.9b13883.

[30] Y. Gu, J.-J. Zheng, K.-I. Otake, K. Sugimoto, N. Hosono, S. Sakaki, F. Li, S. Kitagawa, Structural-deformation-energy-modulation strategy in a soft porous coordination polymer with an interpenetrated framework, Angew. Chem. Int. Ed. 59 (36) (2020) 15517–15521, https://doi.org/10.1002/anie.202003186.

[31] R. Maity, D. Chakraborty, S. Nandi, A.K. Yadav, D. Mullangi, C. Vinod, R. Vaidhyanathan, Aqueous-phase differentiation and speciation of Fe3+ and Fe2+ using water-stable photoluminescent lanthanide-based metal–organic framework, ACS Appl. Nano Mater. 2 (8) (2019) 5169–5178.

[32] J. Wang, Y. Fan, H.-W. Lee, C. Yi, C. Cheng, X. Zhao, M. Yang, Ultrasmall metal–organic framework Zn-MOF-74 nanodots: size-controlled synthesis and application for highly selective colorimetric sensing of iron (III) in aqueous solution, ACS Appl. Nano Mater. 1 (7) (2018) 3747–3753.

[33] X. Fang, X. Chen, Y. Liu, Q. Li, Z. Zeng, T. Maiyalagan, S. Mao, Nanocomposites of Zr (IV)-based metal–organic frameworks and reduced graphene oxide for electrochemically sensing ciprofloxacin in water, ACS Appl. Nano Mater. 2 (4) (2019) 2367–2376.

[34] P. Li, X.-M. Yin, L.-L. Gao, S.-L. Yang, Q. Sui, T. Gong, E.-Q. Gao, Modulating excitation energy of luminescent metal–organic frameworks for detection of Cr (VI) in water, ACS Appl. Nano Mater. 2 (7) (2019) 4646–4654.

[35] N. Zhang, S. Ruan, Y. Yin, F. Li, S. Wen, Y. Chen, Self-sacrificial template-driven LaFeO3/α-Fe2O3 porous nano-octahedrons for acetone sensing, ACS Appl. Nano Mater. 1 (9) (2018) 4671–4681.

[36] K. Wang, C. Wu, F. Wang, G. Jiang, MOF-derived CoP x nanoparticles embedded in nitrogen-doped porous carbon polyhedrons for nanomolar sensing of p-nitrophenol, ACS Appl. Nano Mater. 1 (10) (2018) 5843–5853.

[37] R.N. Widmer, G.I. Lampronti, B. Kunz, C. Battaglia, J.H. Shepherd, S.A. Redfern, T.D. Bennett, Manufacturing macroporous monoliths of microporous metal–organic frameworks, ACS Appl. Nano Mater. 1 (2) (2018) 497–500.

[38] W. Liang, C.J. Coghlan, F. Ragon, M. Rubio-Martinez, D.M. D'Alessandro, R. Babarao, Defect engineering of UiO-66 for CO 2 and H 2 O uptake–a combined experimental and simulation study, Dalton Transac. 45 (11) (2016) 4496–4500.

[39] X. Zhang, S. Zhang, Y. Tang, X. Huang, H. Pang, Recent advances and challenges of metal–organic framework/graphene-based composites, Comp. Part b: Eng. 230 (2022), 109532, https://doi.org/10.1016/j.compositesb.2021.109532.

[40] P. Li, N.A. Vermeulen, C.D. Malliakas, D.A. Gómez-Gualdrón, A.J. Howarth, B. L. Mehdi, A. Dohnalkova, N.D. Browning, M. O'Keeffe, O.K. Farha, Bottom-up construction of a superstructure in a porous uranium-organic crystal, Science 356 (6338) (2017) 624–627, https://doi.org/10.1126/science.aam7851.

[41] C.K. Brozek, V.K. Michaelis, T.-C. Ong, L. Bellarosa, N. López, R.G. Griffin, M. Dincă, Dynamic DMF binding in MOF-5 enables the formation of metastable cobalt-substituted MOF-5 analogues, ACS Central Sci. 1 (5) (2015) 252–260, https://doi.org/10.1021/acscentsci.5b00247.

[42] J.W. Yoon, H. Chang, S.-J. Lee, Y.K. Hwang, D.-Y. Hong, S.-K. Lee, J.S. Lee, S. Jang, T.-U. Yoon, K. Kwac, Y. Jung, R.S. Pillai, F. Faucher, A. Vimont, M. Daturi, G. Férey, C. Serre, G. Maurin, Y.-S. Bae, J.-S. Chang, Selective nitrogen capture by porous hybrid materials containing accessible transition metal ion sites, Nat. Mater. 16 (5) (2017) 526–531, https://doi.org/10.1038/nmat4825.

[43] C. Jiang, X. Wang, Y. Ouyang, K. Lu, W. Jiang, H. Xu, X. Wei, Z. Wang, F. Dai, D. Sun, Recent advances in metal–organic frameworks for gas adsorption/separation, Nanoscale Adv. 4 (9) (2022) 2077–2089, https://doi.org/10.1039/D2NA00061J.

[44] N. Makhanya, B. Oboirien, J. Ren, N. Musyoka, A. Sciacovelli, Recent advances on thermal energy storage using metal-organic frameworks (MOFs), J. Energy Stor. 34 (2021), 102179, https://doi.org/10.1016/j.est.2020.102179.

[45] T. Jia, Y. Gu, F. Li, Progress and potential of metal-organic frameworks (MOFs) for gas storage and separation: a review, J. Environ. Chem. Eng. 10 (5) (2022), 108300, https://doi.org/10.1016/j.jece.2022.108300.
[46] J. Abdi, A.J. Sisi, M. Hadipoor, A. Khataee, State of the art on the ultrasonic-assisted removal of environmental pollutants using metal-organic frameworks, J. Hazard. Mater. 424 (2022), 127558, https://doi.org/10.1016/j.jhazmat.2021.127558.
[47] D.Y. Heo, H.H. Do, S.H. Ahn, S.Y. Kim, Metal-organic framework materials for perovskite solar cells, Polymers 12 (9) (2020) 2061.
[48] H. Ren, T. Wei, Electrochemical synthesis methods of metal-organic frameworks and their environmental analysis applications: a review, ChemElectroChem 9 (13) (2022) e202200196.
[49] M. Varsha, G. Nageswaran, Direct electrochemical synthesis of metal organic frameworks, J. Electrochem. Soc. 167 (15) (2020), 155527.
[50] U. Mueller, M. Schubert, F. Teich, H. Puetter, K. Schierle-Arndt, J. Pastre, Metal–organic frameworks—prospective industrial applications, J. Mater. Chem. 16 (7) (2006) 626–636.
[51] V.F. Yusuf, N.I. Malek, S.K. Kailasa, Review on metal-organic framework classification, synthetic approaches, and influencing factors: applications in energy, drug delivery, and wastewater treatment, ACS Omega 7 (49) (2022) 44507–44531, https://doi.org/10.1021/acsomega.2c05310.
[52] H. Al-Kutubi, J. Gascon, E.J. Sudhölter, L. Rassaei, Electrosynthesis of metal–organic frameworks: challenges and opportunities, ChemElectroChem 2 (4) (2015) 462–474.
[53] M. Jiao, Z. Chen, N. Wang, L. Liu, DFT calculation screened CoCu and CoFe dual-atom catalysts with remarkable hydrogen evolution reaction activity, Appl. Catal. B 324 (2023), 122244.
[54] M. Li, M. Dinca, Reductive electrosynthesis of crystalline metal–organic frameworks, J. Am. Chem. Soc. 133 (33) (2011) 12926–12929.
[55] G. Loget, J. Roche, E. Gianessi, L. Bouffier, A. Kuhn, Indirect bipolar electrodeposition, J. Am. Chem. Soc. 134 (49) (2012) 20033–20036.
[56] S. Yadnum, J. Roche, E. Lebraud, P. Négrier, P. Garrigue, D. Bradshaw, C. Warakulwit, J. Limtrakul, A. Kuhn, Site-selective synthesis of janus-type metal-organic framework composites, Angew. Chem. 126 (15) (2014) 4082–4086.
[57] I. Malytska, C.C. Mézière, M. Kielar, L. Hirsch, G. Wantz, N. Avarvari, A. Kuhn, L. Bouffier, Bipolar electrochemistry with organic single crystals for wireless synthesis of metal–organic Janus objects and asymmetric photovoltage generation, J. Phys. Chem. C 121 (23) (2017) 12921–12927.
[58] M. Fuseini, M.M.Y. Zaghloul, Qualitative and statistical approaches of the electrophoretic deposition kinetics of polyaniline copper coating, Prog. Org. Coat. 171 (2022), 107015.
[59] W.-J. Li, M. Tu, R. Cao, R.A. Fischer, Metal–organic framework thin films: electrochemical fabrication techniques and corresponding applications & perspectives, J. Mater. Chem. A 4 (32) (2016) 12356–12369.
[60] I. Hod, W. Bury, D.M. Karlin, P. Deria, C.W. Kung, M.J. Katz, M. So, B. Klahr, D. Jin, Y.W. Chung, Directed growth of electroactive metal-organic framework thin films using electrophoretic deposition, Adv. Mater. 26 (36) (2014) 6295–6300.
[61] R. Ameloot, L. Pandey, M. Van der Auweraer, L. Alaerts, B.F. Sels, D.E. De Vos, Patterned film growth of metal–organic frameworks based on galvanic displacement, Chem. Commun. 46 (21) (2010) 3735–3737.
[62] A. Ghoorchian, A. Afkhami, T. Madrakian, M. Ahmadi, Electrochemical synthesis of MOFs, Elsevier, Metal-Organic Frameworks for Biomedical Applications, 2020, pp. 177–195.
[63] A.A. Michalchuk, E.V. Boldyreva, A.M. Belenguer, F. Emmerling, V.V. Boldyrev, Tribochemistry, mechanical alloying, mechanochemistry: what is in a name? Front. Chem. 9 (2021), 685789.
[64] P. Baláž, P. Baláž, Mechanochemistry in minerals engineering, Springer, 2008.
[65] T. Friščić, Supramolecular concepts and new techniques in mechanochemistry: cocrystals, cages, rotaxanes, open metal–organic frameworks, Chem. Soc. Rev. 41 (9) (2012) 3493–3510.
[66] A. Pichon, A. Lazuen-Garay, S.L. James, Solvent-free synthesis of a microporous metal–organic framework, CrstEngComm 8 (3) (2006) 211–214.
[67] A. Gedanken, Using sonochemistry for the fabrication of nanomaterials, Ultrason. Sonochem. 11 (2) (2004) 47–55.
[68] N. Stock, S. Biswas, Synthesis of metal-organic frameworks (MOFs): routes to various MOF topologies, Morphologies, and Composites, Chemical Reviews 112 (2) (2012) 933–969, https://doi.org/10.1021/cr200304e.
[69] T. Tsuzuki, Mechanochemical synthesis of metal oxide nanoparticles, Communications Chemistry 4 (1) (2021) 143.
[70] S. Głowniak, B. Szczęśniak, J. Choma, M. Jaroniec, Advances in microwave synthesis of nanoporous materials, Adv. Mater. 33 (48) (2021) 2103477.
[71] H. Furukawa, F. Gandara, Y.-B. Zhang, J. Jiang, W.L. Queen, M.R. Hudson, O. M. Yaghi, Water adsorption in porous metal–organic frameworks and related materials, J. Am. Chem. Soc. 136 (11) (2014) 4369–4381.
[72] J. Klinowski, F.A.A. Paz, P. Silva, J. Rocha, Microwave-assisted synthesis of metal–organic frameworks, Dalton Trans. 40 (2) (2011) 321–330.
[73] N.A. Khan, S.H. Jhung, Synthesis of metal-organic frameworks (MOFs) with microwave or ultrasound: rapid reaction, phase-selectivity, and size reduction, Coord. Chem. Rev. 285 (2015) 11–23.
[74] R. Singh, R. Kumar, D. Singh, R. Savu, S. Moshkalev, Progress in microwave-assisted synthesis of quantum dots (graphene/carbon/semiconducting) for bioapplications: a review, Mater. Today Chem. 12 (2019) 282–314.
[75] G.S. Deyko, L.M. Glukhov, V.I. Isaeva, V.V. Chernyshev, V.V. Vergun, D. A. Archipov, G.I. Kapustin, O.P. Tkachenko, V.D. Nissenbaum, L.M. Kustov, Modifying HKUST-1 crystals for selective ethane adsorption using ionic liquids as synthesis media, Crystals 12 (2) (2022) 279.
[76] K.M. Taylor-Pashow, J. Della Rocca, Z. Xie, S. Tran, W. Lin, Postsynthetic modifications of iron-carboxylate nanoscale metal− organic frameworks for imaging and drug delivery, J. Am. Chem. Soc. 131 (40) (2009) 14261–14263.
[77] Z. Ni, R.I. Masel, Rapid production of metal− organic frameworks via microwave-assisted solvothermal synthesis, J. Am. Chem. Soc. 128 (38) (2006) 12394–12395.
[78] Y.-K. Seo, G. Hundal, I.T. Jang, Y.K. Hwang, C.-H. Jun, J.-S. Chang, Microwave synthesis of hybrid inorganic–organic materials including porous Cu3 (BTC) 2 from Cu (II)-trimesate mixture, Microporous Mesoporous Mater. 119 (1–3) (2009) 331–337.
[79] J.-H. Park, S.-H. Park, S.-H. Jhung, Microwave-syntheses of zeolitic imidazolate framework material, ZIF-8, J. Korean Chem. Soc. 53 (5) (2009) 553–559.
[80] G. Blanita, G. Borodi, M.D. Lazar, A.-R. Biris, L. Barbu-Tudoran, I. Coldea, D. Lupu, Microwave assisted non-solvothermal synthesis of metal–organic frameworks, RSC Adv. 6 (31) (2016) 25967–25974, https://doi.org/10.1039/C5RA26097C.
[81] C. Palomino Cabello, C.O. Arean, J.B. Parra, C.O. Ania, P. Rumori, G. Turnes Palomino, A rapid microwave-assisted synthesis of a sodium–cadmium metal–organic framework having improved performance as a CO2 adsorbent for CCS, Dalton Trans. 44 (21) (2015) 9955–9963, https://doi.org/10.1039/C5DT00909J.
[82] F. Yang, H. Huang, X. Wang, F. Li, Y. Gong, C. Zhong, J.-R. Li, Proton conductivities in functionalized UiO-66: tuned properties, thermogravimetry mass, and molecular simulation analyses, Cryst. Growth Des. 15 (12) (2015) 5827–5833.
[83] H. Guo, Z. Zheng, Y. Zhang, H. Lin, Q. Xu, Highly selective detection of Pb2+ by a nanoscale Ni-based metal–organic framework fabricated through one-pot hydrothermal reaction, Sens. Actuators B 248 (2017) 430–436.
[84] B. Li, Y. Zhang, D. Ma, L. Li, G. Li, G. Li, Z. Shi, S. Feng, A strategy toward constructing a bifunctionalized MOF catalyst: post-synthetic modification of MOFs on organic ligands and coordinatively unsaturated metal sites, Chem. Commun. 48 (49) (2012) 6151–6153, https://doi.org/10.1039/C2CC32384B.
[85] G. Xu, T. Yamada, K. Otsubo, S. Sakaida, H. Kitagawa, Facile "modular assembly" for fast construction of a highly oriented crystalline MOF nanofilm, J. Am. Chem. Soc. 134 (40) (2012) 16524–16527.
[86] A. Anumah, H. Louis, A. Hamzat, O. Amusan, Metal-organic frameworks (MOFs): recent advances in synthetic methodologies and some applications, Chem. Methodol 3 (2019) 283–305.
[87] D. Chen, Y. Zhang, B. Chen, Z. Kang, Coupling effect of microwave and mechanical forces during the synthesis of ferrite nanoparticles by microwave-assisted ball milling, Ind. Eng. Chem. Res. 52 (39) (2013) 14179–14184.
[88] E.R. Parnham, R.E. Morris, Ionothermal synthesis of zeolites, metal–organic frameworks, and inorganic–organic hybrids, Acc. Chem. Res. 40 (10) (2007) 1005–1013.
[89] E.R. Parnham, R.E. Morris, The ionothermal synthesis of cobalt aluminophosphate zeolite frameworks, J. Am. Chem. Soc. 128 (7) (2006) 2204–2205.
[90] Y.-R. Lee, J. Kim, W.-S. Ahn, Synthesis of metal-organic frameworks: a mini review, Korean J. Chem. Eng. 30 (2013) 1667–1680.
[91] Y. Bian, N. Xiong, G. Zhu, Technology for the remediation of water pollution: A review on the fabrication of metal organic frameworks, Processes 6 (8) (2018) 122.
[92] C. Mottillo, T. Friščić, Advances in solid-state transformations of coordination bonds: From the ball mill to the aging chamber, Molecules 22 (1) (2017) 144.
[93] S.F. Ahmed, M. Mofijur, N. Islam, T.A. Parisa, N. Rafa, A. Bokhari, J.J. Klemeš, T. M. Indra Mahlia, Insights into the development of microbial fuel cells for generating biohydrogen, bioelectricity, and treating wastewater, Energy 254 (2022), 124163, https://doi.org/10.1016/j.energy.2022.124163.
[94] J. Ortigueira, T. Pinto, L. Gouveia, P. Moura, Production and storage of biohydrogen during sequential batch fermentation of Spirogyra hydrolyzate by Clostridium butyricum, Energy 88 (2015) 528–536, https://doi.org/10.1016/j.energy.2015.05.070.
[95] J.O. Abe, A.P.I. Popoola, E. Ajenifuja, O.M. Popoola, Hydrogen energy, economy and storage: review and recommendation, Int. J. Hydrogen Energy 44 (29) (2019) 15072–15086, https://doi.org/10.1016/j.ijhydene.2019.04.068.
[96] D. Broom, C. Webb, K. Hurst, P. Parilla, T. Gennett, C. Brown, R. Zacharia, E. Tylianakis, E. Klontzas, G. Froudakis, Outlook and challenges for hydrogen storage in nanoporous materials, Appl. Phys. A 122 (2016) 1–21.
[97] N.L. Rosi, J. Eckert, M. Eddaoudi, D.T. Vodak, J. Kim, M. O'Keeffe, O.M. Yaghi, Hydrogen storage in microporous metal-organic frameworks, Science 300 (5622) (2003) 1127–1129.
[98] R. Singh, A. Altaee, S. Gautam, Nanomaterials in the advancement of hydrogen energy storage, Heliyon 6 (7) (2020) e04487.
[99] H. Furukawa, N. Ko, Y.B. Go, N. Aratani, S.B. Choi, E. Choi, A.Ö. Yazaydin, R. Q. Snurr, M. O'Keeffe, J. Kim, Ultrahigh porosity in metal-organic frameworks, Science 329 (5990) (2010) 424–428.
[100] A. Schoedel, Z. Ji, O.M. Yaghi, The role of metal–organic frameworks in a carbon-neutral energy cycle, Nat. Energy 1 (4) (2016) 1–13.
[101] K. Suresh, D. Aulakh, J. Purewal, D.J. Siegel, M. Veenstra, A.J. Matzger, Optimizing hydrogen storage in MOFs through engineering of crystal morphology and control of crystal size, J. Am. Chem. Soc. 143 (28) (2021) 10727–10734, https://doi.org/10.1021/jacs.1c04926.
[102] M.P. Suh, H.J. Park, T.K. Prasad, D.-W. Lim, Hydrogen storage in metal–organic frameworks, Chem. Rev. 112 (2) (2012) 782–835.

[103] E. Knerelman, Y.A. Karozina, I. Shunina, I. Sedov, Highly porous materials as potential components of natural gas storage systems: part 2 (a review), Pet. Chem. 62 (7) (2022) 677–713.

[104] S. Ma, J. Eckert, P.M. Forster, J.W. Yoon, Y.K. Hwang, J.-S. Chang, C.D. Collier, J. B. Parise, H.-C. Zhou, Further investigation of the effect of framework catenation on hydrogen uptake in metal− organic frameworks, J. Am. Chem. Soc. 130 (47) (2008) 15896–15902.

[105] B.P. Tarasov, P.V. Fursikov, A.A. Volodin, M.S. Bocharnikov, Y.Y. Shimkus, A. M. Kashin, V.A. Yartys, S. Chidziva, S. Pasupathi, M.V. Lototskyy, Metal Hydride hydrogen storage and compression systems for energy storage technologies, Int. J. Hydrogen Energy 46 (25) (2021) 13647–13657.

[106] C. Milanese, T.R. Jensen, B. Hauback, C. Pistidda, M. Dornheim, H. Yang, L. Lombardo, A. Zuettel, Y. Filinchuk, P. Ngene, Complex hydrides for energy storage, Int. J. Hydrogen Energy 44 (15) (2019) 7860–7874.

[107] C. Lang, Y. Jia, X. Yao, Recent advances in liquid-phase chemical hydrogen storage, Energy Storage Mater. 26 (2020) 290–312.

[108] R. Hren, A. Vujanović, Y. Van Fan, J.J. Klemeš, D. Krajnc, L. Čuček, Hydrogen production, storage and transport for renewable energy and chemicals: an environmental footprint assessment, Renew. Sustain. Energy Rev. 173 (2023), 113113.

[109] A. Gupta, G.V. Baron, P. Perreault, S. Lenaerts, R.-G. Ciocarlan, P. Cool, P. G. Mileo, S. Rogge, V. Van Speybroeck, G. Watson, Hydrogen clathrates: next generation hydrogen storage materials, Energy Storage Mater. 41 (2021) 69–107.

[110] N. Kosar, S. Munsif, K. Ayub, T. Mahmood, Storage and permeation of hydrogen molecule, atom and ions (H+ and H−) through silicon carbide nanotube; a DFT approach, Int. J. Hydrogen Energy 46 (13) (2021) 9163–9173.

[111] K. Cousins, R. Zhang, Highly porous organic polymers for hydrogen fuel storage, Polymers 11 (4) (2019) 690.

[112] D. Czarna-Juszkiewicz, J. Cader, M. Wdowin, From coal ashes to solid sorbents for hydrogen storage, J. Clean. Prod. 270 (2020), 122355.

[113] A.G. Wong-Foy, A.J. Matzger, O.M. Yaghi, Exceptional H2 saturation uptake in microporous metal− organic frameworks, J. Am. Chem. Soc. 128 (11) (2006) 3494–3495.

[114] R. Wang, X. Liu, D. Qi, Y. Xu, L. Zhang, X. Liu, J. Jiang, F. Dai, X. Xiao, D. Sun, A Zn metal–organic framework with high stability and sorption selectivity for CO2, Inorg. Chem. 54 (22) (2015) 10587–10592.

[115] A. Sayari, Y. Belmabkhout, R. Serna-Guerrero, Flue gas treatment via CO2 adsorption, Chem. Eng. J. 171 (3) (2011) 760–774.

[116] X. Lin, J. Jia, X. Zhao, K.M. Thomas, A.J. Blake, G.S. Walker, N.R. Champness, P. Hubberstey, M. Schröder, High H2 adsorption by coordination-framework materials, Angew. Chem. 118 (44) (2006) 7518–7524.

[117] M.H. Rosnes, M. Opitz, M. Frontzek, W. Lohstroh, J.P. Embs, P.A. Georgiev, P. D. Dietzel, Intriguing differences in hydrogen adsorption in CPO-27 materials induced by metal substitution, J. Mater. Chem. A 3 (9) (2015) 4827–4839.

[118] B. Xiao, P.S. Wheatley, X. Zhao, A.J. Fletcher, S. Fox, A.G. Rossi, I.L. Megson, S. Bordiga, L. Regli, K.M. Thomas, High-capacity hydrogen and nitric oxide adsorption and storage in a metal− organic framework, J. Am. Chem. Soc. 129 (5) (2007) 1203–1209.

[119] J.A. Villajos, G. Orcajo, C. Martos, J.Á. Botas, J. Villacañas, G. Calleja, Co/ni mixed-metal sited MOF-74 material as hydrogen adsorbent, Int. J. Hydrogen Energy 40 (15) (2015) 5346–5352.

[120] W. Qin, W. Cao, H. Liu, Z. Li, Y. Li, Metal–organic framework MIL-101 doped with palladium for toluene adsorption and hydrogen storage, RSC Adv. 4 (5) (2014) 2414–2420.

[121] J. Kim, S. Yeo, J.-D. Jeon, S.-Y. Kwak, Enhancement of hydrogen storage capacity and hydrostability of metal–organic frameworks (MOFs) with surface-loaded platinum nanoparticles and carbon black, Microporous Mesoporous Mater. 202 (2015) 8–15.

[122] S. Barman, A. Khutia, R. Koitz, O. Blacque, H. Furukawa, M. Iannuzzi, O.M. Yaghi, C. Janiak, J. Hutter, H. Berke, Synthesis and hydrogen adsorption properties of internally polarized 2, 6-azulenedicarboxylate based metal–organic frameworks, J. Mater. Chem. A 2 (44) (2014) 18823–18830.

[123] M. Latroche, S. Surblé, C. Serre, C. Mellot-Draznieks, P.L. Llewellyn, J.H. Lee, J. S. Chang, S.H. Jhung, G. Férey, Hydrogen storage in the giant-pore metal–organic frameworks MIL-100 and MIL-101, Angew. Chem. 118 (48) (2006) 8407–8411.

[124] B. Xiao, Q. Yuan, Nanoporous metal organic framework materials for hydrogen storage, Particuology 7 (2) (2009) 129–140.

[125] K. Sumida, S. Horike, S.S. Kaye, Z.R. Herm, W.L. Queen, C.M. Brown, F. Grandjean, G.J. Long, A. Dailly, J.R. Long, Hydrogen storage and carbon dioxide capture in an iron-based sodalite-type metal–organic framework (Fe-BTT) discovered via high-throughput methods, Chem. Sci. 1 (2) (2010) 184–191.

[126] S.E. Bambalaza, H.W. Langmi, R. Mokaya, N.M. Musyoka, L.E. Khotseng, Experimental demonstration of dynamic temperature-dependent behavior of UiO-66 metal–organic framework: compaction of hydroxylated and dehydroxylated forms of UiO-66 for high-pressure hydrogen storage, ACS Appl. Mater. Interfaces 12 (22) (2020) 24883–24894.

[127] L.Y. Molefe, N.M. Musyoka, J. Ren, H.W. Langmi, M. Mathe, P.G. Ndungu, Polymer-based shaping strategy for zeolite templated carbons (ZTC) and their metal organic framework (MOF) composites for improved hydrogen storage properties, Front. Chem. 7 (2019) 864.

[128] I.A. Ibarra, S. Yang, X. Lin, A.J. Blake, P.J. Rizkallah, H. Nowell, D.R. Allan, N. R. Champness, P. Hubberstey, M. Schröder, Highly porous and robust scandium-based metal–organic frameworks for hydrogen storage, Chem. Commun. 47 (29) (2011) 8304–8306.

[129] Y. Wang, Z. Lan, X. Huang, H. Liu, J. Guo, Study on catalytic effect and mechanism of MOF (MOF= ZIF-8, ZIF-67, MOF-74) on hydrogen storage properties of magnesium, Int. J. Hydrogen Energy 44 (54) (2019) 28863–28873.

[130] N.M. Musyoka, J. Ren, H.W. Langmi, B.C. North, M. Mathe, D. Bessarabov, Synthesis of rGO/Zr-MOF composite for hydrogen storage application, J. Alloy. Compd. 724 (2017) 450–455.

[131] H.J. Choi, M. Dincă, A. Dailly, J.R. Long, Hydrogen storage in water-stable metal–organic frameworks incorporating 1, 3-and 1, 4-benzenedipyrazolate, Energ. Environ. Sci. 3 (1) (2010) 117–123.

[132] S. Yu, G. Jing, S. Li, Z. Li, X. Ju, Tuning the hydrogen storage properties of MOF-650: a combined DFT and GCMC simulations study, Int. J. Hydrogen Energy 45 (11) (2020) 6757–6764.

[133] M. Hirscher, B. Panella, B. Schmitz, Metal-organic frameworks for hydrogen storage, Microporous Mesoporous Mater. 129 (3) (2010) 335–339.

[134] S. Chen, Y. Li, L. Mi, Porous carbon derived from metal organic framework for gas storage and separation: the size effect, Inorg. Chem. Commun. 118 (2020), 107999.

[135] G. Orcajo, H. Montes-Andres, J.A. Villajos, C. Martos, J.A. Botas, G. Calleja, Li-crown ether complex inclusion in MOF materials for enhanced H2 volumetric storage capacity at room temperature, Int. J. Hydrogen Energy 44 (35) (2019) 19285–19293.

[136] L. Xia, Q. Liu, Adsorption of H2 on aluminum-based metal-organic frameworks: a computational study, Comput. Mater. Sci 126 (2017) 176–181.

[137] N.M. Musyoka, K.M. Rambau, N. Manyala, J. Ren, H.W. Langmi, M.K. Mathe, Utilization of waste tyres pyrolysis oil vapour in the synthesis of zeolite templated carbons (ZTCs) for hydrogen storage application, J. Environ. Sci. Health A 53 (11) (2018) 1022–1028.

[138] S. Rochat, K. Polak-Kraśna, M. Tian, L.T. Holyfield, T.J. Mays, C.R. Bowen, A. D. Burrows, Hydrogen storage in polymer-based processable microporous composites, J. Mater. Chem. A 5 (35) (2017) 18752–18761.

[139] A. Ahmed, Y. Liu, J. Purewal, L.D. Tran, A.G. Wong-Foy, M. Veenstra, A. J. Matzger, D.J. Siegel, Balancing gravimetric and volumetric hydrogen density in MOFs, Energ. Environ. Sci. 10 (11) (2017) 2459–2471.

[140] R. Grünker, V. Bon, P. Müller, U. Stoeck, S. Krause, U. Mueller, I. Senkovska, S. Kaskel, A new metal–organic framework with ultra-high surface area, Chem. Commun. 50 (26) (2014) 3450–3452.

[141] Y. Yan, I. Da Silva, A.J. Blake, A. Dailly, P. Manuel, S. Yang, M. Schroder, High volumetric hydrogen adsorption in a porous anthracene-decorated metal–organic framework, Inorg. Chem. 57 (19) (2018) 12050–12055.

[142] J. Liu, R. Zou, Y. Zhao, Recent developments in porous materials for H2 and CH4 storage, Tetrahedron Lett. 57 (44) (2016) 4873–4881.

[143] Z. Yang, W. Xiong, J. Wang, Y. Zhu, Y. Xia, A systematic study on the preparation and hydrogen storage of zeolite 13X-templated microporous carbons, Eur. J. Inorg. Chem. 2016 (13–14) (2016) 2152–2158.

[144] I. Sreedhar, K.M. Kamani, B.M. Kamani, B.M. Reddy, A. Venugopal, A Bird's Eye view on process and engineering aspects of hydrogen storage, Renew. Sustain. Energy Rev. 91 (2018) 838–860.

[145] P. Suksaengrat, V. Amornkitbamrung, P. Srepusharawoot, R. Ahuja, Density functional theory study of hydrogen adsorption in a Ti-decorated Mg-based metal-organic framework-74, ChemPhysChem 17 (6) (2016) 879–884.

[146] D.A. Gómez-Gualdrón, Y.J. Colón, X. Zhang, T.C. Wang, Y.-S. Chen, J.T. Hupp, T. Yildirim, O.K. Farha, J. Zhang, R.Q. Snurr, Evaluating topologically diverse metal–organic frameworks for cryo-adsorbed hydrogen storage, Energ. Environ. Sci. 9 (10) (2016) 3279–3289.

[147] S. Gadipelli, J. Ford, W. Zhou, H. Wu, T.J. Udovic, T. Yildirim, Nanoconfinement and catalytic dehydrogenation of ammonia borane by magnesium-metal–organic-framework-74, Chem.–A Euro. J. 17 (22) (2011) 6043–6047.

[148] D.W. Lim, J.W. Yoon, K.Y. Ryu, M.P. Suh, Magnesium nanocrystals embedded in a metal–organic framework: hybrid hydrogen storage with synergistic effect on physi-and chemisorption, Angew. Chem. Int. Ed. 51 (39) (2012) 9814–9817.

[149] B. Aghel, S. Behaein, F. Alobaid, CO2 capture from biogas by biomass-based adsorbents: a review, Fuel 328 (2022), 125276, https://doi.org/10.1016/j.fuel.2022.125276.

[150] M. Qi, Y. Liu, T. He, L. Yin, C.-M. Shu, I. Moon, System perspective on cleaner technologies for renewable methane production and utilisation towards carbon neutrality: principles, techno-economics, and carbon footprints, Fuel 327 (2022), 125130.

[151] H. Liu, W. Ding, F. Zhou, G. Yang, Y. Du, An overview and outlook on gas adsorption: for the enrichment of low concentration coalbed methane, Sep. Sci. Technol. 55 (6) (2020) 1102–1114.

[152] Y. He, W. Zhou, G. Qian, B. Chen, Methane storage in metal–organic frameworks, Chem. Soc. Rev. 43 (16) (2014) 5657–5678.

[153] B. Li, H.-M. Wen, W. Zhou, J.Q. Xu, B. Chen, Porous metal-organic frameworks: promising materials for methane storage, Chem 1 (4) (2016) 557–580, https://doi.org/10.1016/j.chempr.2016.09.009.

[154] C. Wang, D. Liu, W. Lin, Metal–organic frameworks as a tunable platform for designing functional molecular materials, J. Am. Chem. Soc. 135 (36) (2013) 13222–13234.

[155] P. Wang, Y. Teng, J. Zhu, W. Bao, S. Han, Y. Li, Y. Zhao, H. Xie, Review on the synergistic effect between metal–organic frameworks and gas hydrates for CH4 storage and CO2 separation applications, Renew. Sustain. Energy Rev. 167 (2022), 112807, https://doi.org/10.1016/j.rser.2022.112807.

[156] M. Kondo, T. Yoshitomi, H. Matsuzaka, S. Kitagawa, K. Seki, Three-dimensional framework with channeling cavities for small molecules:{[M2 (4, 4′-bpy) 3 (NO3) 4]· xH2O} n (M=Co, Ni, Zn), Angew. Chem. Int. Ed. Eng. 36 (16) (1997) 1725–1727.

[157] Y. Peng, V. Krungleviciute, I. Eryazici, J.T. Hupp, O.K. Farha, T. Yildirim, Methane storage in metal–organic frameworks: current records, surprise findings, and challenges, J. Am. Chem. Soc. 135 (32) (2013) 11887–11894.
[158] Z. Hulvey, B. Vlaisavljevich, J.A. Mason, E. Tsivion, T.P. Dougherty, E.D. Bloch, M. Head-Gordon, B. Smit, J.R. Long, C.M. Brown, Critical factors driving the high volumetric uptake of methane in Cu3 (btc) 2, J. Am. Chem. Soc. 137 (33) (2015) 10816–10825.
[159] G. Barin, V. Krungleviciute, D.A. Gomez-Gualdron, A.A. Sarjeant, R.Q. Snurr, J. T. Hupp, T. Yildirim, O.K. Farha, Isoreticular series of (3, 24)-connected metal–organic frameworks: facile synthesis and high methane uptake properties, Chem. Mater. 26 (5) (2014) 1912–1917.
[160] J.A. Mason, J. Oktawiec, M.K. Taylor, M.R. Hudson, J. Rodriguez, J.E. Bachman, M.I. Gonzalez, A. Cervellino, A. Guagliardi, C.M. Brown, Methane storage in flexible metal–organic frameworks with intrinsic thermal management, Nature 527 (7578) (2015) 357–361.
[161] K. Seki, W. Mori, Syntheses and characterization of microporous coordination polymers with open frameworks, J. Phys. Chem. B 106 (6) (2002) 1380–1385.
[162] H. Kim, D.G. Samsonenko, S. Das, G.H. Kim, H.S. Lee, D.N. Dybtsev, E. A. Berdonosova, K. Kim, Methane sorption and structural characterization of the sorption sites in Zn2 (bdc) 2 (dabco) by single crystal X-ray crystallography, Chem.–An Asian J. 4 (6) (2009) 886–891.
[163] H. Li, L. Li, R.-B. Lin, W. Zhou, Z. Zhang, S. Xiang, B. Chen, Porous metal-organic frameworks for gas storage and separation: Status and challenges, EnergyChem 1 (1) (2019), 100006, https://doi.org/10.1016/j.enchem.2019.100006.
[164] D. Alezi, Y. Belmabkhout, M. Suyetin, P.M. Bhatt, Ł.J. Weseliński, V. Solovyeva, K. Adil, I. Spanopoulos, P.N. Trikalitis, A.-H. Emwas, MOF crystal chemistry paving the way to gas storage needs: aluminum-based soc-MOF for CH4, O2, and CO2 storage, J. Am. Chem. Soc. 137 (41) (2015) 13308–13318.
[165] T. Tian, Z. Zeng, D. Vulpe, M.E. Casco, G. Divitini, P.A. Midgley, J. Silvestre-Albero, J.-C. Tan, P.Z. Moghadam, D. Fairen-Jimenez, A sol–gel monolithic metal–organic framework with enhanced methane uptake, Nat. Mater. 17 (2) (2018) 174–179.
[166] C.-X. Chen, Z.-W. Wei, J.-J. Jiang, S.-P. Zheng, H.-P. Wang, Q.-F. Qiu, C.-C. Cao, D. Fenske, C.-Y. Su, Dynamic spacer installation for multirole metal–organic frameworks: a new direction toward multifunctional MOFs achieving ultrahigh methane storage working capacity, J. Am. Chem. Soc. 139 (17) (2017) 6034–6037.
[167] J.M. Lin, C.T. He, Y. Liu, P.Q. Liao, D.D. Zhou, J.P. Zhang, X.M. Chen, A metal–organic framework with a pore size/shape suitable for strong binding and close packing of methane, Angew. Chem. 128 (15) (2016) 4752–4756.
[168] Y. Yan, D.I. Kolokolov, I. Da Silva, A.G. Stepanov, A.J. Blake, A. Dailly, P. Manuel, C.C. Tang, S. Yang, M. Schröder, Porous metal–organic polyhedral frameworks with optimal molecular dynamics and pore geometry for methane storage, J. Am. Chem. Soc. 139 (38) (2017) 13349–13360.
[169] S. Bourrelly, P.L. Llewellyn, C. Serre, F. Millange, T. Loiseau, G. Férey, Different adsorption behaviors of methane and carbon dioxide in the isotypic nanoporous metal terephthalates MIL-53 and MIL-47, J. Am. Chem. Soc. 127 (39) (2005) 13519–13521.
[170] P.L. Llewellyn, S. Bourrelly, C. Serre, A. Vimont, M. Daturi, L. Hamon, G. De Weireld, J.-S. Chang, D.-Y. Hong, Y. Kyu Hwang, High uptakes of CO2 and CH4 in mesoporous metal organic frameworks mil-100 and mil-101, Langmuir 24 (14) (2008) 7245–7250.
[171] D.Y. Hong, Y.K. Hwang, C. Serre, G. Ferey, J.S. Chang, Porous chromium terephthalate MIL-101 with coordinatively unsaturated sites: surface functionalization, encapsulation, sorption and catalysis, Adv. Funct. Mater. 19 (10) (2009) 1537–1552.
[172] J. Jiang, H. Furukawa, Y.-B. Zhang, O.M. Yaghi, High methane storage working capacity in metal–organic frameworks with acrylate links, J. Am. Chem. Soc. 138 (32) (2016) 10244–10251.
[173] F. Gándara, H. Furukawa, S. Lee, O.M. Yaghi, High methane storage capacity in aluminum metal–organic frameworks, J. Am. Chem. Soc. 136 (14) (2014) 5271–5274.
[174] J.A. Mason, M. Veenstra, J.R. Long, Evaluating metal–organic frameworks for natural gas storage, Chem. Sci. 5 (1) (2014) 32–51.
[175] M. Zhang, W. Zhou, T. Pham, K.A. Forrest, W. Liu, Y. He, H. Wu, T. Yildirim, B. Chen, B. Space, Fine tuning of MOF-505 analogues to reduce low-pressure methane uptake and enhance methane working capacity, Angew. Chem. 129 (38) (2017) 11584–11588.
[176] H.M. Wen, B. Li, L. Li, R.B. Lin, W. Zhou, G. Qian, B. Chen, A metal–organic framework with optimized porosity and functional sites for high gravimetric and volumetric methane storage working capacities, Adv. Mater. 30 (16) (2018) 1704792.
[177] Y. Peng, G. Srinivas, C.E. Wilmer, I. Eryazici, R.Q. Snurr, J.T. Hupp, T. Yildirim, O.K. Farha, Simultaneously high gravimetric and volumetric methane uptake characteristics of the metal–organic framework NU-111, Chem. Commun. 49 (29) (2013) 2992–2994.
[178] R.D. Kennedy, V. Krungleviciute, D.J. Clingerman, J.E. Mondloch, Y. Peng, C. E. Wilmer, A.A. Sarjeant, R.Q. Snurr, J.T. Hupp, T. Yildirim, Carborane-based metal–organic framework with high methane and hydrogen storage capacities, Chem. Mater. 25 (17) (2013) 3539–3543.
[179] Z. Chen, P. Li, R. Anderson, X. Wang, X. Zhang, L. Robison, L.R. Redfern, S. Moribe, T. Islamoglu, D.A. Gómez-Gualdrón, Balancing volumetric and gravimetric uptake in highly porous materials for clean energy, Science 368 (6488) (2020) 297–303.
[180] D. Yuan, D. Zhao, D. Sun, H.C. Zhou, An isoreticular series of metal–organic frameworks with dendritic hexacarboxylate ligands and exceptionally high gas-uptake capacity, Angew. Chem. 122 (31) (2010) 5485–5489.
[181] X. Duan, C. Wu, S. Xiang, W. Zhou, T. Yildirim, Y. Cui, Y. Yang, B. Chen, G. Qian, Novel microporous metal–organic framework exhibiting high acetylene and methane storage capacities, Inorg. Chem. 54 (9) (2015) 4377–4381.
[182] C.Ö. Karacan, F.A. Ruiz, M. Cotè, S. Phipps, Coal mine methane: a review of capture and utilization practices with benefits to mining safety and to greenhouse gas reduction, Int. J. Coal Geol. 86 (2–3) (2011) 121–156.
[183] B. Li, H.-M. Wen, H. Wang, H. Wu, T. Yildirim, W. Zhou, B. Chen, Porous metal–organic frameworks with Lewis basic nitrogen sites for high-capacity methane storage, Energ. Environ. Sci. 8 (8) (2015) 2504–2511.
[184] W. Zhou, H. Wu, M.R. Hartman, T. Yildirim, Hydrogen and methane adsorption in metal− organic frameworks: a high-pressure volumetric study, J. Phys. Chem. C 111 (44) (2007) 16131–16137.
[185] J.C. Chien, Polyacetylene: chemistry, physics, and material science, Elsevier, 2012.
[186] Y. He, B. Li, M. O'Keeffe, B. Chen, Multifunctional metal–organic frameworks constructed from meta-benzenedicarboxylate units, Chem. Soc. Rev. 43 (16) (2014) 5618–5656.
[187] R. Matsuda, R. Kitaura, S. Kitagawa, Y. Kubota, R.V. Belosludov, T.C. Kobayashi, H. Sakamoto, T. Chiba, M. Takata, Y. Kawazoe, Highly controlled acetylene accommodation in a metal–organic microporous material, Nature 436 (7048) (2005) 238–241.
[188] S. Xiang, W. Zhou, J.M. Gallegos, Y. Liu, B. Chen, Exceptionally high acetylene uptake in a microporous metal− organic framework with open metal sites, J. Am. Chem. Soc. 131 (34) (2009) 12415–12419.
[189] S. Xiang, W. Zhou, Z. Zhang, M.A. Green, Y. Liu, B. Chen, Open metal sites within isostructural metal–organic frameworks for differential recognition of acetylene and extraordinarily high acetylene storage capacity at room temperature, Angew. Chem. 122 (27) (2010) 4719–4722.
[190] X. Rao, J. Cai, J. Yu, Y. He, C. Wu, W. Zhou, T. Yildirim, B. Chen, G. Qian, A microporous metal–organic framework with both open metal and Lewis basic pyridyl sites for high C 2 H 2 and CH 4 storage at room temperature, Chem. Commun. 49 (60) (2013) 6719–6721.
[191] H.-M. Wen, H. Wang, B. Li, Y. Cui, H. Wang, G. Qian, B. Chen, A microporous metal–organic framework with lewis basic nitrogen sites for high C2H2 storage and significantly enhanced C2H2/CO2 separation at ambient conditions, Inorg. Chem. 55 (15) (2016) 7214–7218.
[192] F. Moreau, I. Da Silva, N.H. Al Smail, T.L. Easun, M. Savage, H.G. Godfrey, S. F. Parker, P. Manuel, S. Yang, M. Schröder, Unravelling exceptional acetylene and carbon dioxide adsorption within a tetra-amide functionalized metal-organic framework, Nat. Commun. 8 (1) (2017) 14085.
[193] M. Zhang, B. Li, Y. Li, Q. Wang, W. Zhang, B. Chen, S. Li, Y. Pan, X. You, J. Bai, Finely tuning MOFs towards high performance in C 2 H 2 storage: synthesis and properties of a new MOF-505 analogue with an inserted amide functional group, Chem. Commun. 52 (45) (2016) 7241–7244.
[194] J. Pang, F. Jiang, M. Wu, C. Liu, K. Su, W. Lu, D. Yuan, M. Hong, A porous metal-organic framework with ultrahigh acetylene uptake capacity under ambient conditions, Nat. Commun. 6 (1) (2015) 7575.
[195] S. Yang, J. Sun, A.J. Ramirez-Cuesta, S.K. Callear, W.I. David, D.P. Anderson, R. Newby, A.J. Blake, J.E. Parker, C.C. Tang, Selectivity and direct visualization of carbon dioxide and sulfur dioxide in a decorated porous host, Nat. Chem. 4 (11) (2012) 887–894.
[196] Y. Cui, Y. Yue, G. Qian, B. Chen, Luminescent functional metal–organic frameworks, Chem. Rev. 112 (2) (2012) 1126–1162.
[197] X. Cui, K. Chen, H. Xing, Q. Yang, R. Krishna, Z. Bao, H. Wu, W. Zhou, X. Dong, Y. Han, Pore chemistry and size control in hybrid porous materials for acetylene capture from ethylene, Science 353 (6295) (2016) 141–144.
[198] J. Cai, H. Wang, H. Wang, X. Duan, Z. Wang, Y. Cui, Y. Yang, B. Chen, G. Qian, An amino-decorated NbO-type metal–organic framework for high C 2 H 2 storage and selective CO 2 capture, RSC Adv. 5 (94) (2015) 77417–77422.
[199] J.-P. Zhang, X.-M. Chen, Optimized acetylene/carbon dioxide sorption in a dynamic porous crystal, J. Am. Chem. Soc. 131 (15) (2009) 5516–5521.
[200] C.-T. He, Z.-M. Ye, Y.-T. Xu, D.-D. Zhou, H.-L. Zhou, D. Chen, J.-P. Zhang, X.-M. Chen, Hyperfine adjustment of flexible pore-surface pockets enables smart recognition of gas size and quadrupole moment, Chem. Sci. 8 (11) (2017) 7560–7565.
[201] T. Ghanbari, F. Abnisa, W.M.A. Wan Daud, A review on production of metal organic frameworks (MOF) for CO2 adsorption, Sci. Total Environ. 707 (2020), 135090, https://doi.org/10.1016/j.scitotenv.2019.135090.
[202] L. Li, H.S. Jung, J.W. Lee, Y.T. Kang, Review on applications of metal–organic frameworks for CO2 capture and the performance enhancement mechanisms, Renew. Sustain. Energy Rev. 162 (2022), 112441, https://doi.org/10.1016/j.rser.2022.112441.
[203] M. Thema, T. Weidlich, M. Hörl, A. Bellack, F. Mörs, F. Hackl, M. Kohlmayer, J. Gleich, C. Stabenau, T. Trabold, Biological CO2-methanation: an approach to standardization, Energies 12 (9) (2019) 1670.
[204] M. Hervy, J. Maistrello, L. Brito, M. Rizand, E. Basset, Y. Kara, M. Maheut, Power-to-gas: CO2 methanation in a catalytic fluidized bed reactor at demonstration scale, experimental results and simulation, J. CO2 Utiliz. 50 (2021), 101610, https://doi.org/10.1016/j.jcou.2021.101610.
[205] S. Chakrabortty, J. Nayak, B. Ruj, P. Pal, R. Kumar, S. Banerjee, M. Sardar, P. Chakraborty, Photocatalytic conversion of CO2 to methanol using membrane-integrated Green approach: a review on capture, conversion and purification,

J. Environ. Chem. Eng. 8 (4) (2020), 103935, https://doi.org/10.1016/j.jece.2020.103935.
[206] S. Chakrabortty, J. Nayak, P. Pal, R. Kumar, S. Banerjee, P.K. Mondal, M. Pal, B. Ruj, Catalytic conversion of CO2 to biofuel (methanol) and downstream separation in membrane-integrated photoreactor system under suitable conditions, Int. J. Hydrogen Energy 45 (1) (2020) 675–690, https://doi.org/10.1016/j.ijhydene.2019.10.220.
[207] S.S. Cordova, M. Gustafsson, M. Eklund, N. Svensson, Potential for the valorization of carbon dioxide from biogas production in Sweden, J. Clean. Prod. 370 (2022), 133498, https://doi.org/10.1016/j.jclepro.2022.133498.
[208] Y. Liu, Z.U. Wang, H.C. Zhou, Recent advances in carbon dioxide capture with metal-organic frameworks, Greenhouse Gases Sci. Technol. 2 (4) (2012) 239–259.
[209] D. Britt, H. Furukawa, B. Wang, T.G. Glover, O.M. Yaghi, Highly efficient separation of carbon dioxide by a metal-organic framework replete with open metal sites, Proceedings of the National Academy of Sciences 106(49) (2009) 20637-20640.
[210] J. Duan, Z. Yang, J. Bai, B. Zheng, Y. Li, S. Li, Highly selective CO 2 capture of an agw-type metal–organic framework with inserted amides: Experimental and theoretical studies, Chem. Commun. 48 (25) (2012) 3058–3060.
[211] S. Kazemi, V. Safarifard, Carbon dioxide capture on metal-organic frameworks with amide-decorated pores, Nanochem. Res. 3 (1) (2018) 62–78, https://doi.org/10.22036/ncr.2018.01.007.
[212] D.-X. Xue, Q. Wang, J. Bai, Amide-functionalized metal–organic frameworks: syntheses, structures and improved gas storage and separation properties, Coord. Chem. Rev. 378 (2019) 2–16.
[213] Z. Lu, J. Bai, C. Hang, F. Meng, W. Liu, Y. Pan, X. You, The utilization of amide groups to expand and functionalize metal-organic frameworks simultaneously, Chem. – A Euro. J. 22 (18) (2016) 6277–6285, https://doi.org/10.1002/chem.201504907.
[214] N.A. Qasem, R. Ben-Mansour, M.A. Habib, An efficient CO2 adsorptive storage using MOF-5 and MOF-177, Appl. Energy 210 (2018) 317–326.
[215] H. Zhou, J. Zhang, J. Zhang, X.-F. Yan, X.-P. Shen, A.-H. Yuan, Spillover enhanced hydrogen storage in Pt-doped MOF/graphene oxide composite produced via an impregnation method, Inorg. Chem. Commun. 54 (2015) 54–56.
[216] A.A. Ensafi, M. Jafari-Asl, A. Nabiyan, B. Rezaei, M. Dinari, Hydrogen storage in hybrid of layered double hydroxides/reduced graphene oxide using spillover mechanism, Energy 99 (2016) 103–114.
[217] N.F. Attia, M. Jung, J. Park, H. Jang, K. Lee, H. Oh, Flexible nanoporous activated carbon cloth for achieving high H2, CH4, and CO2 storage capacities and selective CO2/CH4 separation, Chem. Eng. J. 379 (2020), 122367.
[218] M. Li, W. Yin, J. Pan, Y. Zhu, N. Sun, X. Zhang, Y. Wan, Z. Luo, L. Yi, L. Wang, Hydrogen spillover as a promising strategy for boosting heterogeneous catalysis and hydrogen storage, Chem. Eng. J. 471 (2023), 144691, https://doi.org/10.1016/j.cej.2023.144691.
[219] L. Liu, W. Cui, C. Lu, A. Zain, W. Zhang, G. Shen, S. Hu, X. Qian, Analyzing the adsorptive behavior of Amoxicillin on four Zr-MOFs nanoparticles: functional groups dependence of adsorption performance and mechanisms, J. Environ. Manag. 268 (2020), 110630, https://doi.org/10.1016/j.jenvman.2020.110630.
[220] K. Koizumi, K. Nobusada, M. Boero, Hydrogen storage mechanism and diffusion in metal–organic frameworks, Phy. Chem. Chem. Phy. 21 (15) (2019) 7756–7764, https://doi.org/10.1039/C8CP07467D.
[221] B. Zhang, Y. Sun, H. Xu, X. He, Hydrogen storage mechanism of metal–organic framework materials based on metal centers and organic ligands, Carbon Neutralization n/a(n/a) (2023). https://doi.org/https://doi.org/10.1002/cnl2.91.
[222] J.-H. Guo, S.-J. Li, Y. Su, G. Chen, Theoretical study of hydrogen storage by spillover on porous carbon materials, Int. J. Hydrogen Energy 45 (48) (2020) 25900–25911.
[223] W. Zhou, Methane storage in porous metal− organic frameworks: current records and future perspectives, Chem. Rec. 10 (3) (2010) 200–204.
[224] H. Wu, J.M. Simmons, Y. Liu, C.M. Brown, X.S. Wang, S. Ma, V.K. Peterson, P. D. Southon, C.J. Kepert, H.C. Zhou, Metal–organic frameworks with exceptionally high methane uptake: where and how is methane stored? Chem.–A Euro. J. 16 (17) (2010) 5205–5214.
[225] H. Wu, W. Zhou, T. Yildirim, High-capacity methane storage in metal− organic frameworks M2 (dhtp): the important role of open metal sites, J. Am. Chem. Soc. 131 (13) (2009) 4995–5000.
[226] S.M. Lucena, P.G. Mileo, P.F. Silvino, C.L. Cavalcante Jr, Unusual adsorption site behavior in PCN-14 metal–organic framework predicted from Monte Carlo simulation, J. Am. Chem. Soc. 133 (48) (2011) 19282–19285.
[227] S. Ma, D. Sun, J.M. Simmons, C.D. Collier, D. Yuan, H.-C. Zhou, Metal-organic framework from an anthracene derivative containing nanoscopic cages exhibiting high methane uptake, J. Am. Chem. Soc. 130 (3) (2008) 1012–1016.
[228] J. Getzschmann, I. Senkovska, D. Wallacher, M. Tovar, D. Fairen-Jimenez, T. Düren, J.M. Van Baten, R. Krishna, S. Kaskel, Methane storage mechanism in the metal-organic framework Cu3 (btc) 2: An in situ neutron diffraction study, Microporous Mesoporous Mater. 136 (1–3) (2010) 50–58.
[229] H. Wu, W. Zhou, T. Yildirim, Methane sorption in nanoporous metal− organic frameworks and first-order phase transition of confined methane, J. Phys. Chem. C 113 (7) (2009) 3029–3035.
[230] M. Zhang, B. Li, Y. Li, Q. Wang, W. Zhang, B. Chen, S. Li, Y. Pan, X. You, J. Bai, Finely tuning MOFs towards high performance in C2H2 storage: synthesis and properties of a new MOF-505 analogue with an inserted amide functional group, Chem. Comm. 52 (45) (2016) 7241–7244, https://doi.org/10.1039/C6CC03198F.
[231] W. Gong, H. Cui, Y. Xie, Y. Li, X. Tang, Y. Liu, Y. Cui, B. Chen, Efficient C2H2/CO2 separation in ultramicroporous metal-organic frameworks with record C2H2 storage density, J. Am. Chem. Soc. 143 (36) (2021) 14869–14876, https://doi.org/10.1021/jacs.1c07191.
[232] L. Valenzano, B. Civalleri, S. Chavan, G.T. Palomino, C.O. Areán, S. Bordiga, Computational and experimental studies on the adsorption of CO, N2, and CO2 on Mg-MOF-74, J. Phys. Chem. C 114 (25) (2010) 11185–11191.
[233] W.L. Queen, C.M. Brown, D.K. Britt, P. Zajdel, M.R. Hudson, O.M. Yaghi, Site-specific CO2 adsorption and zero thermal expansion in an anisotropic pore network, J. Phys. Chem. C 115 (50) (2011) 24915–24919.
[234] M.K. Rana, H.S. Koh, J. Hwang, D.J. Siegel, Comparing van der Waals density functionals for CO2 adsorption in metal organic frameworks, J. Phys. Chem. C 116 (32) (2012) 16957–16968.
[235] X.-J. Hou, P. He, H. Li, X. Wang, Understanding the adsorption mechanism of C2H2, CO2, and CH4 in isostructural metal–organic frameworks with coordinatively unsaturated metal sites, J. Phys. Chem. C 117 (6) (2013) 2824–2834.
[236] D.-A. Yang, H.-Y. Cho, J. Kim, S.-T. Yang, W.-S. Ahn, CO 2 capture and conversion using Mg-MOF-74 prepared by a sonochemical method, Energ. Environ. Sci. 5 (4) (2012) 6465–6473.
[237] J.H. Choe, H. Kim, C.S. Hong, MOF-74 type variants for CO2 capture, Mater. Chem. Front. 5 (14) (2021) 5172–5185, https://doi.org/10.1039/D1QM00205H.
[238] Y.B.N. Tran, P.T.K. Nguyen, Q.T. Luong, K.D. Nguyen, Series of M-MOF-184 (M = Mg Co, Ni, Zn, Cu, Fe) metal-organic frameworks for catalysis cycloaddition of CO2, Inorg. Chem. 59 (22) (2020) 16747–16759, https://doi.org/10.1021/acs.inorgchem.0c02807.
[239] H. Kim, M. Sohail, K. Yim, Y.C. Park, D.H. Chun, H.J. Kim, S.O. Han, J.-H. Moon, Effective CO2 and CO Separation using [M2(DOBDC)] (M = Mg Co, Ni) with unsaturated metal sites and excavation of their adsorption sites, ACS Appl. Mater. Interf. 11 (7) (2019) 7014–7021, https://doi.org/10.1021/acsami.8b20450.
[240] S.R. Caskey, A.G. Wong-Foy, A.J. Matzger, Dramatic tuning of carbon dioxide uptake via metal substitution in a coordination polymer with cylindrical pores, J. Am. Chem. Soc. 130 (33) (2008) 10870–10871.
[241] P.P. Pescarmona, Cyclic carbonates synthesised from CO2: applications, challenges and recent research trends, Curr. Opin. Green Sustain. Chem. 29 (2021), 100457.
[242] J. Tapiador, E. García-Rojas, P. López-Patón, G. Calleja, G. Orcajo, C. Martos, P. Leo, Influence of divalent metal ions on CO2 valorization at room temperature by isostructural MOF-74 materials, J. Environ. Chem. Eng. 11 (2) (2023), 109497.
[243] W.L. Queen, M.R. Hudson, E.D. Bloch, J.A. Mason, M.I. Gonzalez, J.S. Lee, D. Gygi, J.D. Howe, K. Lee, T.A. Darwish, Comprehensive study of carbon dioxide adsorption in the metal–organic frameworks M 2 (dobdc)(M= Mg, Mn, Fe Co, Ni, Cu, Zn), Chem. Sci. 5 (12) (2014) 4569–4581.
[244] E. Haldoupis, J. Borycz, H. Shi, K.D. Vogiatzis, P. Bai, W.L. Queen, L. Gagliardi, J. I. Siepmann, Ab initio derived force fields for predicting CO2 adsorption and accessibility of metal sites in the metal–organic frameworks M-MOF-74 (M= Mn Co, Ni, Cu), The J. Phy. Chem. C 119 (28) (2015) 16058–16071.
[245] P.D. Dietzel, V. Besikiotis, R. Blom, Application of metal–organic frameworks with coordinatively unsaturated metal sites in storage and separation of methane and carbon dioxide, J. Mater. Chem. 19 (39) (2009) 7362–7370.
[246] J.M. Simmons, H. Wu, W. Zhou, T. Yildirim, Carbon capture in metal–organic frameworks—a comparative study, Energ. Environ. Sci. 4 (6) (2011) 2177–2185.
[247] B. Basak, S.M. Patil, S. Saha, M.B. Kurade, G.-S. Ha, S.P. Govindwar, S.S. Lee, S. W. Chang, W.J. Chung, B.-H. Jeon, Rapid recovery of methane yield in organic overloaded-failed anaerobic digesters through bioaugmentation with acclimatized microbial consortium, Sci. Total Environ. 764 (2021), 144219, https://doi.org/10.1016/j.scitotenv.2020.144219.
[248] L. Yang, X. Ge, C. Wan, F. Yu, Y. Li, Progress and perspectives in converting biogas to transportation fuels, Renew. Sustain. Energy Rev. 40 (2014) 1133–1152, https://doi.org/10.1016/j.rser.2014.08.008.
[249] A. Khan, M.A. Qyyum, H. Saulat, R. Ahmad, X. Peng, M. Lee, Metal–organic frameworks for biogas upgrading: recent advancements, challenges, and future recommendations, Appl. Mater. Today 22 (2021), 100925, https://doi.org/10.1016/j.apmt.2020.100925.
[250] A.R. Millward, O.M. Yaghi, Metal−organic frameworks with exceptionally high capacity for storage of carbon dioxide at room temperature, J. Am. Chem. Soc. 127 (51) (2005) 17998–17999, https://doi.org/10.1021/ja0570032.
[251] A. Chidambaram, D.H. Le, J.A.R. Navarro, K.C. Stylianou, Robust metal-organic frameworks for dry and wet biogas upgrading, Appl. Mater. Today 22 (2021), 100933, https://doi.org/10.1016/j.apmt.2020.100933.
[252] X.Y. Chen, H. Vinh-Thang, A.A. Ramirez, D. Rodrigue, S. Kaliaguine, Membrane gas separation technologies for biogas upgrading, RSC Adv. 5 (31) (2015) 24399–24448.
[253] H. Gong, C.Y. Chuah, Y. Yang, T.-H. Bae, High performance composite membranes comprising Zn(pyrz)2(SiF6) nanocrystals for CO2/CH4 separation, J. Ind. Eng. Chem. 60 (2018) 279–285, https://doi.org/10.1016/j.jiec.2017.11.014.
[254] T.H. Bae, J.R. Long, CO2/N2 separations with mixed-matrix membranes containing Mg2(dobdc) nanocrystals, Energy Environ. Sci. 6 (12) (2013) 3565–3569, https://doi.org/10.1039/c3ee42394h.
[255] Y. Yang, K. Goh, R. Wang, T.-H. Bae, High-performance nanocomposite membranes realized by efficient molecular sieving with CuBDC nanosheets, Chem. Comm. 53 (30) (2017) 4254–4257, https://doi.org/10.1039/C7CC00295E.

[256] O.T. Qazvini, R. Babarao, S.G. Telfer, Selective capture of carbon dioxide from hydrocarbons using a metal-organic framework, Nat. Commun. 12 (1) (2021) 197, https://doi.org/10.1038/s41467-020-20489-2.
[257] J. Glover, E. Besley, A high-throughput screening of metal–organic framework based membranes for biogas upgrading, Faraday Discuss. 231 (2021) 235–257, https://doi.org/10.1039/D1FD00005E.
[258] H. Gong, C.Y. Chuah, Y. Yang, T.-H. Bae, High performance composite membranes comprising Zn (pyrz) 2 (SiF6) nanocrystals for CO2/CH4 separation, J. Ind. Eng. Chem. 60 (2018) 279–285.
[259] J. Ding, T. Tsuzuki, P.G. McCormick, Microstructural evolution of Ni-NaCl mixtures during mechanochemical reaction and mechanical milling, J. Mater. Sci. 34 (21) (1999) 5293–5298, https://doi.org/10.1023/A:1004736602847.